THE IMPACT OF SHADOW ENHANCEMENT ALGORITHMS ON REMOTELY SENSED IMAGES OF COMPLEX URBAN ENVIRONMENTS

WAN CHEUK YAN

M.Phil

The Hong Kong Polytechnic University

2013

The Hong Kong Polytechnic University

Department of Land Surveying and
Geo-Informatics

The Impact of Shadow Enhancement Algorithms on Remotely Sensed Images of Complex Urban Environments

Wan Cheuk Yan

A thesis submitted in partial fulfillment of the requirements for the degree of Master of Philosophy

August, 2012

CERTIFICATE OF ORIGINALITY

I hereby declare that this thesis is my own work and that, to the best of my knowledge and belief, it reproduces no material previously published or written, nor material that has been accepted for the award of any other degree or diploma, except where due acknowledgement has been made in the text.

____

WAN Cheuk Yan

Abstract

Large portions of shadowed areas in satellite images of urban areas can affect the accuracy of classification and thus reduce an image's effectiveness in urban remote sensing applications. This is particularly acute in cities such as Hong Kong where dense high-rise buildings cast many long shadows across a variety of different surface types. One solution to this problem is to enhance shadowed areas so their spectral range becomes closer to their corresponding non-shadowed areas. In this thesis the Spectral Shape Index was used to identify shadowed areas and two techniques, Gamma Correction and Linear Correlation Correction, were applied for the enhancement of three study sites of 2.4m spatial resolution multispectral Quickbird image. The selected study sites represent typical urban types of Hong Kong, ranging from high-rise commercial to low-rise residential areas. The performance of the shadow detection algorithm and its limitations are discussed. The histograms of the corresponding non-shadowed areas, the original and the enhanced shadow areas are used to compare the spectral range. Problems associated with shadow enhancement are discussed and the possibility of using a non-linear model for enhancement is examined. The results show that Linear Correlation Correction is more suitable when applied to complex environments and the enhanced areas as in band ratios, such as NDVI, show greater similarity after enhancement. For shadows that are still darker after enhancement, a

second iteration was performed and the results were examined. It was found that when the shadows are extremely dark the spectral information will be damaged and cannot be enhanced effectively.

Acknowledgement

I would like to express my deep and sincere appreciation to my supervisors, Dr. Bruce King and Prof. Zhilin Li, for their detailed and constructive comments, and for their support throughout this work. I would not have been able to complete the project without their guidance and encouragement throughout the project.

I would also like to thank Prof. Janet Nichol, my undergraduate supervisor, who has provided me with the necessary satellite images and technical support. Moreover, special thanks also go to Dr. Rebecca Tse, who gave valuable comments and suggestions for the project.

Lastly, I would like to express my gratitude to my parents and friends for their care and support throughout the project.

Table of contents

List of figures

List of tables

Chapter 1. Introduction

1.1 The importance of shadow enhancement

1.1.1 Negative effects of shadows

From a spectral signature point of view, shadows that exist in satellite images will affect the spectral signature. When less reflected energy is received by the sensor, spectral signature will normally be narrower and darker than those under sunlight. It would not be a problem for human eyes to identify ground features even when they are under shadows, but training the computers to identify various types of shadows is more difficult. For example, shadows on a bright surface and dark surface will have different behavior in the RGB brightness. If the dark pixels are considered only, shadows on bright surfaces cannot be extracted. For a complex urban environment, different types of surface like asphalt, concrete, metallic and vegetation, the brightness pattern in each band will behave differently. This spectral signature can be used to recognize features, but when it is being affected, identification and extraction of certain land surfaces cannot be done correctly. This situation will be more complicated and serious when more surface types are involved in an urban area.

Shadow compensation is one of the solutions to minimize the shadow effect and extract useful information within. Two major steps are involved to deal with these effects, shadow detection followed by enhancement. Pixel values after enhancement should be much closer to its surrounding so that part of the details within shadows can be recovered. Shadow enhancement can provide better visualization, and different algorithms of shadow enhancement have been investigated for this purpose. However, the enhanced areas may still appear darker and the spectral signature cannot be preserved. Any information loss during the shadow enhancement procedure will produce insignificant improvement for further applications like classification or feature extraction. This research is to examine if the effect of shadows can be minimized by such a process and be used for further image analysis tasks.

1.1.2 Previous research on the impact of shadows in satellite imagery

According to Massalabi et al. (2004a), with very high spatial resolution urban images, small features can be observed with more details, but the amount of shadow also increases due to the presence of tall buildings and trees. They also reported that, no matter when the satellite images (day time) were taken, shadows could not be avoided. Chen et al. (2007) mentioned that the existence of shadows in an image strongly disturb the image analysis results. Low reflected energy also causes information loss. Arevalo et al. (2006) also commented on the shadow problems that radiometric information may be totally lost which leads to failed analysis results. This suggested that higher radiometric resolution is preferable for shadow enhancement as it allows more details to be preserved after radiometric correction of shadowed pixels.

Yamazaki et al. (2009) pointed out that the presence of shadows has a negative effect on the accuracy of urban change detection. When multi-temporal images are used, the time and seasonal effect of image acquisition leads to change in shadow direction and shape. “Changes” will then be found near these shadows and wrong analysis results may be carried out even when there are no structural changes in a time series. This agrees with Xia et al. (2009), who mentioned that shadows cause wrong color tone and thus affect image processing performance. In Hong Kong, the land cover map of urban areas cannot be generated by image classification easily due to the problems of occlusion and shadows caused by high-rise buildings. As the surfaces (including roads, buildings, vegetation, water and bare ground) are under shadow, training software to identify certain land covers becomes a very difficult task. Especially for water bodies and shadows with similar spectral signature, existing algorithms for extracting water bodies in urban areas are application specific and shadows formed by tall buildings could hardly be avoided (Nath & Deb, 2010).

1.1.3 Importance of spectral signature

Satellite images are the main data sources of remote sensing applications. There are many sensors carried by remote satellites which may be combined to produce a range of image types, one of the most useful being the multispectral image. For satellite images, one of their valuable features is that multi-spectral sensors are available on the satellite; sensors are sensitive to different spectral energy. Different bands of reflected energy can be captured by the sensor and the resulting image can then be separated into different layers. In order to classify different land covers, there are many algorithms developed, including various spectral classification methods and band ratios. No matter which algorithm is applied, the classification accuracy strongly depends on the accuracy of the per-pixel recorded band energies. As the presence of shadows will affect the energy received from the sensor, the classification accuracy will also be affected.

1.1.4 The Hong Kong situation

Hong Kong is a small but famous city, with limited flat land available. Buildings are usually tall in order to maximize the use of land resources. In urban areas, it is common to find commercial and residential buildings having more than 30 storeys. Besides the buildings' height, building density is another issue that makes Hong Kong a complex urban environment. Buildings and constructions with different functionalities are closely packed within an area. For example, small recreation areas may be surrounded by 60 storey commercial buildings. This unique structure makes Hong Kong a representative place for studying shadow enhancement in complex urban environment.

Figure 1-1 presents a typical urban area in Hong Kong. It can be seen that the building density is high and long shadows are formed by tall buildings. When we want to develop an environmental assessment within this area using the satellite image, the existence of shadows would be a problem when the sampling location exactly falls onto the shadows inside the image. When this is the case, the correlation establishment using in-situ sampling data would be affected. Also, for shadow enhancement, the existence of water surfaces, asphalt roof tops and the difference in illuminating condition would have serious impact on classifying shadows and other non-shadow dark surfaces.

Figure 1-1 Typical urban area in Hong Kong

Although there are successful cases of shadow enhancement in different countries, an application in Hong Kong is a more challenging task. Three typical urban areas of Hong Kong are selected for case study. These areas contain complex environments that are representative of most of the extreme cases in shadow enhancement. Parts of them are surrounded by polluted water so that shadows and water may easily get misclassified. There are cases that shadows fall onto water surfaces. Besides that, the high-rise buildings are densely distributed so that a large portion of land surface is under shadow and the land covers are more complicated than found in previous studies.

1.1.5 Problems associated with shadows in Hong Kong satellite imagery

Figure 1-2 is used to illustrate the problem of shadows in Hong Kong urban imagery. As mentioned before, water features are easily mixed with shadows when image classification is being done. In Hong Kong, some districts (as shown in figure 1-2 yellow circle) are close to water bodies and sometimes shadows even fall onto the surface. The water quality varies from location to location, making the separation process of water and shadow a difficult task.

Land covers in Hong Kong are rather complicated and some of the shadow enhancement algorithms are not likely to work. The red circle in figure 4-7 shows that a rather long shadow falls onto the ground. Within that shadowed areas, land covers include vegetation, flyover, road, bare ground and pavements. Under this situation, an algorithm such as histogram matching cannot work efficiently (Dare, 2005). For histogram matching, the minimum, mean and maximum pixel values of a shadowed region are adjusted close to the same type of surface. If the shadows only fall onto one certain land cover, histogram matching can be applied easily. However, in this case, the spectral range of all the land covers within the shadows has to be considered, and it involves the process of classifying shadows based on their land covers.

Figure 1-2 problems associated with urban imagery

1.1.6 Significance of this study

The presence of shadows in images will make the pixels much darker than the surrounding and thus have lower pixel values. The differences in color tone affect the accuracy of image classification and feature extraction. For in-situ data sampling, correlation is made with the pixel values on corresponding locations in the satellite image. Shadows may be found and would strongly affect the correlation accuracy. Shadow information restoration can help to correct these darker pixels so they can become brighter and natural to its surrounding regions. With much closer color tone to its surrounding area, these negative impacts of shadows can be reduced.

Although the colors of shadow regions can be restored, the spectral properties may still be damaged during the process as the negative effect of shadows may not be eliminated successfully. This study provides proof that if spectral properties can also be preserved through different algorithms, scientists can make full use of these enhanced regions during their analysis. This also indicates whether shadow enhanced images can be used as an image source for further analysis in an image covering a densely built-up area. The existence of shadows will then have less impact on the image analysis process.

1.2 Research objectives

To examine the shadow enhancement results in complex urban areas, two different enhancement algorithms (Gamma Correction and Linear Correlation Correction) will be compared and tested to see if they are suitable for further image analysis (through simple band ratios). The possibilities of iterating enhancement process and the performance of modified shadow enhancement algorithm will be tested.

1.3 Structure of this thesis

This report is divided into six parts. After the introduction, the significance of the study and the research objective are stated. Some of the previous studies are then discussed. The research methodology is delineated, followed by the results and analysis. The report ends with the discussion and conclusion.

Chapter 2. Procedures and techniques for shadow enhancement

2.1 Shadow detection

According to Massalabi et al. (2004b), shadow detection methods mainly make use of the color and spectral properties, and geometric properties can be used to improve the accuracy of shadow detection. Xia et al. (2009) also commented that an accurate shadow detection algorithm is necessary for any uses of shadow information. They also pointed out that training computers to identify shadows effectively is a difficult task when many different types of surfaces are involved. For the two existing approaches, properties based and model based detection algorithms, they commented that the properties based required less geometrical information (urban structures) and is more commonly used. Cai et al. (2010) summarised shadow detection methods into two types: model based and shadow attribute (properties) based. They pointed out that model based detection is used for special situations that acquire much higher detection accuracy while attribute based detection makes use of the knowledge of shadow properties and is applied more generally. They also commented that using model based detection requires more knowledge and information about urban structures (buildings' models) and lighting conditions (azimuth angle, season and time when the image is taken), which can be used to improve the detection accuracy.

2.1.1 Properties based shadow detection

According to Cai et al. (2010), properties based shadow detection makes use of spectral and geometric characteristics to detect shadows. The spectral characteristics can be regarded as the intensity of shadow pixels and geometric information such as shadow orientation, angle and its position to improve the detection accuracy. By different band ratios and colour spaces used, the shadows can be detected and extracted if the image histogram has more than one peak that is able to isolate most of the shadows.

Cai further illustrated that it requires a threshold value for separating target features from shadows and stated that shadows usually have low intensity, high saturation and high hue value. In Cai's study, 3 different indices based on HSI transformation were suggested and the uses of NDVI were combined in order to extract shadow areas by choosing a suitable threshold value. They found that the shadow detection accuracy is improved compared with HSI transformation only. However, in most of studies, some coverage such as non-shadow dark surfaces and polluted water surfaces will be misidentified due to the fact that they have similar spectral properties.

Sarabandi et al. (2004) suggested using Color Invariant Indices for classifying shadows.

$C_1C_2C_3$ color space (Gevers & Smeulders, 1999) was transformed from RGB. Texture and edge filter were then applied to the C_3 layer in order to classify the shadow boundaries. Arevalo et al. (2006) also made use of C_3 color space for shadow detection, while they commented that this component is quite noisy and not stable for certain color values. With the help of RGB and HSI spaces and the use of region growing techniques, shadows can be detected. Although their study showed that the number of false positives decrease, some of the shadow edges were not successfully detected.

Tsai (2006) compared the effectiveness of different invariant color spaces for shadow detection, including HSI, HSV, HCV, YIQ and YC_bC_r models. He concluded that HSI, YIQ and YC_bC_r are the most suitable color spaces for shadow detection. However, the study only covered small areas for testing. It is necessary to examine its ability to deal with complex situations like water bodies and dark surface.

Chen et al. (2007) suggested another algorithm to deal with the misclassification between water bodies and shadows. They introduced five sets of indices to separate water and shadows and named the one with better performance "Spectral Shape Index". However, in Chen et al.'s (2007) study, the Spectral Shape Index being recommended (Red+Blue-2×Green) did not produce fair shadow detection results in the preliminary test using Hong Kong satellite image. In fact, another formula ([Green-Red] ÷ [Red+NIR]) produces more reasonable shadow detection results that shadows can be separated from water features, and the name Spectral Shape Index is adopted for this formula and used for the rest of the thesis. All the formulas are listed in Appendix A.

Wang & Wang (2009) suggested the use of Principal Component Analysis (PCA) to transform RGB image into luminance and chrominance components. Histogram threshold was used to detect shadows in the luminance layer. Although some bright surfaces under shadow cannot be detected, the techniques of PCA can be applied to reduce the number of spectral bands involved. For example, a RGB image (3 bands: Red, Green and Blue) is represented using 2 principal components luminance and chrominance. If an image contains many spectral bands, PCA can be used to reduce the number of layers involved. The new layers are called principal components and are able to explain most of the variations within an image (dataset).

2.1.2 Model based shadow detection

Model based detection makes use of extra information in order to best simulate the real situation and estimate the shadows location, size and direction. The information may include digital building model (DBM), digital terrain model (DTM), together with sun azimuth angle, season and time of image taken. With this information, higher shadow detection accuracy can be obtained, but what kind of information needed and its availability may vary from place to place.

In Zhou's (2005) study of true orthoimage generation that deals with occlusions, shadows and incorrect building's spatial position, he considered the problem of self-shadow (shadow cast on the object by itself) and made use of digital building model (DBM) and digital surface model (DSM) to accurately simulate the urban area so that shadow detection can be made. Nakajima et al. (2002) made use of Airborne Laser Scanning data and Digital Surface Model of the urban area for shadow simulation. They also combined the sun angle and azimuth information of the image acquisition time in order to estimate the location of shadows in the image. However, asphalt surfaces that are mixed with shadows cannot be distinguished easily. Nakajima et al. commented that the algorithm used requires a high accuracy DSM/DEM to produce a fair result.

Based on the DSM model derived from ALS data, Zhan et al. (2005) applied the object-based approach for shadow detection. Each pixel is considered to have 4 connections (4 sides of a pixel square). The pixel values are compared to identify if they belong to the same object. Shadow objects smaller than a certain size will be eliminated for fear that noises are treated as shadows. Both studies require an accurate DSM/DEM which is not available to the public in Hong Kong; it would be a problem especially when dealing with a hilly landform with densely distributed buildings.

2.1.3 Other shadow detection algorithms

In this section, the way of how images are being classified and the use of extra information for shadow detection will be discussed. They can be classified as improvement of detection accuracy.

Xia et al. (2009) made use of Affinity Propagation Clustering for shadow detection based on the HSI color space. The possible center of cluster is calculated for HSI layer and the shadow detected images can be produced. According to the author, this algorithm provide better detection accuracy than K-means clustering and traditional histogram threshold segmentation, and is able to distinguish dark objects from shadows which is suitable for the case study of Hong Kong. However, the author also commented that applying Affinity Propagation to the image directly will consume large amount of system resources and is necessary to divide the image into smaller portions before clustering. It would be another concern of how the images are being divided and how small the areas should be in order to give better results. Further investigation is needed for the image dividing mechanism.

Guo et al. (2008) made use of the sun angle and the direction of the shadows to develop structure lines for shadow edges. After the line constraint was established, statistical comparison of grey levels along these lines was used to decide whether those pixels along the lines belong to shadow or not. More customized constraints are then used to extract the boundary of shadows. However, the straight shadow edges of low-rise buildings are not clear and may not have a unique pattern which means that many more constraints may have to be considered in order to produce an accurate result.

2.2 Shadow enhancement

There are three shadow enhancement algorithms that are commonly used: Histogram Matching, Gamma Correction and Linear Correlation Correction. Histogram Matching is the most common algorithm that adjusts the pixel values' mean and variance of shadowed areas so that they are closer to the non-shadowed areas. Gamma Correction treats shadow as a multiplicative noise source that affects the pixel brightness and can enhanced using specific equation with a Gamma parameter estimated from training datasets. Linear Correlation Correction makes use of pixel values from both shadowed and representative non-shadowed areas to create different sets of linear regression model for enhancement purpose.

These three techniques plus the more recent Retinex techniques and the problems associated with shadow enhancement will be discussed in the following sections.

2.2.1 Histogram Matching

According to Sarabandi et al. (2004), histogram matching works by correcting the brightness distribution of two given images so they become as close as possible. For shadow detection, the brightness of shadowed and non-shadowed areas of the same class will be compared and adjusted. With the use of two same size windows for comparison and correction, they commented that the window size would affect the shadow enhancement quality. Quad-Tree partitioning was used to automatically identify suitable window size. Sarabandi compared the three enhancement algorithms listed above and commented that histogram matching is capable for shadow enhancement, but it is not as effective as Linear Correlation Correction. Tsai (2006) made use of histogram matching for shadow detection in aerial images but noted that the resulting image is quite noisy. The problem of dark surfaces is not discussed. Dare (2005) commented that neighboring shadows will be agglomerated into single shadow region. The algorithm only works well while the histogram information of nearby regions is used; local equalization parameters should be used, not global ones. Zheng & Wang (2008) reported that it is difficult to extract histogram information of the same type of surfaces and that the resulting image quality will be degraded when histogram stretching is applied due to limited number of pixels being involved.

2.2.2 Gamma Correction

According to Sarabandi et al. (2004), Gamma Correction treats shadow as a source of noise that affects the brightness of shadowed pixels. For an 11-bit image, the Gamma Correction equation can be written as:

$$\frac{DN_{non\,shadow}}{2047} = \frac{(DN_{shadow})^{\frac{1}{\gamma}}}{2047} \qquad (1)$$

DN refers to the pixel number. One Gamma parameter γ for each image band is estimated based on the average pixel values of shadowed and non-shadowed areas. The highest possible pixel value (2047) is used to standardize the differences between each band.

For the effectiveness of Gamma Correction, Nakajima et al. (2002) reported that trees and ground surfaces can be correctly enhanced, but asphalt surfaces (roads / roof tops) cannot be successfully enhanced due to the fact that these surfaces cannot be identified correctly during shadow detection. Massalabi et al. (2004a) had a different result showing that the precision of the land-use map created increases when a Gamma Corrected image is used. This agrees with Sarabandi et al. (2004) who commented that Gamma Correction is capable of shadow enhancement, but Linear Correlation Correction produces better final results.

2.2.3 Linear Correlation Correction (LCC)

According to Sarabandi et al. (2004), if shadow is treated as a combination of additive and multiplicative noise, the brightness of shadows can be enhanced by a linear function. Chen et al. (2007) further explained the algorithm that radiance recorded by satellite sensors consists of three components, reflectance of atmosphere (Rs), reflectance of object by direct sunlight (Rdr), and reflectance of object by scattered sunlight (Rsr). As sunlight is the primary source of energy, Rs and Rsr are assumed to be proportional to Rdr. Radiance in the shadow area and non-shadow area should then have a linear relationship. It is also the relationship of illumination condition between the shadow areas and non-shadow areas. Chen et al. (2007) established the linear equations based on the mean and standard deviation of grey values in shadowed and non-shadowed areas. Yamazaki et al. (2009) established the equations simply by using linear regression model obtained from 11 pairs of pixel values (under sunlight and shadow). Each spectral band will have its own linear equation for enhancement use; the enhanced image will be fused with the original image. For the visible RGB bands, a stronger linear relationship between shadow and non-shadow areas can be observed, and for Near-Infrared band the relationship is not as strong as the visible bands, but linear regression can still be used for enhancement.

For the effectiveness of Linear Correlation Correction, Sarabandi et al. (2004) compared the enhancement result using Histogram Matching, Gamma Correction and Linear Correlation Correction. He pointed out that Linear Correlation Correction gave the closest pixel value with respect to its neighbor pixels. However, only one set of sampling data was used for the comparison so the claim is not well supported by evidence. Zheng & Wang (2008) also compared the effectiveness of the three approaches. From a visualization point of view, they commented that Linear Correlation Correction preserves more details within the shadow area than Gamma Correction and the color tone is similar to its surrounding. They also commented that it is not easy to find sampling areas with the same surface type for Histogram Matching in urban areas. The resulting image tone may easily be distorted.

2.2.4 Retinex technique

Retinex is a technique that is usually applied in computer graphics. Huang et al. (2004) stated that Retinex Theory is used for removing discrepancy between observation and image. According to Wang & Wang (2009), the goal of Retinex is to decompose the brightness information into a reflectance image and an illuminance image so that the effect of shadow can be cancelled separately. A luminance image is formed by multiplying an illuminance image and a reflectance image. They used PCA for separating different components and pointed out that only luminance (brightness) is being enhanced but the chrominance layers remain unchanged and are transformed back to RGB image by inverse PCA.

For the effectiveness of Retinex, Wang & Wang (2009) commented that this approach can distinguish greenish objects from shadows and improve the visibility of features in shadowed areas without affecting non-shadow areas. This is an approach worth using as it can distinguish objects with similar color tone. However, the algorithm has to be implemented in programs like MATLAB. These studies made use of aerial photos which normally consist of RGB layers only, but high-resolution satellite images usually contains an additional Infrared band. The mechanism of defining luminance and chrominance layers using images with infrared band will be different. Further investigation is required on the performance of enhancing the Infrared layer using Retinex.

2.2.5 The penumbra problem (semi-shadow region)

According to Dare (2005), when high-resolution images are used, it is not appropriate to assume the light source as a point at infinity and it is necessary to consider shadow umbra and penumbra. Umbra (shadow) is the region where sunlight is totally blocked while penumbra (semi-shadow) is the region around the umbra where sunlight is partially blocked. Penumbra is thus slightly darker than its non-shadowed surrounding without sharp edges and is not easy to be separated. Dare (2005) reported that the width of penumbra is proportional to the building height and approximately 1 pixel penumbra region will be created for a 50m tall building. Shu & Freeman (1990) suggested solving the penumbra problem by considering the semi-shadow regions during shadow detection (shadow, semi-shadow and non-shadow areas). The enhancement can then be done on each region individually. However, Dare (2005) believed that under complex structural urban areas, it is difficult to distinguish these classes clearly and thus may not produce better enhancement results.

Zheng and Wang (2008) observed that the shadow edges will look brighter if enhancement is involved within the edges, but they will look darker when shadow detection cannot successfully extract these edges. They suggested that a buffer zone should be set up at the shadow edges and a median filter is applied until the gradient is within a given threshold.

Guo et al. (2008) considered the companion area of shadow for the edges and both umbra and penumbra regions are involved for Gamma Correction enhancement. Although the color tone after enhancement was not close to its surrounding, it was found that the penumbra region was already taken into account and the color tone difference is due to the enhancement algorithm.

In fact, different color tone of enhanced penumbra regions could hardly be avoided. In this study, the problems associated with penumbra regions were not tackled specifically and some of these regions were enhanced while some were not. The effect of penumbra regions under complex urban structure can be observed in the results presented in later sections.

2.3 Quality assessment of shadow enhancement

In an ideal shadow enhancement result, for any type of surface, the pixel value distribution within shadowed areas should be almost the same as the one in non-shadowed areas. The smaller the differences between enhanced pixel and non-shadowed pixel values, the higher the enhancement quality. Quality assessment plays an important role that reflects the performance of each algorithm. With higher enhancement quality, the negative effect of shadowed regions could be reduced and those regions may be used normally. These results also reflect how good these enhanced regions can be classified and extracted in further process. Common assessment techniques include Bias of Mean (BM) that compares the average pixel values; Entropy, which measures information changes; and band ratios (vegetation index is used in this study), which reflect the ability of classifying shadowed regions after enhancement.

Sarabandi et al. (2004) examined how close the pixel value of enhanced shadow area and its neighbor are. However, only one set of data from the final image is used to draw the conclusion, which is not scientific enough. Zhan et al. (2005) presented the histogram of one of the sampling data before and after enhancement to show the pattern of each spectral band. Most of the studies considered the visual-improvement after enhancement is done.

Massalabi et al. (2004a) suggested the use of classification to assess the quality of enhanced image, and concluded that classification on shadow enhanced image increases the precision of the land use map produced. Yamazaki et al. (2009) compared the NDVI image before and after enhancement, which shows that more vegetation can be identified from the image. Unsupervised classification was then carried out showing that no shadow class exists after enhancement.

In Han et al.'s (2008) studies on image fusion techniques, they suggested using Bias of Mean (BM) and Correlation Coefficient to assess the spectral fidelity and made use of Entropy to assess the information after image fusion. The concept of Bias of Mean can be used to assess the spectral properties between enhanced areas and non-shadow areas of the same surface material. An ideal value of Bias of Mean is 0, which indicates that two areas (equal size) have the same mean pixel value. The Correlation Coefficient between enhanced shadow and its neighbor non-shadow areas can also be used to assess the spectral fidelity. For correlation coefficient, selected areas are close to each other and have the same surface type to ensure that the effect of sunlit condition in different locations can be minimized. Entropy is a measure of information and has been used for assessing the information changes during image processing. Han et al. (2008) commented that if the Entropy increases after image processing, more information is available in the resulting image. However, Lau et al. (2001) pointed out that the extra information available can be in the form of noise which may not be useful. It is still possible to use Entropy to assess the information content of a shadow enhanced image, not by comparing the whole image before and after enhancement, but by comparing the enhanced shadow and its non-shadow neighbor (same size and type of surface).

To summarize the quality assessment techniques on spectral fidelity, most research related to shadow enhancement focused on visual improvement rather than spectral preservation. Some of them compared the histogram pattern before and after shadow enhancement, and some of them calculated the vegetation index to examine the usefulness of the final enhanced image.

Chapter 3. Design of experiments for comparative analysis of shadow enhancement

3.1 General Strategy

In order to achieve the objectives of this research, several steps have to be taken. Firstly, the shadows must be extracted in order to separate shadows from non-shadows and water features so that different processes can be applied to these areas. Shadow detection algorithms used should minimize the omission error and commission error of shadows identification. However, in complex urban environments, these errors are unavoidable and can only be reduced. The effects of penumbra were varied and the impact on the enhancement will be illustrated by example in section 4.2.3, but the corresponding solution requires further investigation and is not addressed in this paper.

Secondly, shadow enhancement algorithms are applied to the extracted shadows. Two methods will be compared: Gamma Correction and Linear Correlation Correction. As mentioned in section 2.2.1, Histogram Matching is not likely to work in complex urban environments and therefore only two methods are compared. Previous studies compared the performance of these two methods but their relative performance in complex urban environments was not clear.

Histogram Matching was not compared due to the fact that surface types under shadows were hidden, errors will be introduced in data sampling process. When one single shadow casted on several surface types, it would not be easy to select appropriate non-shadowed areas for a reference histogram.

Finally, the spectral fidelity testing assessment methods will be studied. It was observed that most of the techniques used for spectral fidelity assessment can be found in image fusion related papers but not many focused on shadow enhancement. In order to examine the quality of spectral preservation for the final product, quantitative analysis is necessary. How the assessment can be made will be a key issue for this research.

3.2 Work flow

After the selection of source images, a shadow mask will be created. Unlike the Spectral Shape Index used by Chen et al. (2007) the Spectral Shape Index used here will be calculated from the Red, Green and Infrared bands in order to isolate water bodies from shadows. Spectral Shape Index (eq. 2) is listed as below:

$$SSI = (Green - Red) \div (Red + NIR) \qquad (2)$$

The shadow mask will then be applied to each spectral band to extract shadow regions and is followed by the various shadow enhancement processes for each spectral band. The enhanced image will be merged with the non-shadow image in order to produce the shadow enhanced image. Different techniques will then be used to examine the quality of the enhanced image produced.

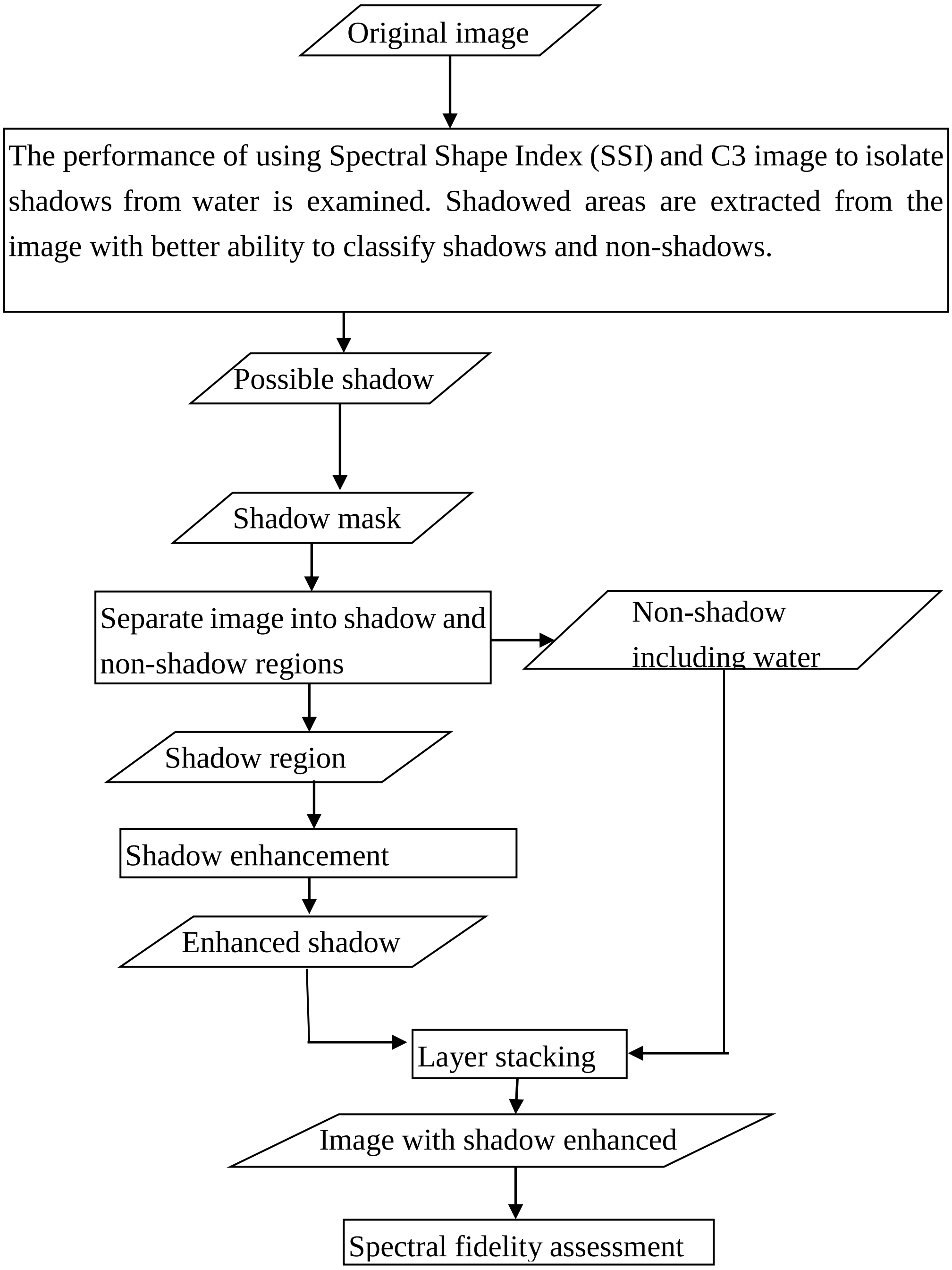

Figure 3-3-1 Flowchart of the research process

3.3 Selection of study areas

Two sets of Quickbird images with 2.4m spatial resolution covering different parts of Hong Kong are used in this study. One of the images (figure 3-2) covers the whole of the Kowloon Peninsula and part of northern Hong Kong Island and the other (figure 3-3) covers the Ma On Shan area. As the images contain both urban and non-urban areas the results of using the whole images would not be representative of complex urban areas. Instead, 3 districts which cover most of the complex scenarios of Hong Kong were selected. They are Central, Ma On Shan and Sham Shui Po. An overview map of the selected areas is given in figure 3-4.

3.3.1 Central

Central (figure 3-5) is located in the northern part of Hong Kong Island, and lies between the mountainous terrain of The Peak and Victoria Harbor. It is the CBD of Hong Kong and is made up of high rise residential buildings inland and even taller commercial buildings (including the world's 10^{th} tallest building, the Two International Finance Centre, 88 storeys, 415m tall) close to the coastline. Buildings in this district are built up to 50 or even 60 storeys high. Some of the road surfaces can hardly be seen in the satellite image. Victoria Harbor is the water body close to Central and from figure 3-2, it can be seen that the water is slightly polluted. Shadows in Central are mainly caused by buildings and fall across a variety of surfaces including low vegetation, asphalt roads and concrete.

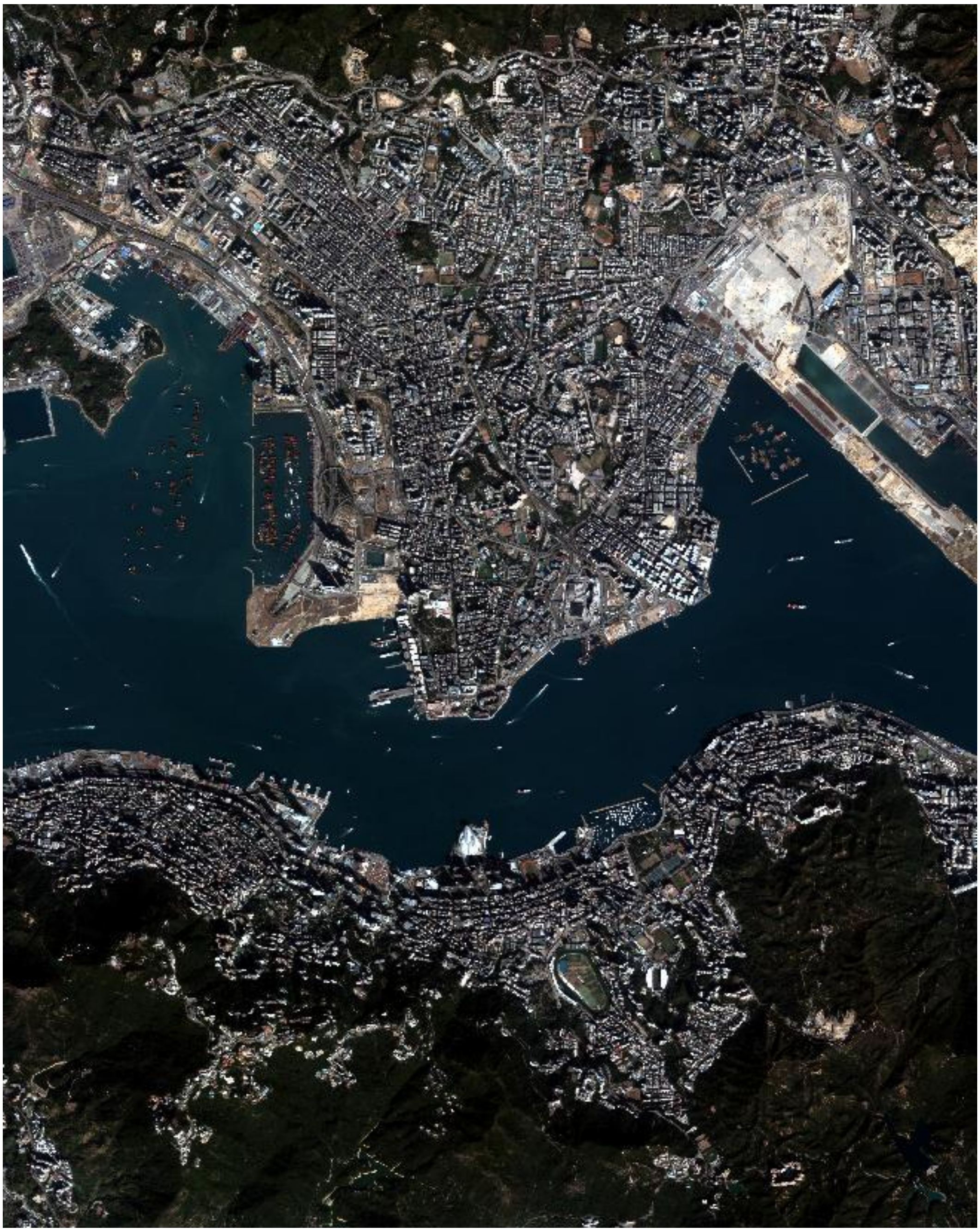

Figure 3-2 Coverage of the Kowloon Peninsula and Hong Kong Island Quickbird image

Figure 3-3 Coverage of the Ma On Shan Quickbird image

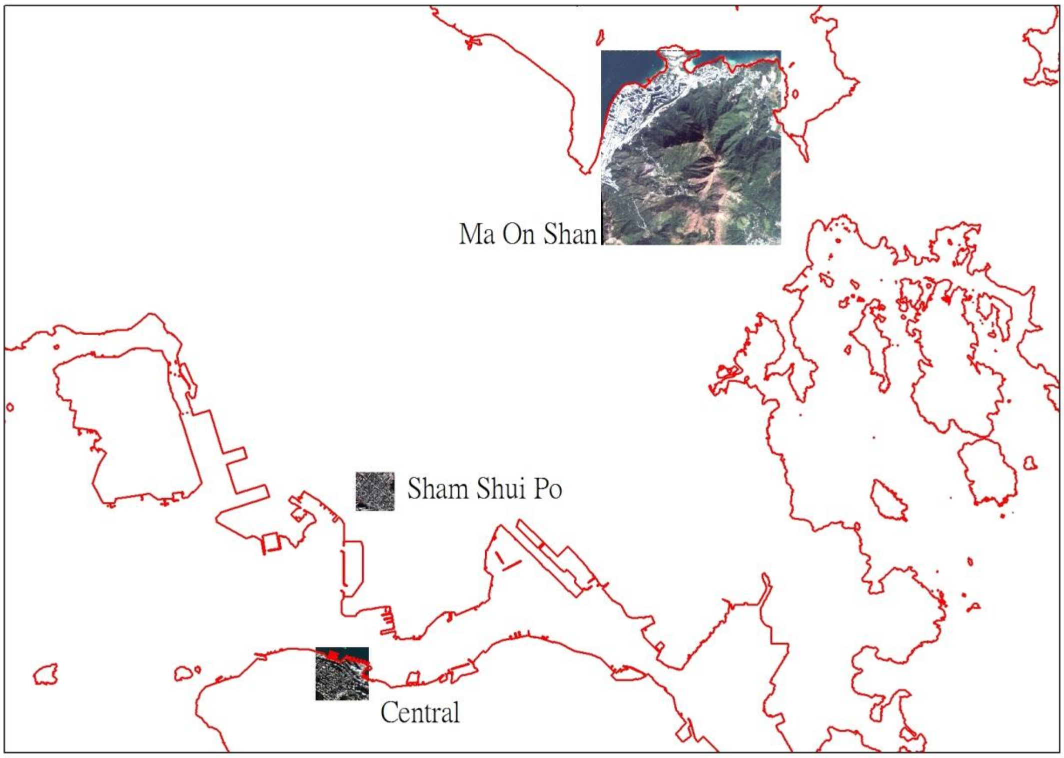

Figure 3-4 Overview map of the selected study areas

Figure 3-5 The Central study area (IFC located inside the red circle)

3.3.2 Ma On Shan

Ma On Shan (figure 3-6) is a newly developed town located in the north east of Hong Kong with lower building density. It is beside a country park and close to natural coast. Not many buildings in this district are tall. Some of them are around 30-40 storeys tall while most of the others are lower. Water depth within this area is much less compared with that in Central. Beach side and natural coast can be found. Shadows in Ma On Shan are from buildings and mountainous terrain within the country park. Only part of the original image is being used because shadows by mountainous terrain have similar behavior and the remaining portion is representative enough.

Figure 3-6 The Ma On Shan study area

Figure 3-7 The Sham Shui Po study area

3.3.3 Sham Shui Po

Sham Shui Po (figure 3-7) is located in the center of the Kowloon Peninsula of Hong Kong. It is an early developed area with high building density and narrow roads. Sham Shui Po is not close to the coastline and the terrain is rather flat. Most of the buildings in Sham Shui Po are around 10 storeys tall and are closely packed into regular building blocks. Shadows are formed in this district mainly by buildings.

3.4 Selection of images

In order to perform shadow enhancement, satellite images with high radiometric resolution are preferable (Arevalo et al., 2006). As the spectral signature under shadowed areas is usually narrower and darker than for non-shadow areas, more grey levels available can ensure that small differences between pixels' brightness can be recorded. If small variations in pixel brightness are ignored and represented by the same pixel values, only one single color tone can be obtained within the enhanced shadows and no details can be recovered.

Two Quickbird multispectral satellite images were used. One image covers the Kowloon Peninsula and northern Hong Kong Island and another covers the Ma On Shan area. Both images are of 2.4m resolution at the nadir and 11bit (0-2047) radiometric resolution saved as 16 bit image format so that details within shadowed areas can be preserved better.

A 0.6m panchromatic sharpened image was also available for the Kowloon and Hong Kong areas but not used. According to Chen et al. (2008), remote sensing image fusion is a tradeoff process and spatial visualization and spectral property cannot be improved and preserved at the same time. In order to avoid any information loss due to the image fusion process affecting the quality of the end product, the 2.4m Quickbird multispectral image is selected. Another reason for not using fused imagery is that the file size of each spectral band is large. Considering the processing time and storage space, using smaller files is more efficient.

3.5 Selection of algorithms for shadow detection

Shadow detecting can be divided into two types; one is based on shadow properties, while the other is based on models. Model based detection usually aims at applications that require high shadow detection accuracy. Digital Surface Model (DSM) and 3D building model are required to estimate the shadow areas. Considering that an accurate DSM was not available, and simple 3D models cannot adequately represent the complex shape of urban buildings, properties based detection was used.

For properties based shadow detection, different color spaces are used to distinguish target features. The performance of Color invariant index (C1C2C3) and Spectral Shape Index (SSI) were examined so that shadowed areas can be extracted based on the supervised classification technique. The most commonly used supervised classification technique, Maximum Likelihood, was selected for this task due to its algorithm simplicity and ease of application.

3.6 Selection of algorithms for shadow enhancement

There are three existing approaches for shadow enhancement (or restoration), namely, Gamma Correction, Histogram Matching and Linear Correlation Correction. After reviewing the effectiveness of the enhancement result, Histogram Matching will not be used in the study. Histogram Matching makes use of the same class of value to estimate the range and mean of shadowed pixel. Since land covers in Hong Kong are complex and mixed, it is difficult to decide which land covers should be involved and how to classify them effectively. From the visualization point of view, enhancement using Gamma Correction may not give natural color tone when compared with its neighbor pixels, but it is worth testing if it could be used in this study. Apart from these reasons, Linear Correlation Correction has been proved that it gives more reliable results (Sarabandi et al., 2004; Zheng & Wang, 2008). Shadowed pixels will be recalculated based on the linear regression model between shadowed and non-shadowed areas. As Quickbird imagery is used, 4 linear equations will be generated for all spectral bands. 17 pairs of sample areas with size 4x4 pixels covering a variety of shadowed and adjacent non-shadowed areas were selected from each case study area. The average pixel value from each pair of sampling area is used to establish both Gamma parameters and linear regression models for each spectral band. The average Gamma parameter estimated from the 17 sampling data is used to enhance the whole image. After the extracted shadows are enhanced, an image that contains shadows only is overlaid on the non-shadow image and the two parts are merged together into one completed shadow enhanced image. The enhancement quality by the two algorithms can then be compared.

3.7 Selection of algorithms for assessment

The spectral range of common land covers is used as an indicator to show if the enhanced areas were darker than non-shadowed areas. The histogram pattern of enhanced shadow areas was assessed and compared with its neighbor pixels. Similar to the approach in data sampling for model establishment, average pixel value was extracted from 17 pairs of sample areas with the size 4x4 pixels covering enhanced shadowed areas and adjacent non-shadowed areas. The differences between each pair of sampling areas are used to judge the enhancement quality. Vegetation index is used to examine whether the shadow enhancing process can improve the performance of using band ratio and this is also an indicator to check if shadow enhanced image is capable for further analysis.

3.8 Selection of software platforms

3.8.1 ER Mapper

ER Mapper mainly focuses on raster data image processing, with many built-in functions that help in image analysis. An advantage of using ER Mapper is that procedures of training data for classification are not complicated. Also, it allows a pixel to have a value of "NULL", which makes calculation easier and avoids misleading classification results. No matter how many spectral bands are involved, two files are used to store the information of one set of images. Image files can then be managed more efficiently. However, there are fewer functions for vector data modeling. For example, the overlay of boundary data (vector) onto the raster image and extract useful information cannot be done using ER Mapper.

3.8.2 IDRISI

IDRISI is a cheaper software and all-round more functional software compared to ER Mapper. There are many conversion functions for data transformation between different common file formats. It also provides built-in functions for image processing and raster vector conversion so that extraction of image values is possible. Both raster data and vector data can be used in spatial analysis.

An advantage of IDRISI is that image segmentation is available and there are many statistical analysis tools that can be chosen. Calculating band ratio in IDRISI is rather flexible. Spectral bands are stored individually so that mathematic and logical operators can be used. There are no limits to the number of bands used for calculation. Unlike ERMapper, "NULL" values cannot be set for a pixel; they may only be assigned a value of "0" which can sometimes produce misleading results. As spectral bands are stored individually, file management is sometimes not very convenient.

One of the problems of IDRISI is the registration points used to define the image coordinate system are different from ER Mapper. Therefore conversion between data formats may affect its georeference information. The resulting image will have incorrect coordinates which means it cannot be overlaid with other map data. However, ER Mapper can be used to alter/modify its georeference information by correcting the registration points' coordinates.

3.8.3 ArcMap

As different remote sensing software is involved for image processing, ArcMap is used to display satellite images in order to ensure the georeferencing is correct. It has been found that the georeference of the satellite image will have problems during format conversion from IDRISI to ERMapper, due to the difference in coordinate system origin of software used. When two layers cannot be directly overlaid, each spectral layer cannot be stacked and form a RGB image. Therefore, it is necessary to correct the georeference information of the .ERS file.

Chapter 4. Comparative analysis of shadow enhancement processes

4.1 Comparative analysis of shadow detection algorithms

4.1.1 Results by color invariant index C3 and Spectral Shape Index (SSI)

Both color invariant index layer C3 and Spectral Shape Index were applied in order to examine which one produces the better shadow extraction result. Figure 4-1 presents the C3 image of Central area and figure 4-2 refers to the Spectral Shape Index. In Figure 4-1, light blue refers to shadows; dark blue represents non-shadows while orange is water feature. In Figure 4-2, yellow refers to shadows; blue represents non-shadows while orange is water.

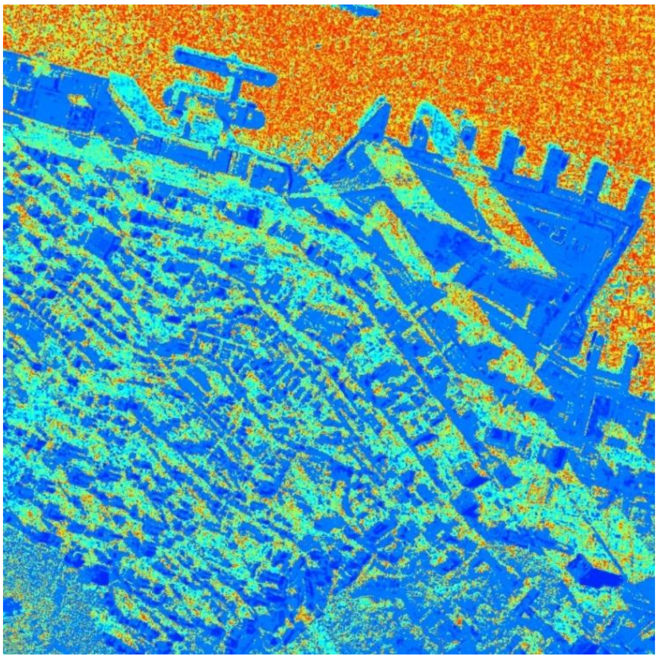

Figure 4-1 Color invariant index (C3) of Central

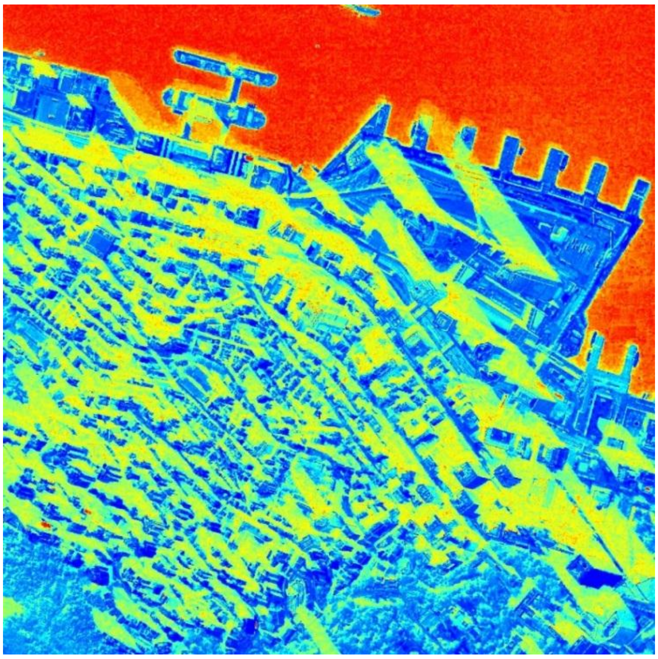

Figure 4-2 Spectral Shape Index of Central

After comparing the two images created, it can be seen that C3 layer is quite noisy and some of the shadows have similar values as water features. From figure 4-2, it can be seen that the shadows, non-shadows and water features are more uniform than the C3 image. The SSI image is also smoother. The image histograms (figure 4-3) illustrate the difference in performance between the two methods. They show that the SSI image has much clearer peaks than that of color invariant index C3 layer. This also indicates the ease SSI provides when classifying images. Water features will have a larger value while non-shadow land features will be lowest and shadows are in between.

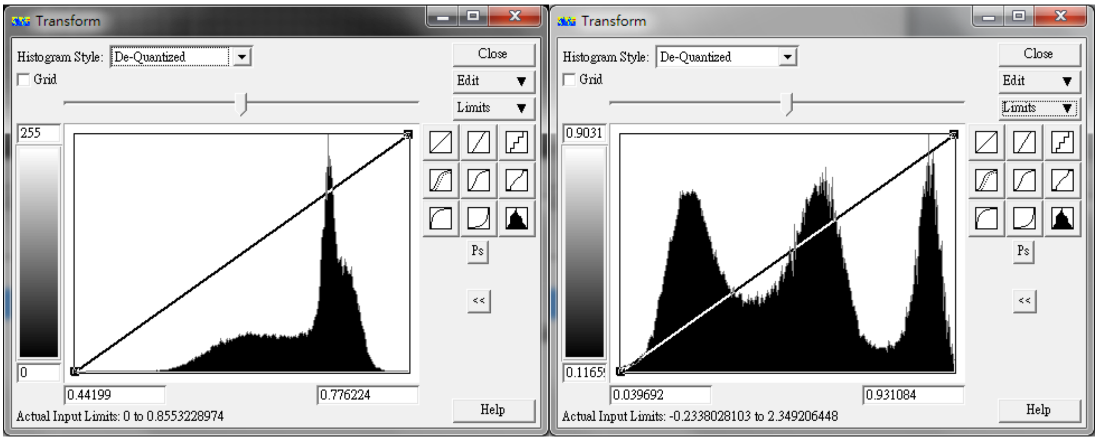

Figure 4-3 Histogram of C3 layer (left) and Spectral Shape Index (right)

Although the color invariant index layer C3 has been recommended for shadow detection after applying low pass filter to smooth the noise, the differences between features are not clear when compared to the resulting image produced by the Spectral Shape Index. Three classes are created as supervised classification training datasets. They are “water”, “shadow” and “non-shadow” (“non-shadow” refers to neither water nor shadow). Supervised classification result of the C3 layer (figure 4-4) shows that some of the shadows are wrongly classified as water, while some of the water features are classified as shadows. Since only three classes were used in the supervised classification process, it may require more classes if color invariant index C3 is being used.

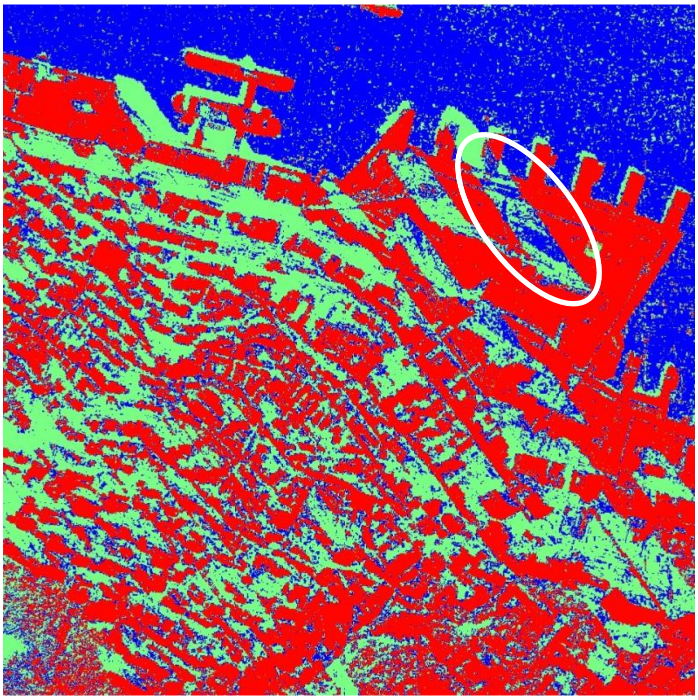

Figure 4-4 Supervised classification result of C3 layer (blue: water; red: non-shadows; green: shadows)

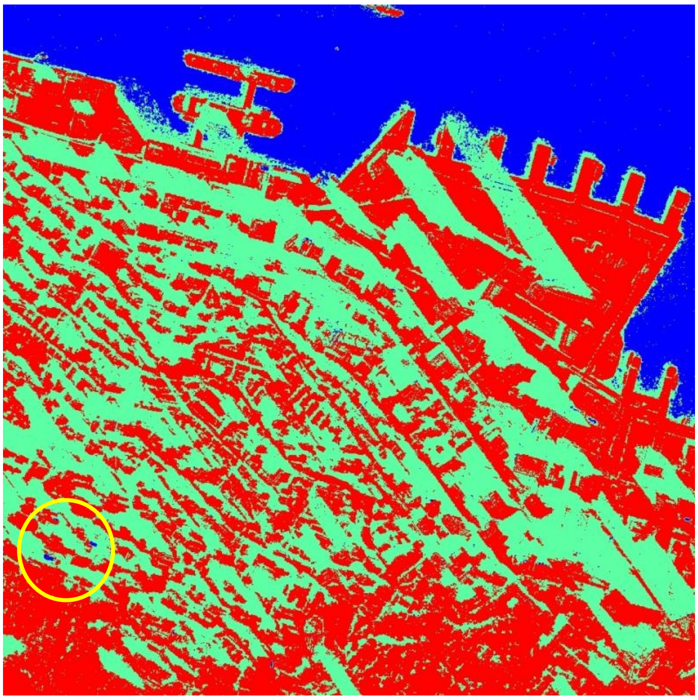

Figure 4-5 Supervised classification result of Spectral Shape Index (blue: water; red: non-shadows; green: shadows)

In comparison, the result generated by the Spectral Shape Index (figure 4-5), water surfaces are extracted with less omission error, except for those shadows that fall onto the water surfaces. It is also observed that even water features such as swimming pools (appearing in blue within the yellow circle in figure 4-5) can be identified using the Spectral Shape Index. Most of the noise in the image is on the water surfaces, especially when shadows fall onto it. Based on these results, the color invariant index layer C3 is not used for the other two study areas. Only Spectral Shape Index is applied to create the shadow mask for the later shadow enhancement procedure.

4.1.2 Shadow detection results of each study area

Supervised classification was done on the Spectral Shape Index image. Class “shadow” was used to create the shadow mask while both “water” and “non-shadow” class were treated as non-shadow regions. For shadows that fall onto water surface, most of them are classified as shadow. The shadow mask was created for extracting shadowed regions so that these regions could be enhanced, while the pixel values of non-shadowed regions remain unchanged. The shadow masks created for each study area are presented in figure 4-6, 4-7 and 4-12 for the Central, Ma On Shan and Sham Shui Po study areas respectively.

Central

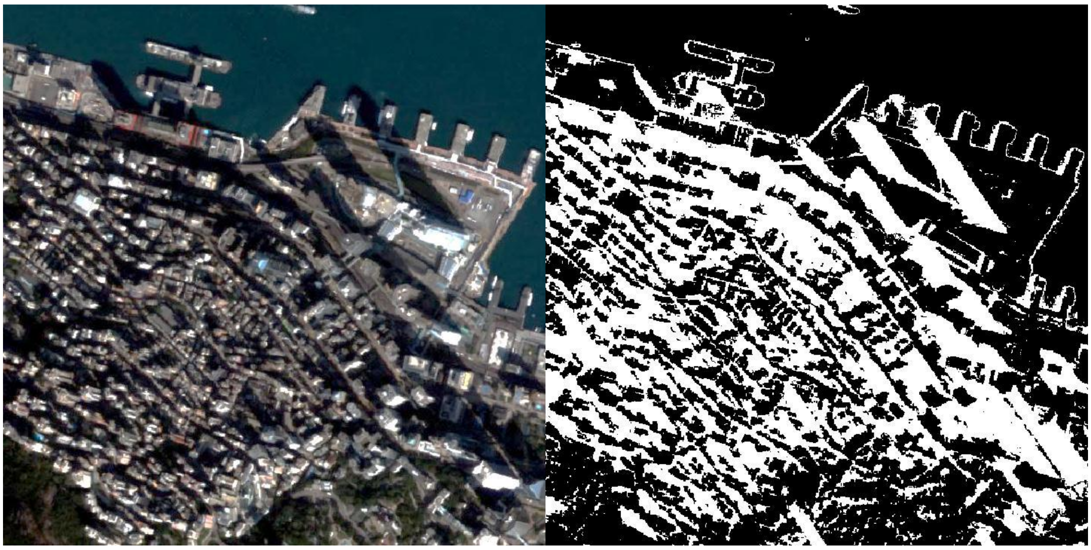

Figure 4-6 Original image and shadow mask of Central (shadows are white in the mask image)

In figure 4-6, it can be seen that a large amount of shadows are caused by buildings within Central area and almost 50% of the areas is under shadow. For misclassification, not all the shadows that fall onto water surfaces can be extracted. It appears to be quite noisy for those areas. If the surfaces are naturally dark like those made of asphalts (roof surfaces), the Spectral Shape Index is not able to identify all of them correctly. It is also found that the edges of the coastline are classified as shadows, which are not easy to be justified using bare eyes. This is due to the fact that maximum likelihood decision rule is based on the probability that a pixel belongs to a particular class under the assumption that these probabilities are equal for all classes (Myint et al., 2011). Average pixel values obtained from the training dataset are used to judge whether a pixel should be assigned to a particular class. As it concerns how to classify a pixel, the spatial autocorrelation of nearby pixels is ignored.

Ma On Shan

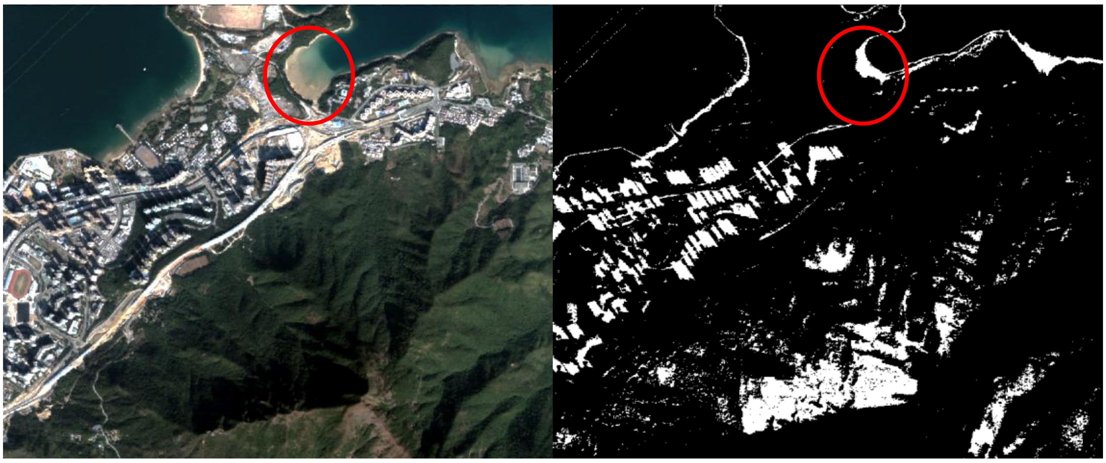

Figure 4-7 Original image and shadow mask of Ma On Shan

For Ma On Shan, shadows formed by mountainous areas and buildings are extracted. However, the natural coast areas are being misclassified as shadows. These areas are in fact shallow water (shown in figure 4-7). The shadow detection results show that the Spectral Shape Index algorithm is not able to identify shallow water from sandy seabed. These misclassified shadows can also be seen in the histogram (figure 4-8); it is observed that, unlike the Central study area, there is no sharp peak between water features and non-shadow land features. Figure 4-99 andFigure 4-1010 show an enlarged view of the Ma On Shan image and its corresponding Spectral Shape Index image. It is noticed that the algorithm applied for shadow detection is able to identify water features like the swimming pool circled and most of the sea surfaces, but is not able to deal with shallow water surfaces. Salt water with a sandy bottom (0.5m depth) will have a higher reflectance than deep water (2m depth); the sandy background will dominate most of the spectral properties of the water surface (YCEO, 2012). When the SSI equation [Green-Red] ÷ [Red+NIR] is used, water surface (deep) has larger pixel values in the Green band and lower pixel values in Red and NIR will result in higher SSI value. However, the pixel values of sandy background water are increased in all 3 bands (sharp increase for green band) so the numerator will decrease while the denominator will increase. The SSI obtained will be much lower than that of deep water surface.

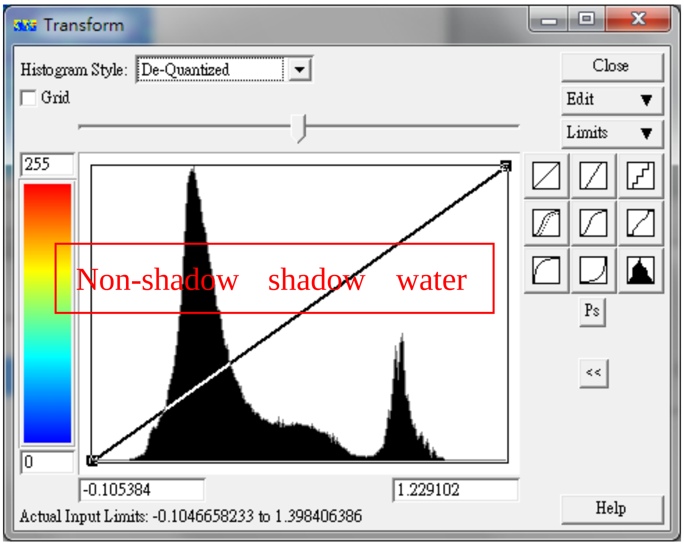

Figure 4-8 Image histogram of Ma On Shan Spectral Shape Index image

Figure 4-9 Enlargement of Ma On Shan

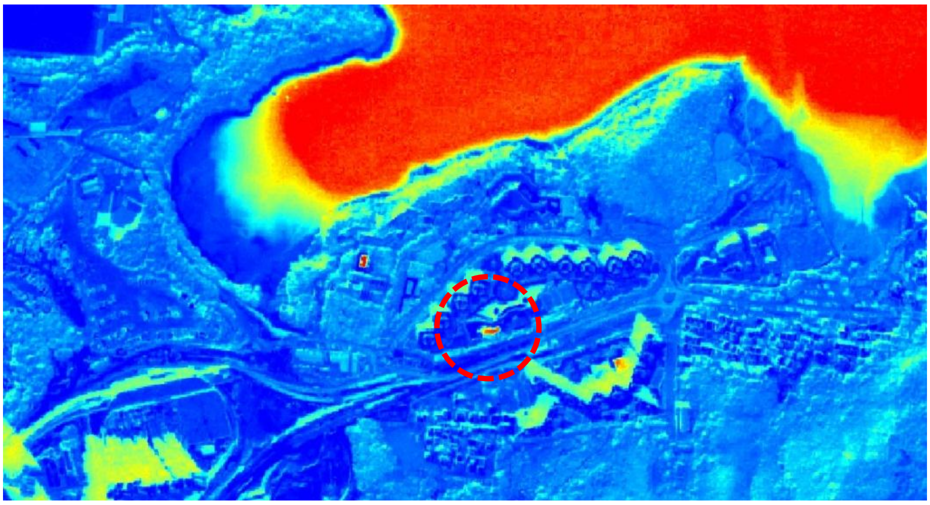

Figure 4-10 Enlargement of Spectral Shape Index image of Ma On Shan

Sham Shui Po

Compared to the previous two districts, this selected part of Sham Shui Po does not have significant water features and shadows are mainly formed by buildings. The absence of water features can also be supported by the image histogram (figure 4-11) which shows there are two sharp peaks which correspond to shadow and non-shadow classes. For the size of shadows, except for one large shadow in the lower left corner, all are small in size. The shadow extraction result is as shown in figure 4-12.

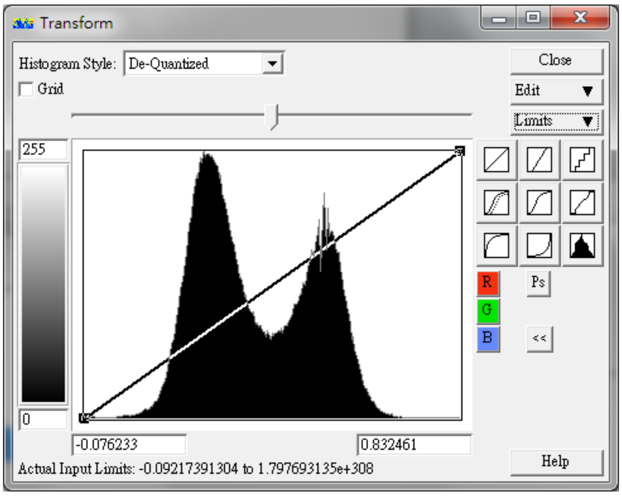

Figure 4-11 Image histogram of Sham Shui Po Spectral Shape Index image

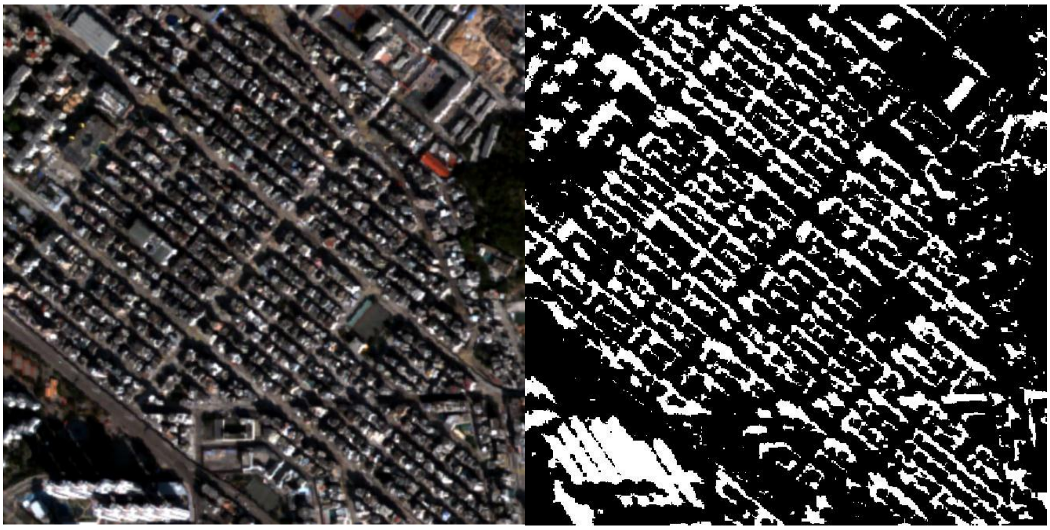

Figure 4-12 Original image and shadow mask of Sham Shui Po

4.2 Comparative analysis of shadow enhancement algorithms

4.2.1 Gamma correction

4.2.1.1 Gamma value estimation

For Gamma correction, a number of area pairs are randomly selected in each study area and their average pixel values in each spectral band are recorded. Each pair consists of a 4 pixel by 4 pixel (around 10m by 10m on ground) square of shadowed area and adjacent non-shadowed area. The Gamma equation (eq. 2) was used and is listed as below:

$$DN_{output} = 2047 \times \left(DN_{input} \div 2047\right)^{\frac{1}{\gamma}} \quad (2)$$

DN_{output} refers to the pixel values of non-shadow regions, while DN_{input} is the pixel values of shadow regions having the same surface material. When the average pixel values are recorded, the value of Gamma (γ) is able to be calculated using simple logarithm function. Each average pixel value is calculated from 16 pixels in order to minimize the effect of extreme pixel values of noise. With a fixed sampling size of 4 pixel by 4 pixel, the number of sampling data is limited under such a high building density area. For example, the distance between two shadows is too close and adjacent non-shadowed regions are small for data sampling. Some shadows are large and fall across side of buildings so it is not easy to confirm the adjacent non-shadowed regions are of the same surface type. A minimum of 16 sampling pairs are made when the surface type can be identified in both shadowed and adjacent non-shadowed area.

Table 4-1 Overall Gamma value estimation result of Central

Central	Gamma Min	Gamma Max	Average Gamma value	Standard deviation
Blue	1.046	1.587	1.201	0.152
Green	1.112	2.396	1.402	0.326
Red	1.166	2.472	1.433	0.326
NIR	0.915	2.987	1.573	1.463

Table 4-2 Overall Gamma value estimation result of Ma On Shan

Ma On Shan	Gamma Min	Gamma Max	Average Gamma value	Standard deviation
Blue	1.015	1.480	1.170	0.139
Green	1.044	2.045	1.357	0.295
Red	1.064	2.049	1.439	0.296
NIR	1.095	2.237	1.680	0.283

Table 4-3 Overall Gamma value estimation result of Sham Shui Po

Sham Shui Po	Gamma Min	Gamma Max	Average Gamma value	Standard deviation
Blue	1.096	1.225	1.163	0.034
Green	1.197	1.472	1.326	0.072
Red	1.214	1.579	1.398	0.113
NIR	1.351	1.715	1.553	0.089

For Central, a total of 16 pairs of sampling area and thus 16 Gamma values are calculated for each spectral band. The number of sampling data for Ma On Shan and Sham Shui Po is 18 and 17 respectively and the overall Gamma value estimations are presented in table 4-1 to table 4-3.

As the Gamma values are estimated using different surface materials randomly selected, it is difficult to choose a single Gamma measurement representing the whole spectral band. From the above tables, it can be seen that the range of Gamma values in some of the spectral bands are large. Most of the standard deviations are small except the NIR band in Central. This is because the average shadow pixel value is larger than the average non-shadow pixel value and the Gamma value calculated is less than 1. Z-test was used to detect outliers and it was found that only Gamma values computed from extreme bright surface in Central were classified as outliers (Gamma values were almost twice as much as the average value in one set of sampling data). These surfaces are highly reflective and the pixel values recorded are abnormally high compared to the rest of the sampling data. Although the Gamma values estimated were large, they were real data from the complex environments in Central and were not omitted.

It is possible to further sub-divide the study areas into smaller regions so as to compute the Gamma parameters more accurately for that specific area, but the problems of different land covers within shadows cannot be solved. It resulted in the fact that one Gamma value is being applied to all land covers within a small region and the shadow enhancement result may vary a lot. Some previous studies suggested that the image can be classified according to the surface types and one Gamma value is used for each land cover. However, in a complex environment (like Hong Kong), this will involve classifying shadowed regions before they are enhanced. Considering the complexity of sub-dividing the study area and the possibility of classifying shadows, the average Gamma value of each spectral band will be used for enhancing shadow regions.

4.2.1.2 Results by Gamma Correction

Since the average Gamma values are used, it is expected that the shadow enhancement results will not be satisfactory for some regions. However, the resulting image is able to show whether Gamma correction can be applied with high complexity land covers. The shadow enhancement results are presented below:

Central

Upon comparing the image enhanced by Gamma Correction (figure 4-13) and the original Central image (figure 3-5), it is clear that the visual improvement is not significant. From figure 4-13, it is found that all the shadows are much brighter than the original dark pixels. However the color tone is not natural and appears to be hazy compared to its surrounding. Details within shadows cannot be seen after enhancement. A zoomed in view of Central image is presented in figure 4-14, with the original portion on the left.

Figure 4-13 Shadow enhancement by Gamma correction – Central

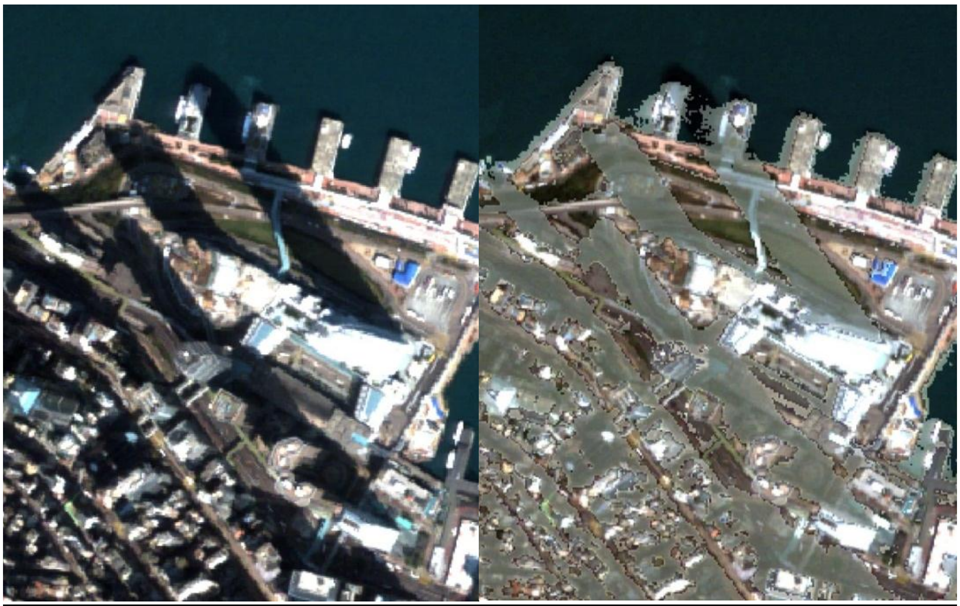

Figure 4-14 Enlargement view of part of the Central by Gamma Correction

Ma On Shan and Sham Shui Po

Figure 4-15 Shadow enhancement by Gamma correction - Ma On Shan

Similar to Central, the shadow enhanced regions of both Ma On Shan (figure 4-15) and Sham Shui Po (figure 4-16) appeared grey and hazy. The color tone of the enhanced areas is not natural compared to its neighbor. No matter which land cover it is, the enhanced regions looks similar and is like replacing the dark pixels with brighter grey pixels. For Gamma Correction, it is expected that the grey level of the enhanced regions is uniformly increased. Previous studies also pointed out that this uniform grey level will lead to larger color differences between enhanced regions and adjacent non-shadowed regions with different surface type.

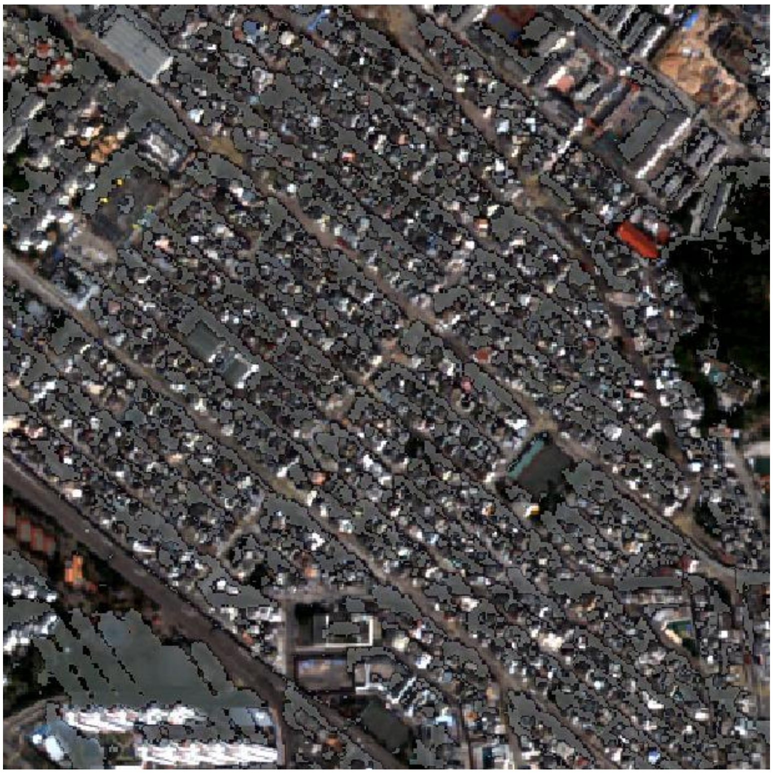

Figure 4-16 Shadow enhancement by Gamma correction - Sham Shui Po

4.2.2 Linear Correlation Correction

4.2.2.1 Establish linear regression model

Unlike the Gamma correction where only one Gamma value is applied to the whole image, Linear Correlation Correction made use of all the area pairs to generate the regression model. For example, 16 shadow and non-shadow pairs in Central (the same data as in Gamma correction) are used to form the linear regression model for each of the 4 bands – one each for the Red, Green, Blue and Near-Infrared band respectively. The linear regression models (where x is the DN of shadows and y is the DN of non-shadows) and their corresponding correlation coefficients are presented as follows (All relevant graphs are presented in Appendix B):

Table 4-4 Linear regression model of Central (16 pairs of sampling data)

Central	Regression model by 16 data pairs	Correlation coefficient
Blue	$y = 3.624x - 497.13$	0.947
Green	$y = 4.445x - 727.62$	0.943
Red	$y = 5.672x - 442.62$	0.933
NIR	$y = 7.552x - 525.31$	0.950

Table 4-5 Linear regression model of Ma On Shan (18 pairs of sampling data)

Ma On Shan	Regression model by 18 data pairs	Correlation coefficient
Blue	$y = 3.396x - 426.79$	0.981
Green	$y = 4.144x - 600.49$	0.975
Red	$y = 5.404x - 372.94$	0.958
NIR	$y = 7.765x - 489.00$	0.913

Table 4-6 Linear regression model of Sham Shui Po (17 pairs of sampling data)

Sham Shui Po	Regression model by 17 data pairs	Correlation coefficient
Blue	$y = 2.795x - 317.17$	0.881
Green	$y = 3.463x - 484.84$	0.850
Red	$y = 5.37x - 443.57$	0.905
NIR	$y = 4.179x - 175.67$	0.888

All the linear regression models were locally derived, and it could be seen that the equation of the same spectral band (e.g. equations of all NIR band) appeared to be different. It is not suitable to use one set of global formulas for all study areas due to the fact that the urban environments vary from location to location. Although there is a strong correlation between shadow and non-shadow pairs, there are some problems associated with these regression models such as the penumbra regions and they will be discussed in section 4.2.3 and 4.2.4.

4.2.2.2 Results by Linear Correlation Correction

Two mask images are created for each study area, shadow mask and non-shadow mask. The regression models are applied to the image that only contains shadowed regions. After enhancing the shadowed regions in each spectral band, a simple image overlay is performed in order to merge the enhanced regions with the non-shadowed regions. The shadow enhancement results are shown below:

<u>Central</u>

Figure 4-17 (the enhancement results of Central) shows that the visual improvement is more significant compared to the one by Gamma correction. Part of the details under shadows can be seen after the enhancement process. The red circle in figure 4-17 is an example of successful shadow enhancement (zoomed in view in figure 4-18). Vegetation has similar color tone compared to its neighbor. Although the color of a flyover nearby is slightly darker after enhancement, it is much better compared to the original image. The yellow circle in figure 4-17 shows one of the regions that is still dark even after enhancement was performed. This indicates that the linear regression model used is not able to enhance this and similar regions correctly.

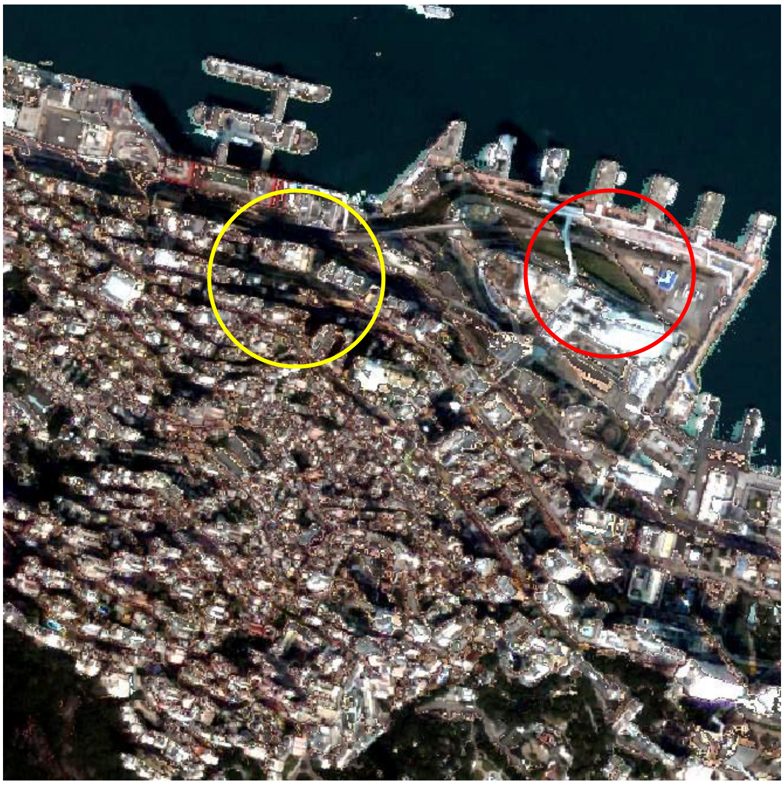

Figure 4-17 Shadow enhancement by Linear Correlation Correction – Central

Figure 4-18 Enlargement view of linear enhanced Central image

In order to explain why the enhancement results have such a big difference, the building structures of the two circled regions are compared. Central is the main CBD of Hong Kong. Here buildings are tall and the distances between buildings are small, which results in a special form of building structure – walled buildings. It refers to buildings that are constructed like a wall, which block the view of other buildings, block the sunlight penetrating through gaps between buildings and block air ventilation channels. In this case, the presence of walled buildings block all the sun energy penetrating between buildings and no other surfaces can reflect sun energy to these shadows. In the open space within the red circle, no buildings block the direction of sun light (bottom right), making the shadows within less dense than those in the yellow circle area. The difference in enhancement of the two areas, despite being within a short distance of each other, implies that using one set of regression model may not be able to enhance all the regions properly, giving rise to the idea of using locally derived regression models in different areas. The issue of when and how different regression models should be applied then comes up. The use of different regression models and its results will be discussed in chapter 5.

Ma On Shan

Figure 4-19 Shadow enhancement by Linear correlation correction - Ma On Shan

For Ma On Shan, except for the natural coast areas being wrongly extracted and enhanced, most of the shadows are natural to its surrounding. After enhancement, road features can be viewed as one object, not broken into several segments by shadows. Compared to the enhancement results by Gamma correction, shadows enhanced by Linear Correlation Correction are more similar to their surroundings demonstrated by significant visual improvement. Because of the lower building height and density compared to Central, one set of regression models is able to give promising results.

Sham Shui Po

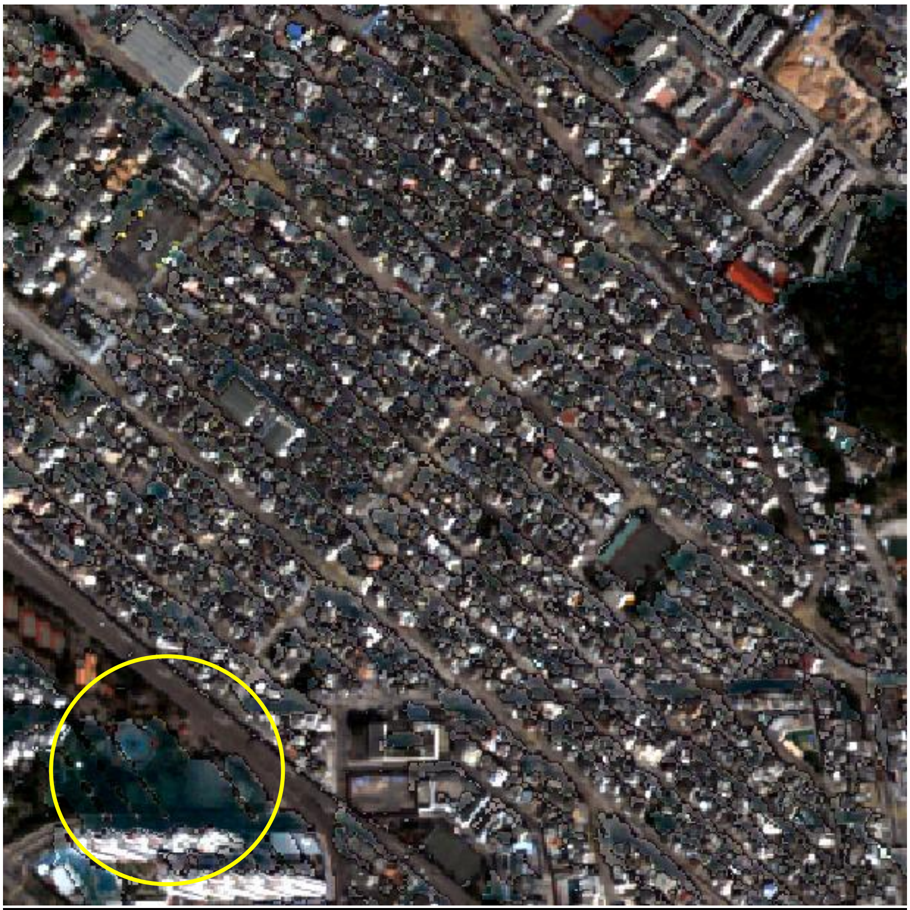

Figure 4-20 Shadow enhancement by Linear Correlation Correction - Sham Shui Po

Sham Shui Po has high building density and shadows are formed between buildings. This is similar to the condition in Central, but the buildings are much lower, meaning that the shadows mostly fall across roads and very few fall across mixed surfaces. Therefore, the regression models are mainly generated from asphalt surface pairs. Very few vegetated pairs can be found and, therefore, the enhancement of such areas as shown for a park area (yellow circle in figure 4-20) appears significantly different to its surroundings. The result also shows that when sun energy is blocked by walled-buildings, shadows are not likely to be enhanced successfully. However, the enhanced shadows in yellow circle show some more details and higher contrast. It is considered that these areas could be further enhanced by establishing another set of regression models.

4.2.3 Penumbra enhancement

Enhancement of the penumbra regions produced variable results. Across the three study areas it was seen the penumbra were not easily detected by the shadow detection algorithm. In the Central image (figure 4-18), some of these edges were extracted and enhanced, with the result that the enhanced edges were brighter than both non-shadow regions and enhanced shadow regions. Prior to enhancement the penumbra was not obvious. When they are extracted, the linear regression model will make these edges brighter due to the fact that penumbra regions are not as dark as shadows. When they cannot be extracted during shadow detection, it remains dark compared to the enhanced regions. The amount and appearance of penumbra will strongly be affected by the urban structure and lighting condition. If low pass filter is applied, some of the details may be lost after processing. It is suggested that specific smoothing filter is applied to the edges in order to lower the difference in between, because either extracting penumbra or enhancing the edges separately have not been well developed yet.

4.2.4 Problems of using Linear Correlation Correction

Although the enhancement by Linear Correlation Correction gave better visual improvement, some problems were found afterwards. Apart from the penumbra effect, it was observed that some of the pixels are not being enhanced when the regression model is applied. This problem is found mostly in the red and near infrared bands. Pixel values are lowered after enhancement was done. Both Central and Ma On Shan encountered this problem. Take Central as an example, one of the darkest shadowed pixels is located on a road surface and has the pixel value 53 in the infrared band. When the value 53 is substituted into the equation listed in table 4-4, which is $7.552 \times (53) - 525.31$, the result will be -125.054. For some other bright surfaces under shadows, the pixel values after enhancement (figure 4-21) will exceed 2047, which is the maximum value with an 11-bit image. Even when extreme pixel values are involved during sampling process, averaging 16 pixel values and fitting it into a linear regression model will lower such a large difference. There is no doubt that more pixels involved in sampling process will reduce the effect of extreme pixel brightness, but balancing the number of pixels, a specific surface type can be recognized and the number of sampling data, 16 pixels (10m by 10m ground resolution) is considered to be an optimum sampling size. This out-of-range circumstance is found in the red and near infrared band of both Central and Ma On Shan image. If the scale of each spectral band is not the same, it would have problems when calculating band ratios such as vegetation index. Therefore, it is necessary to keep the pixel values of all spectral bands within the 0-2047 level.

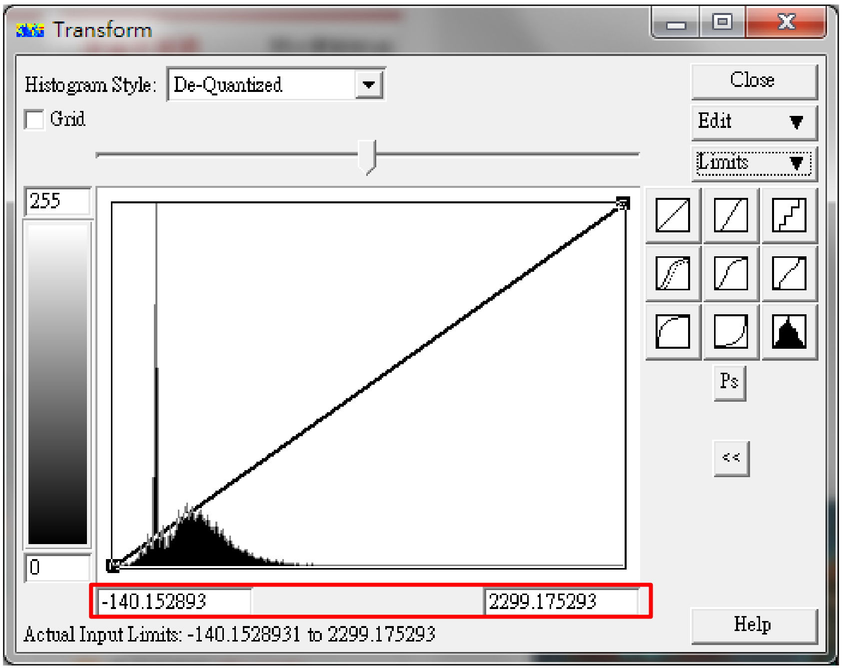

Figure 4-21 Histogram of NIR after Linear Correlation Correction

The first attempt to deal with this issue is to set cut off values. If any pixel values exceed the boundary of 0-2047, either 0 or 2047 is assigned to that pixel depending on whether it is smaller than 0 or larger than 2047. However, the enhanced pixel values are of relative sense, and it is not likely to obtain pixel values 0 or 2047 within a normal image. This is the simplest way to deal with this situation, but there are certain drawbacks. If the pixel values are lower than 0, setting it as 0 means that pixel values are not being enhanced. A pixel having value 53 may become 0 in this case, which is not increased. Using 0 as a cut off value will also result in inaccurate band ratios calculations. For example, vegetation index NDVI will have extreme negative or positive values which are not within the range -1 to +1.

The second attempt is to reconstruct the pixel values range (-140 to 2299 as shown in figure 4-21) by keeping their relative difference. This is done by first getting the range information of this raster dataset, then computing the percentage for each pixel values and finally multiplying by 2047. For example, if the lowest pixel value is -140, the minimum pixel value “-140” is subtracted, then divide by 2439 (range of this dataset) and then multiplied by 2047. The output value will become 0. Although the relative difference between each pixel value is maintained, the pixel values that originally satisfy the linear regression model are altered. When the pixel values of these shadow enhanced regions are compared with their surrounding non-shadow areas, the difference in between will be enlarged. The effect of Linear Correlation Correction is thus being cancelled out.

The third attempt is to use the original shadowed pixel values to replace the enhanced results under the condition that the pixel value after enhancement is lower than the original one. For pixel values that exceed the number 2047, the maximum pixel values from the original unprocessed image are used to replace the enhanced results. This method can ensure that all the pixel values after enhancement are within the range 0-2047, and most of the results being linearly enhanced are maintained. However, replacing original pixel values with the enhancement pixels will result in these pixels not being enhanced at all. When they are used for further image interpretation like the making of vegetation index map, these regions may not have any changes compared to the original image.

4.3 Assessment of enhancement results

4.3.1 Comparison of the enhancement results

After the enhancement process, the pixel values from the original image, Gamma correction and Linear Correlation Correction were compared. Similar to the process of establishing linear correlation model and computing Gamma parameters, a number of areas pairs (4 pixels by 4 pixels) for both non-shadows and enhanced shadows were randomly selected for comparison. Each pair of areas is of the same type of surface based on the users' judgments and interpretations and was not used in the enhancement process. The means and standard deviations of the pixel value differences (enhanced shadow minus non-shadow) for each image band was computed for assessing the spread of the difference among each enhancement algorithm. The results are presented in Table 4-7 to 4-9.

Table 4-7 Statistics before and after enhancement - Central

Central	Mean of the pixel value difference			Standard Deviation of the difference		
	Original	Gamma correction	Linear regression	Original	Gamma correction (% change from Original)	Linear regression
Blue	-70	-3	-14	31.70	28.53 (10%)	31.39 (1%)
Green	-151	-4	-28	66.94	60.75 (9%)	54.04 (19%)
Red	-144	-15	-41	67.60	58.52 (13%)	50.62 (25%)
NIR	-227	-32	-125	97.48	85.87 (12%)	80.04 (18%)

Table 4-8 Statistics before and after enhancement - Ma On Shan

MOS	Mean of the pixel value difference			Standard Deviation of the difference		
	Original	Gamma correction	Linear regression	Original	Gamma correction (% change from Original)	Linear regression
Blue	-78	4	-2	73.24	67.91 (7%)	21.58 (71%)
Green	-166	14	-11	141.99	130.40 (8%)	37.28 (74%)
Red	-157	4	-15	123.51	106.82 (14%)	34.56 (72%)
NIR	-252	-10	-36	97.61	84.58 (13%)	58.16 (40%)

Table 4-9 Statistics before and after enhancement - Sham Shui Po

SSP	Mean of the pixel value difference			Standard Deviation of the difference		
	Original	Gamma correction	Linear regression	Original	Gamma correction (% change from Original)	Linear regression
Blue	-68	13	20	32.46	29.90 (8%)	19.87 (39%)
Green	-141	32	38	68.73	64.04 (7%)	50.72 (26%)
Red	-143	15	14	53.24	44.74 (16%)	41.96 (21%)
NIR	-195	9	-9	52.49	46.69 (11%)	41.10 (22%)

For an ideal situation, the mean of the difference would be 0 after shadow enhancement algorithm is applied. As expected, the mean of the difference for the original shadows is large and this can be seen in the tables corresponding to Central, Ma On Shan and Sham Shui Po respectively. Also, a larger standard deviation of the difference between original shadows and their neighboring non-shadows is observed. The standard deviation is lowered after enhancement. This larger standard deviation is also expected when shadows are formed under different illumination conditions. The contrast between shadows and non-shadows can have large variations. For example, the shadows formed under walled-buildings in Central have higher contrasts with their surroundings. This makes the standard deviation of the differences larger.

From the enhancement results shown in the above tables the mean values for Gamma Correction is lower than Linear Correlation Correction and closer to zero. However, this is due to the fact that the variation is quite large in the difference. There are extreme values within; therefore the mean values may not be a good indicator to judge the quality of enhancement. For example, two extreme values are obtained in the green band dataset of Central by Gamma correction; one is 90.44 while the other one is -156.4. It could also be seen that there is no pattern observed for the mean values among all the spectral bands and study areas.

Under this circumstance, standard deviation is used to examine the spread of the difference. For an ideal enhancement result, the pixel value differences should be small and close to zero and thus resulting in smaller standard deviation. Table 4-7 to 4-9 show that the standard deviation decreases when enhancement was done. This can be explained by the extremely dark pixels under walled-buildings; the difference after enhancement is still large compared to other testing areas. For Gamma Correction, the standard deviation of difference is slightly lower than that of the original shadows while Linear Correlation Correction gives much lower standard deviations. Comparing the results in Central and Sham Shui Po which contains high building density, the standard deviation is only slightly lowered. However, in Ma On Shan which is of lower building density, there is a large decrease in standard deviation when Linear Correlation Correction is applied. However, the large difference observed in Ma On Shan could be also due to the fact that it is from a different set of image, but the performance of Gamma Correction and Linear Correlation Correction can also be seen and compared.

Table 4-10 Standard deviation of all pixel values in the sampling data in Central

Central	Standard Deviation			
	Non-shadow	shadow	Gamma enhanced	Linear enhanced
Blue	51.95	21.62	24.80	78.33
Green	95.85	30.86	37.63	137.18
Red	85.43	20.20	30.55	114.55
NIR	111.45	18.03	33.97	133.11

Table 4-11 Standard deviation of all pixel values in the sampling data in Ma On Shan

MOS	Standard Deviation			
	Non-shadow	shadow	Gamma enhanced	Linear enhanced
Blue	101.46	29.16	34.30	99.01
Green	185.17	44.33	55.88	183.72
Red	150.06	27.63	44.50	149.30
NIR	111.66	16.18	32.02	125.62

Table 4-12 Standard deviation of all pixel values in the sampling data in Sham Shui Po

SSP	Standard Deviation			
	Non-shadow	shadow	Gamma enhanced	Linear enhanced
Blue	47.02	16.96	19.89	47.38
Green	88.22	25.33	31.68	87.73
Red	68.32	17.28	27.24	92.79
NIR	61.01	12.37	22.43	51.69

In fact, it is possible that the smaller standard deviation of differences between shadowed pixels and non-shadowed pixels is due to a brightness shift. Therefore, the standard deviations of the sampling data are used for further support. In table 4-10 to 4-12, comparing the spread of data between non-shadowed regions and shadowed regions, the standard deviation of linear enhanced regions is more similar to the non-shadowed regions. These tables show that Linear Correlation Correction is more capable than Gamma Correction to reproduce the spread of pixel values within shadowed regions.

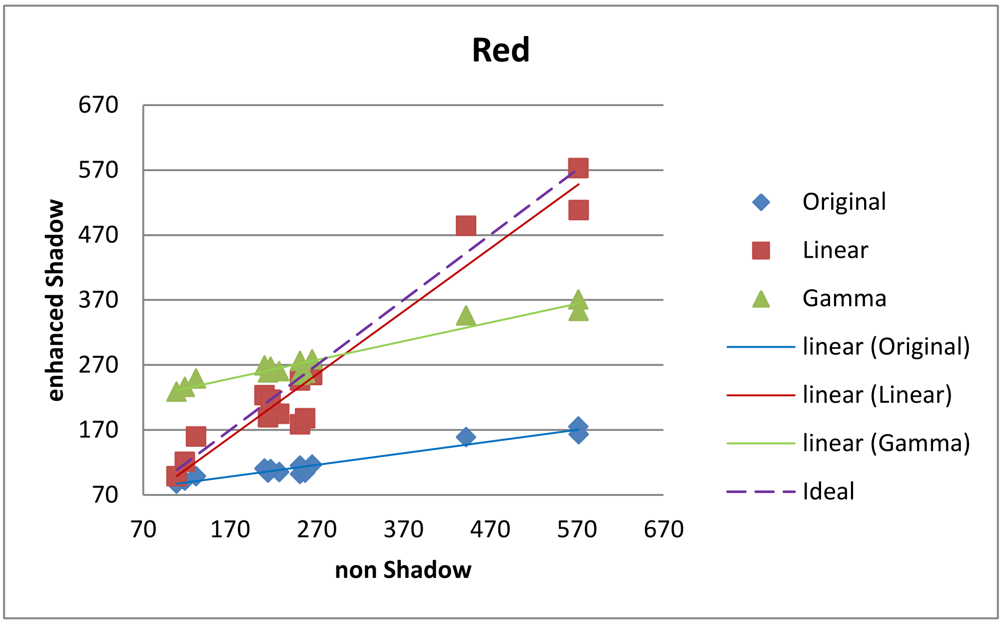

Figure 4-22 Relationship between enhanced shadows and non-shadows - Ma On Shan (Red)

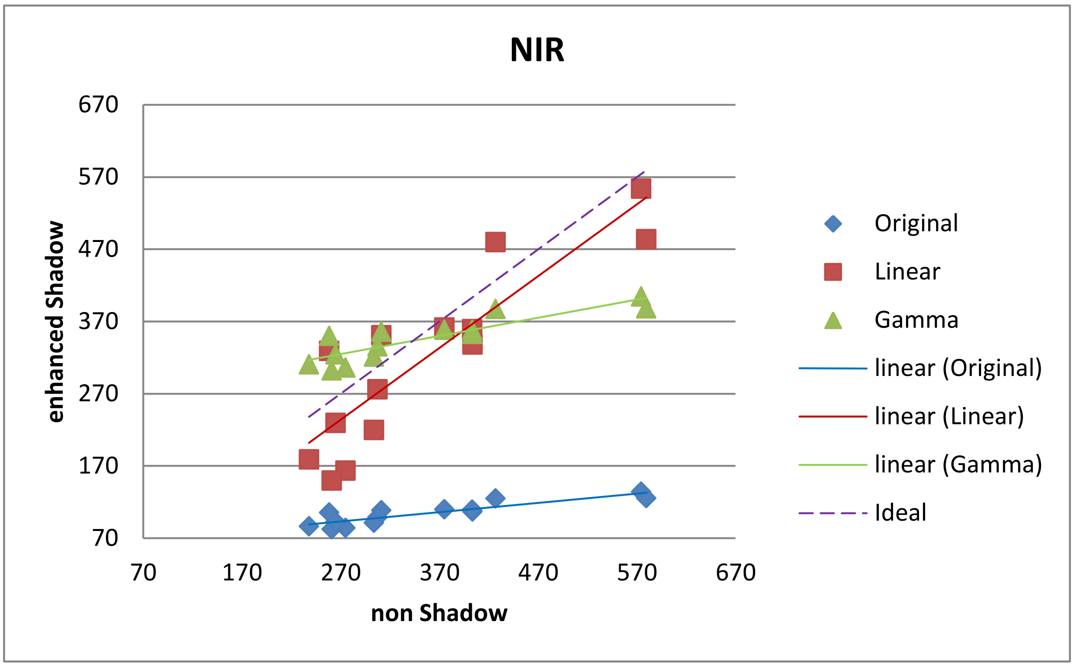

Figure 4-23 Relationship between enhanced shadows and non-shadows - Ma On Shan (NIR)

For an ideal situation, the enhanced results should be close to its surrounding. Figure 4-22 and 4-23 show the graphs of the two selected bands, red and near-infrared, from Ma On Shan. It is observed that the regression line by Linear Correlation Correction is the closest to the ideal situation while the one by Gamma Correction is nearly parallel to the original one. These graphs show that the large variation of difference in Gamma Correction, which can also be seen visually from the enhancement result, is not satisfactory. The graphs for all three study areas are listed in Appendix C.

The problems of Linear Correlation Correction with respect to the darkest group of pixel values being reduced rather than enhanced have been discussed in the previous section. It can also be shown in the above two figures. From the graph, it is expected that the regression line of the original shadows and the linear enhanced shadow will have an intersection when the original pixel values are small. Even if the darkest pixel is involved in the sampling process, averaging 16 pixel values will reduce its effect in the dataset. In fact, both blue band and green band have similar graph behavior (figures 4-24 and 4-25). However, the darkest pixel value will not be lower than the original data after enhancement. Although the behavior of Linear Correlation Correction is closer to the ideal case, it is also observed that the pixel values are generally lower than that of the surrounding environment (regression line of Linear Correlation Correction is beneath the ideal case).

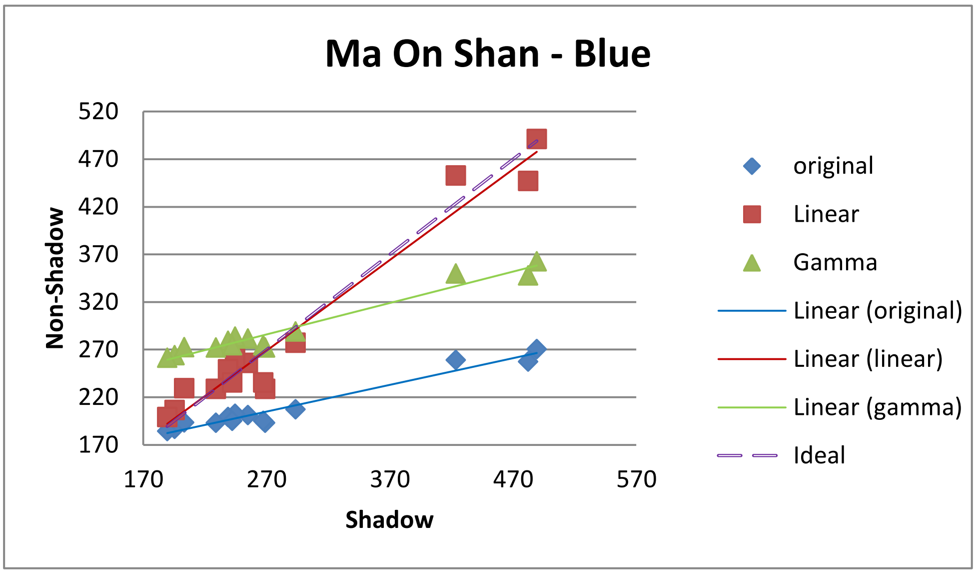

Figure 4-24 Relationship between enhanced shadows and non-shadows - Ma On Shan (Blue)

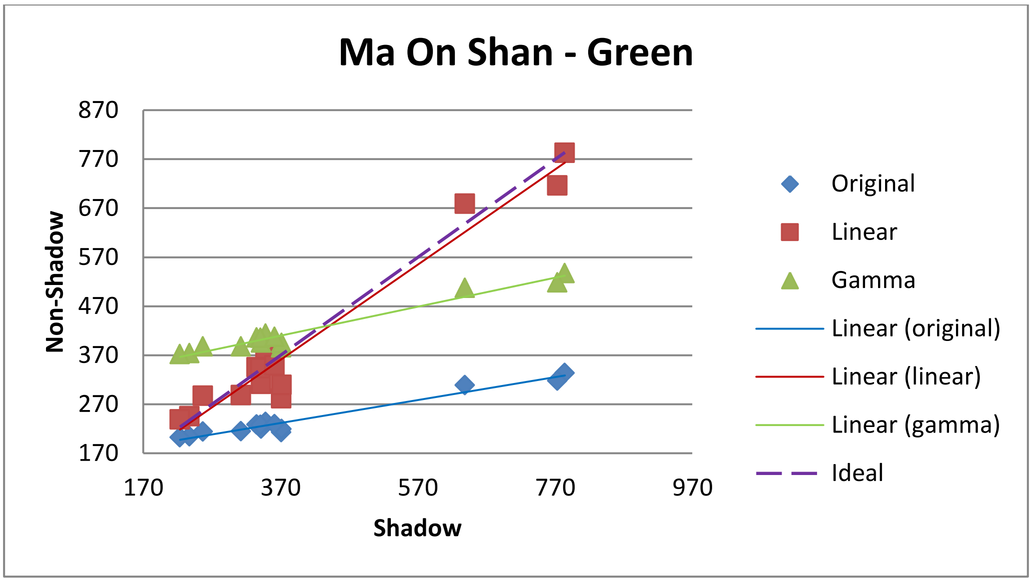

Figure 4-25 Relationship between enhanced shadows and non-shadows - Ma On Shan (Green)

Table 4-13 Assessment result of Linear Correlation Correction (data from Central image)

	NIR Surrounding	enhanced Shadow	RED Surrounding	enhanced shadow	GREEN Surrounding	enhanced shadow	BLUE Surrounding	enhanced shadow
Road								
Min	164	75.00	174	124.54	299	214.70	236	209.53
Max	379	290.32	361	323.05	482	432.50	329	292.88
Mean	261.02	142.52	251.53	195.44	373.00	325.68	268.51	248.49
Median	266.46	108.64	255.81	174.94	378.35	321.05	270.88	238.51
Bare ground								
Min	244	101.51	228	209.61	368	330.27	266	245.77
Max	483	297.87	429	328.72	502	485.84	326	325.50
Mean	307.81	188.94	287.84	254.77	411.69	390.87	287.63	275.39
Median	295.35	192.02	276.68	254.74	403.59	388.00	284.98	267.26
vegetation								
Min	256	146.83	109	50.81	228	205.81	193	184.16
Max	572	554.64	206	215.29	334	356.94	233	238.52
Mean	425.45	321.30	138.87	154.31	268.37	294.54	207.08	218.27
Median	412.77	320.47	127.95	163.89	258.64	312.07	203.00	223.87

Table 4-13 shows the pixel values difference between enhanced (Linear Correlation Correction) shadows and its adjacent non-shadows. Data were collected using Central image. Three classes: road, bare ground and vegetation were selected and statistics from the enhanced image were recorded. It can be seen that the pixel values after enhancement are generally darker than its surrounding areas.

4.3.2 Assessment based on band ratios – vegetation index

To examine if the spectral properties within enhanced regions are capable of improving classification accuracy in shadowed areas, the performance of the commonly used vegetation index NDVI is tested. The NDVI images of the original, the Gamma enhanced and the Linear enhanced were compared to examine if the vegetation under shadows can be extracted after shadow enhancement process.

For Central, a total number of 4 images are presented to illustrate the results of using NDVI for vegetation detection. They are the original image, gamma enhanced image, and two linear enhanced images (with and without correcting the boundary pixel values of the red and NIR band).

<u>Central</u>

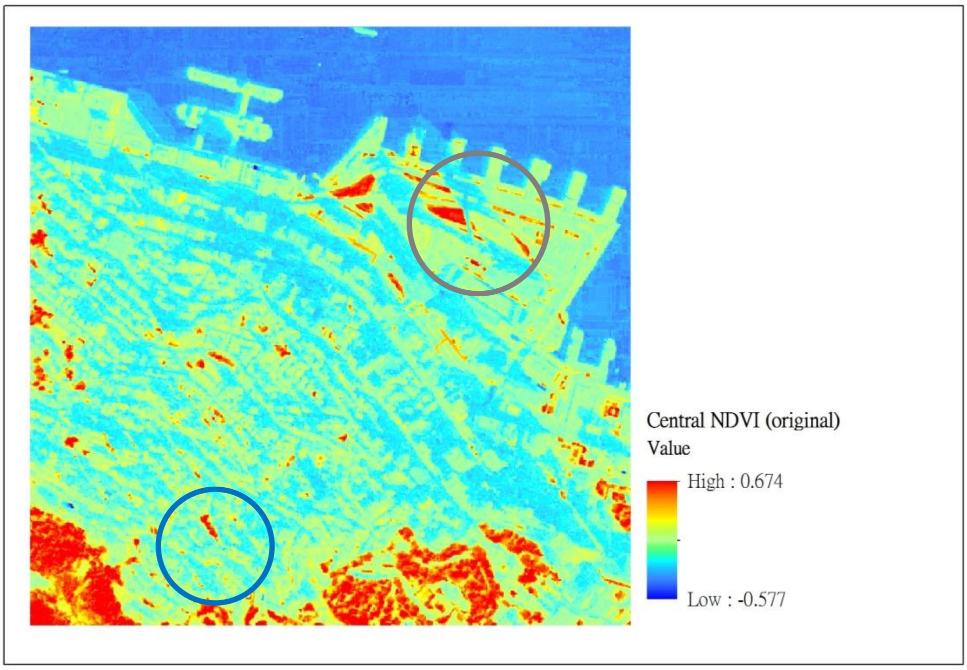

Figure 4-26 Original NDVI of Central

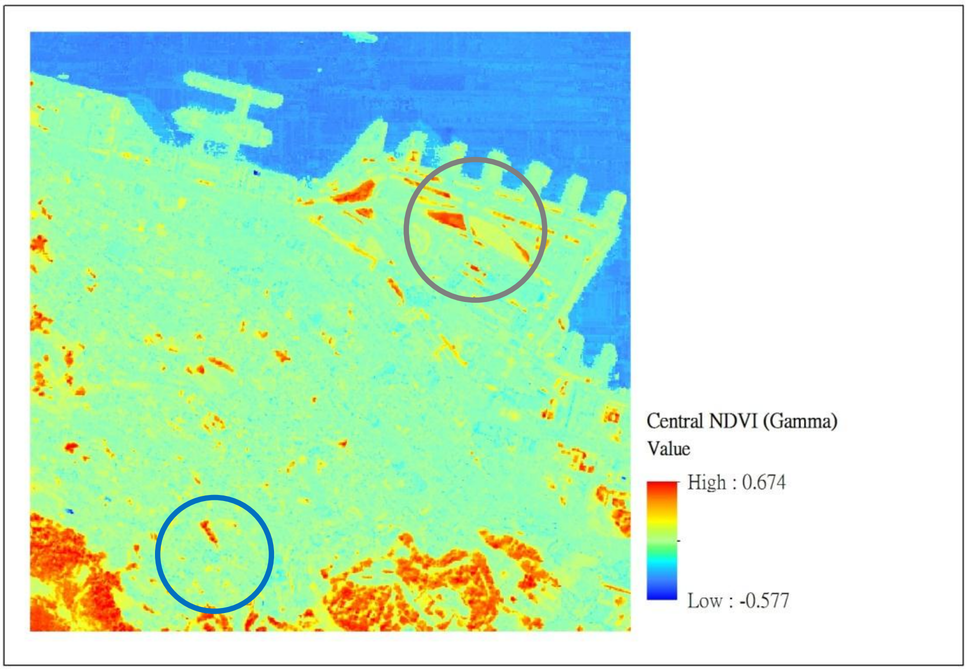

Figure 4-27 Gamma enhanced NDVI of Central

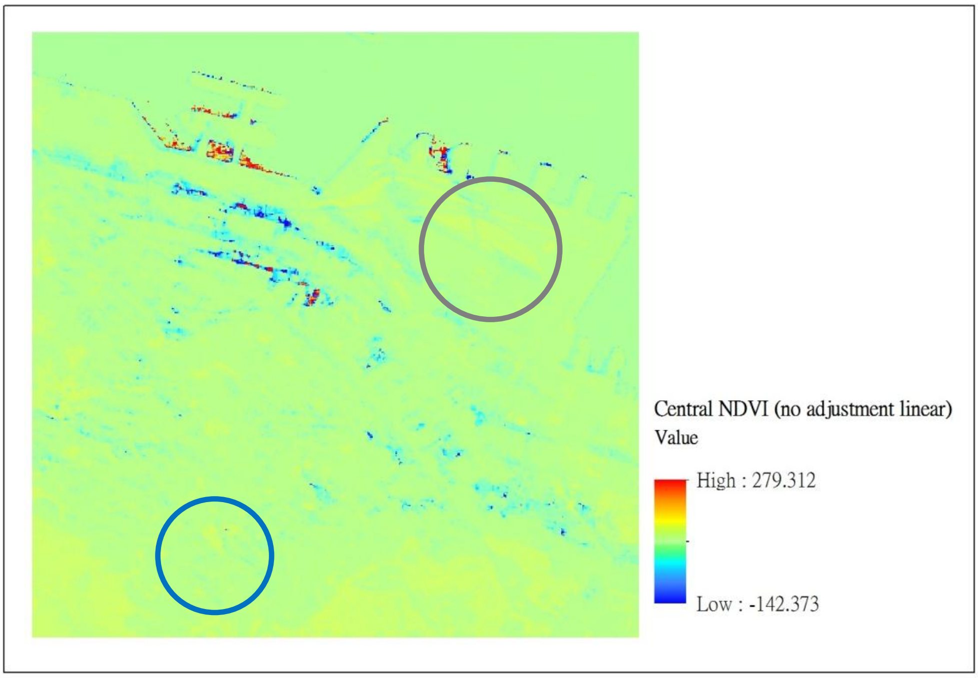

Figure 4-28 Linear enhanced NDVI of Central (without correcting red and NIR band)

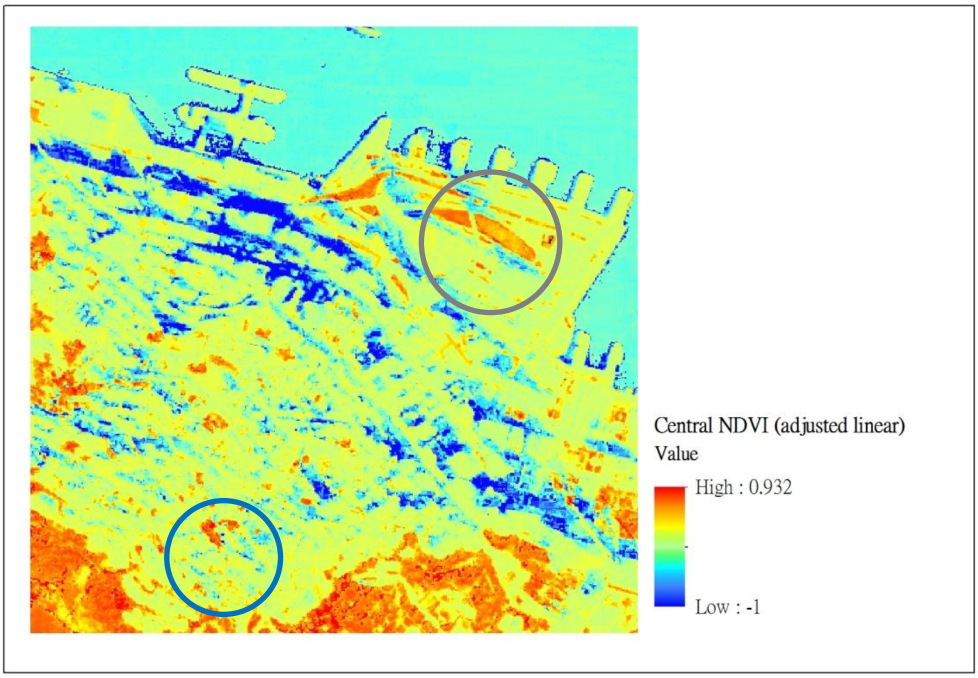

Figure 4-29 Linear enhanced NDVI of Central (with red and NIR band corrected)

The normal range of NDVI is from -1 to +1 (standardized) and values larger than 0.2

are classified as vegetation. In figure 4-26 the original NDVI image inside the grey circle is a grassed garden and a footbridge. The part which is not under shadow has a higher NDVI value (~0.5) compared to the part under shadow (~0.09) and can be seen by the color difference. Comparing figure 4-27 (Gamma enhanced image) with figure 4-26, the results appear to be similar in that the vegetation under shadow cannot be detected. Although the pixel values were increased after Gamma Correction, it can be seen that the spread of data in Gamma Correction is similar to the original shadow (figures 4-22 and 4-23). Therefore, the NDVI computed within shadowed regions will not have a significant change and thus the range of NDVI remains the same (lowest and highest NDVI are obtained from non-shadowed regions). Figure 4-28 shows the NDVI image created from the Linear Correlation Correction enhanced image where the range of pixel values in red and NIR bands were not adjusted to the range 0-2047. The NDVI values calculated are not within -1 to +1 due to the inconsistent scale used in the two different spectral bands. When the problems associated with wrong scale is fixed, figure 4-29 shows a more reasonable image. Within the blue circle in figure 4-29, part of the vegetation is under shadow while the other part can be detected by the NDVI. Comparing the amount of vegetation detected in two circles, it can be seen that figure 4-29 shows more detected vegetation than the one in figure 4-26 (original) and figure 4-27 (Gamma). With a wider spread of pixel values, the NDVI values calculated using Linear Correlation Correction image have more significant changes. The location of the footbridge in grey circle is now clearly seen.

The results indicate that an image with shadows enhanced by Linear Correlation Correction is able to show vegetation to a higher degree of accuracy when compared to the Gamma Correction. However, from figure 4-29 there are certain areas having the value -1, showing a large contrast with the surrounding. How this situation is caused mainly depends on the way the range in red and NIR band are being adjusted. In figure 4-29, cut off value 0 is applied to those pixel values lower than 0. When computing NDVI, zero value in one of the spectral bands will lead to extreme NDVI value (NDVI equals 1 or -1). The result can be validated by the scanned aerial photo of Central from Hong Kong Guide (2005) (Figure 4-30) where the circled area is vegetated.

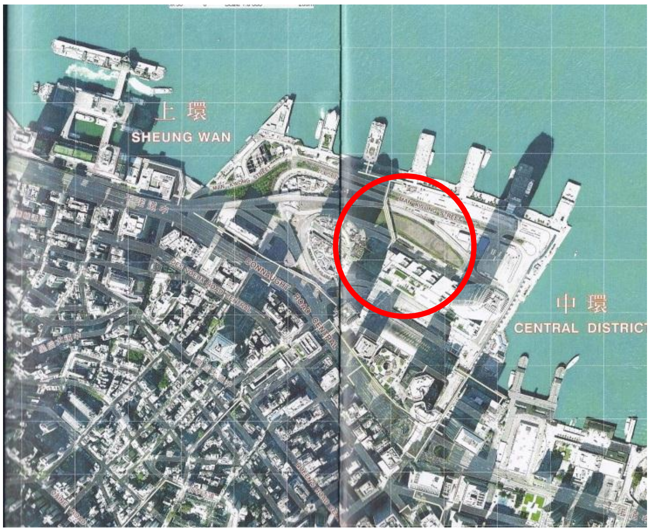

Figure 4-30 Aerial photo of Central

Ma On Shan

The results of original NDVI and Gamma enhanced NDVI in Ma On Shan are similar to that of Central, but the result by Linear Correlation Correction in figure 4-33 is slightly different. In fact, in this set of images, the method used to deal with out-of-range pixel values is not the same as in Central. Figure 4-34 shows the Ma On Shan NDVI image adjusted by replacing any pixel values that are lowered after enhancement (algorithm same as the Central NDVI in figure 4-29). For those values that are larger than 2047, the original local maximum is used. From figure 4-33, it can be seen that the NDVI calculated is having extreme value of -1 and +1. In fact, the shadows in the mountainous area are vegetated and contain the darkest group of pixel values, but the NDVI image shows a large difference in between. The NDVI values in the non-shadowed areas are around 0.4-0.6, while those being linearly enhanced are +1. Although the areas inside the circle can be extracted as vegetation, the values are misleading and would become a serious problem for image interpretation process.

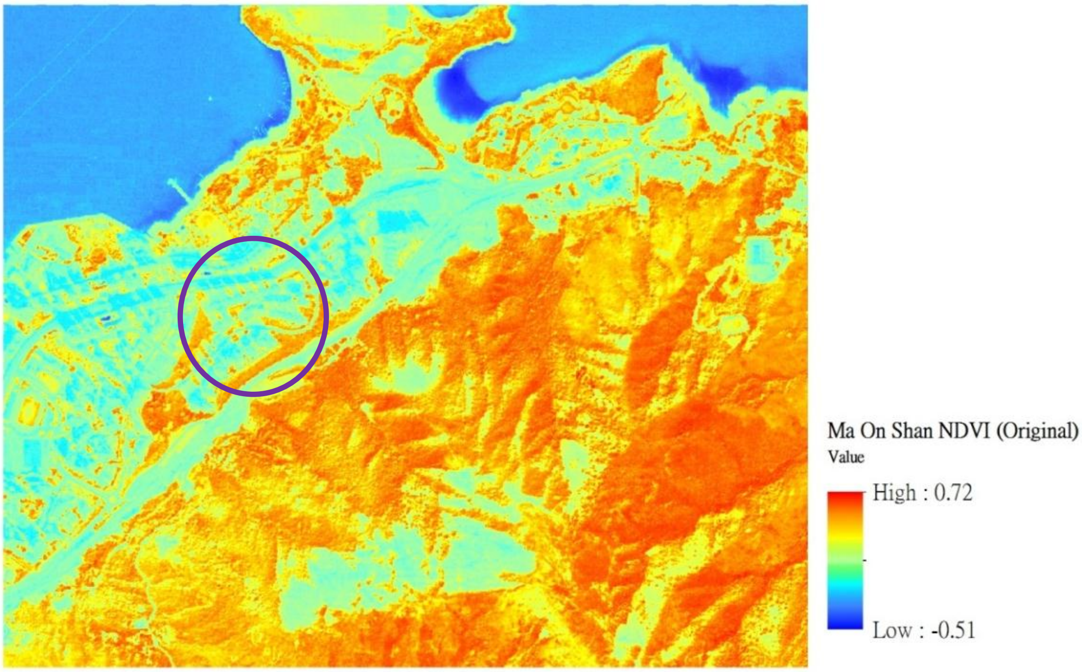

Figure 4-31 Original NDVI of Ma On Shan

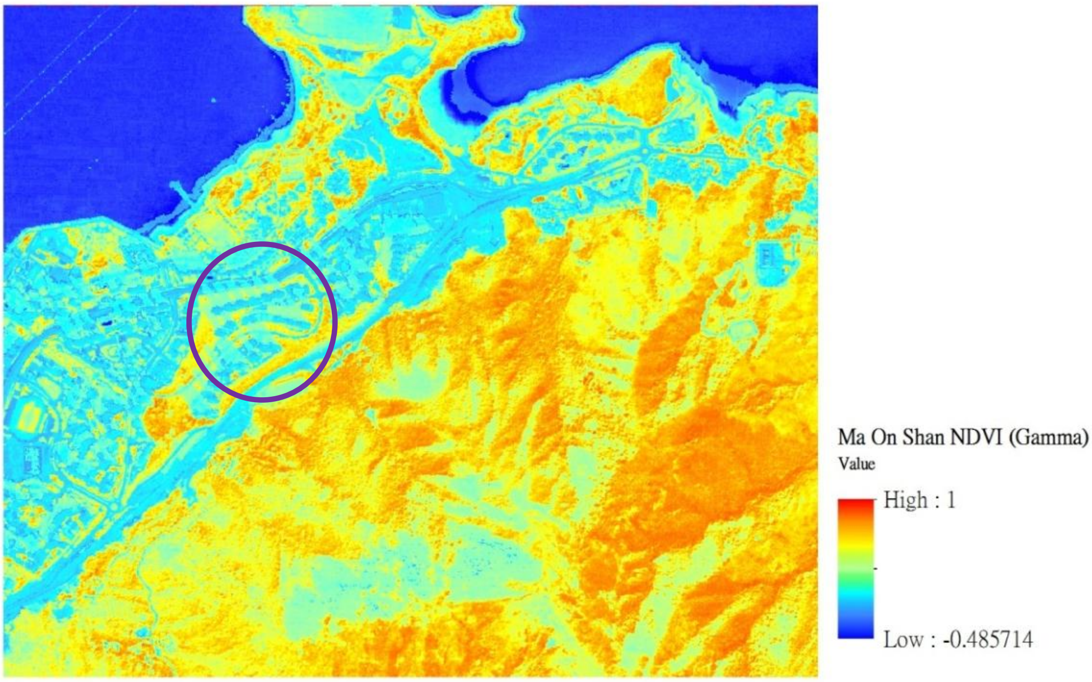

Figure 4-32 Gamma enhanced NDVI of Ma On Shan

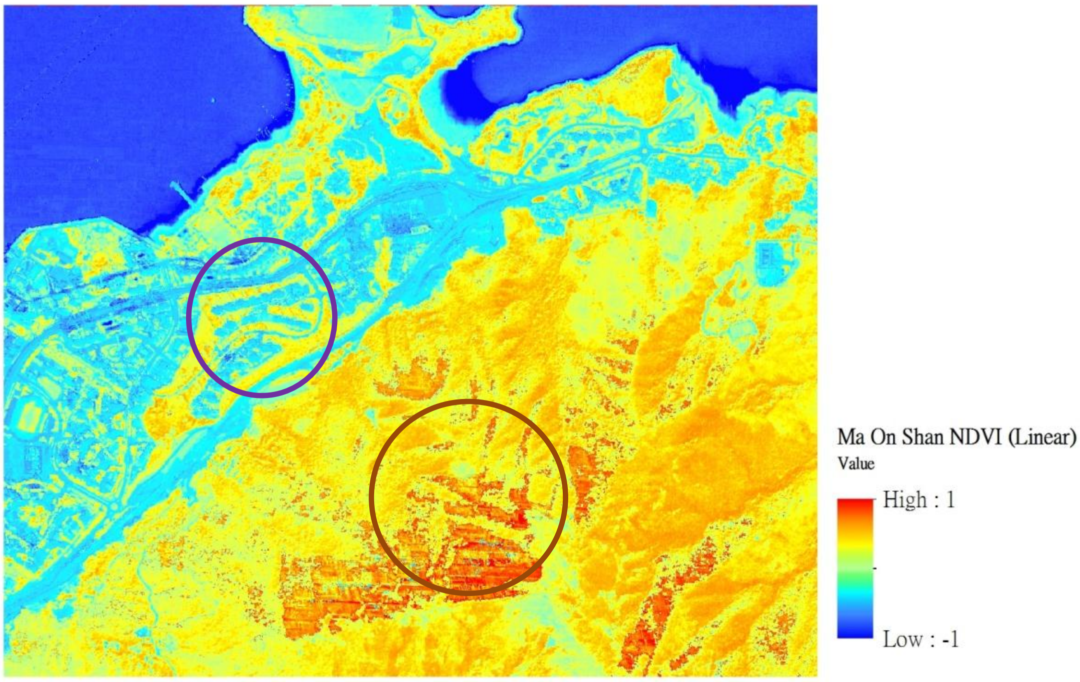

Figure 4-33 Linear enhanced NDVI of Ma On Shan (corrected by setting cut off value)

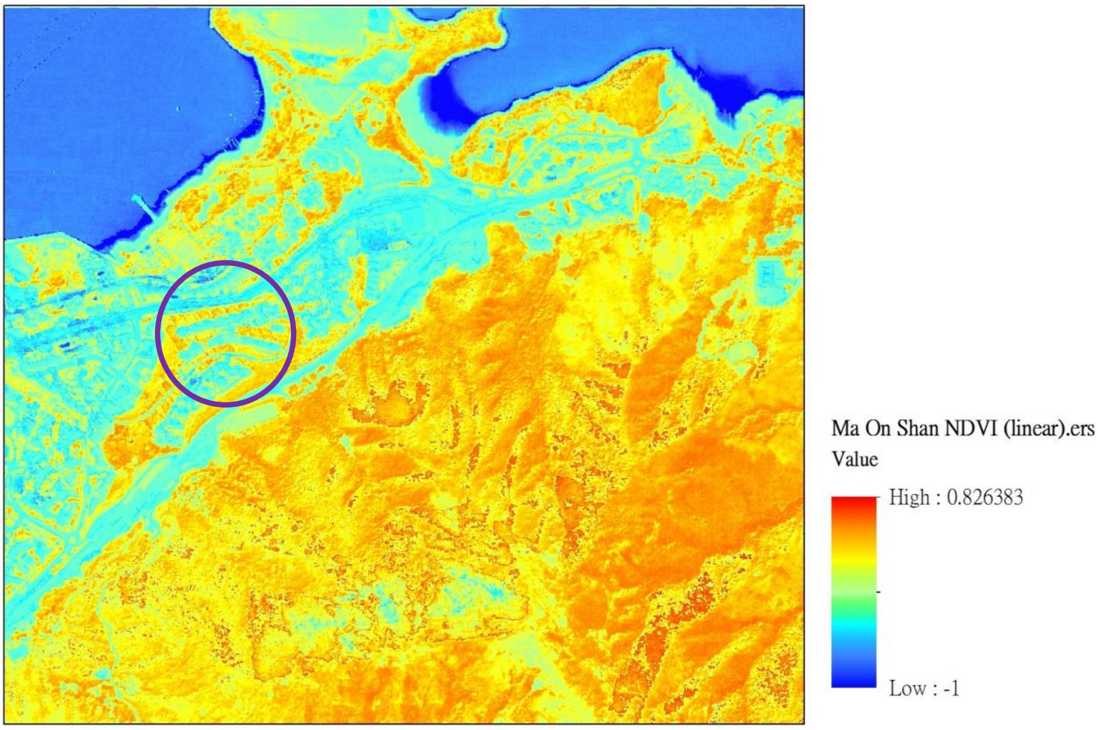

Figure 4-34 Linear enhanced NDVI of Ma On Shan (corrected by replacing original pixel value)

Figure 4-35 Aerial photo of Ma On Shan

Different from the algorithm that use cut-off value, NDVI obtained in figure 4-34 (replacing original pixel values) are much closer to its surrounding and are less misleading than applying cut-off value. However, replacing original pixel values means that some of the NDVI values would be the same as the original NDVI image and would not be able to classify as vegetation. This indicates the importance of choosing a suitable method to deal with the scale problem when Linear Correlation Correction is being used. Although the scanned aerial photo of Ma On Shan (Figure 4-35) is not able to cover the same area size as the satellite image, the circled area (in purple) is vegetated and only Linear Correlation Correction is able to extract it successfully.

Sham Shui Po

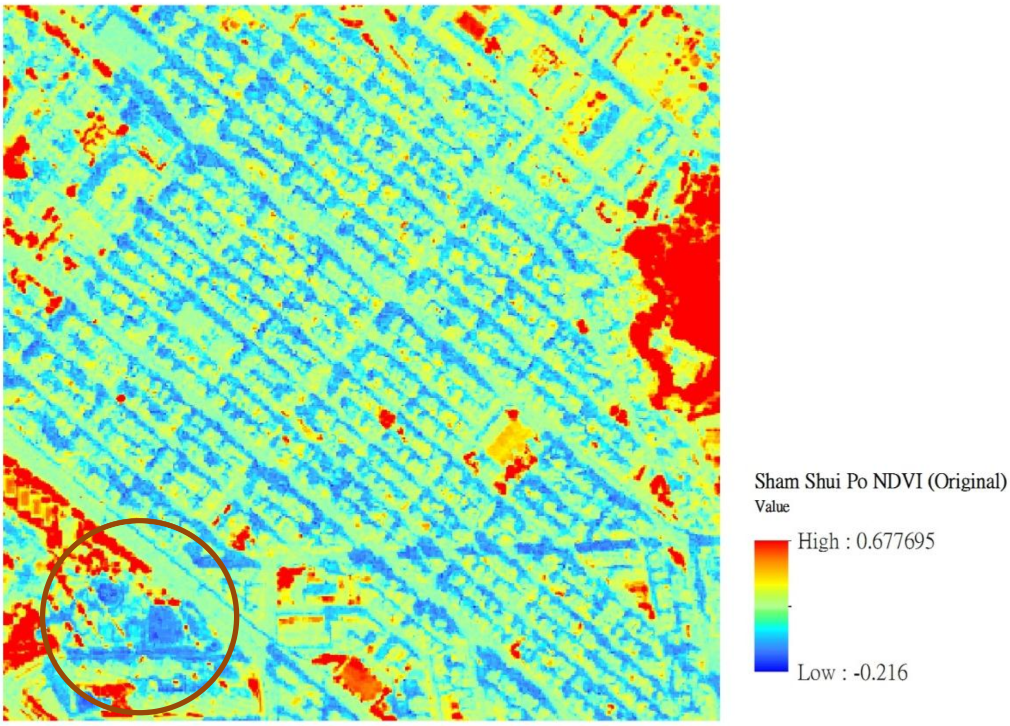

Figure 4-36 Original NDVI of Sham Shui Po

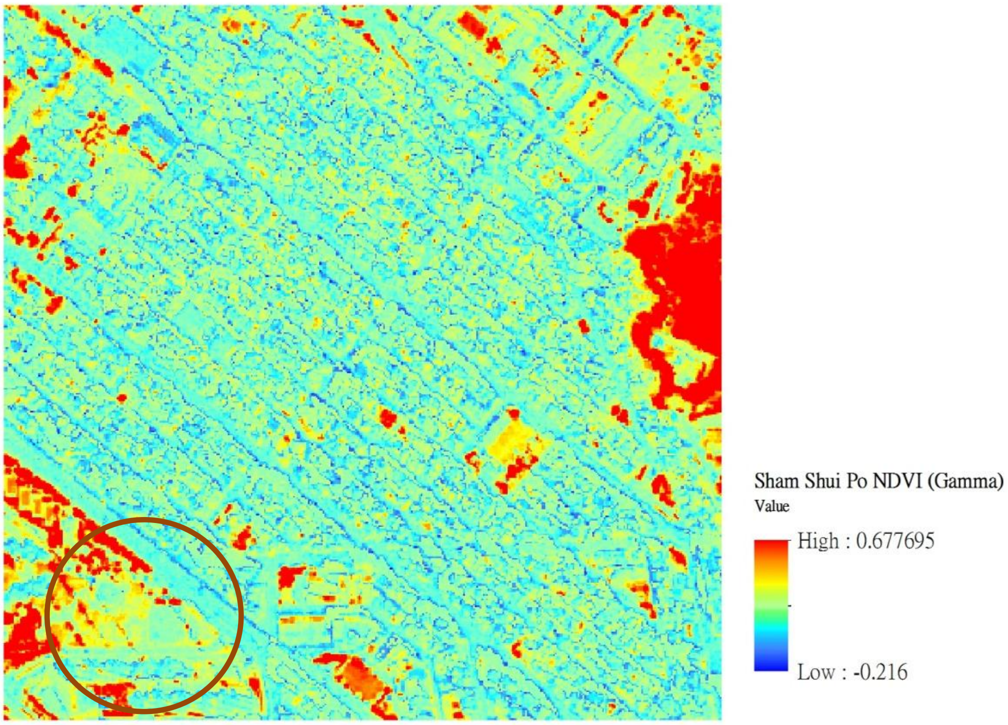

Figure 4-37 Gamma enhanced NDVI of Sham Shui Po

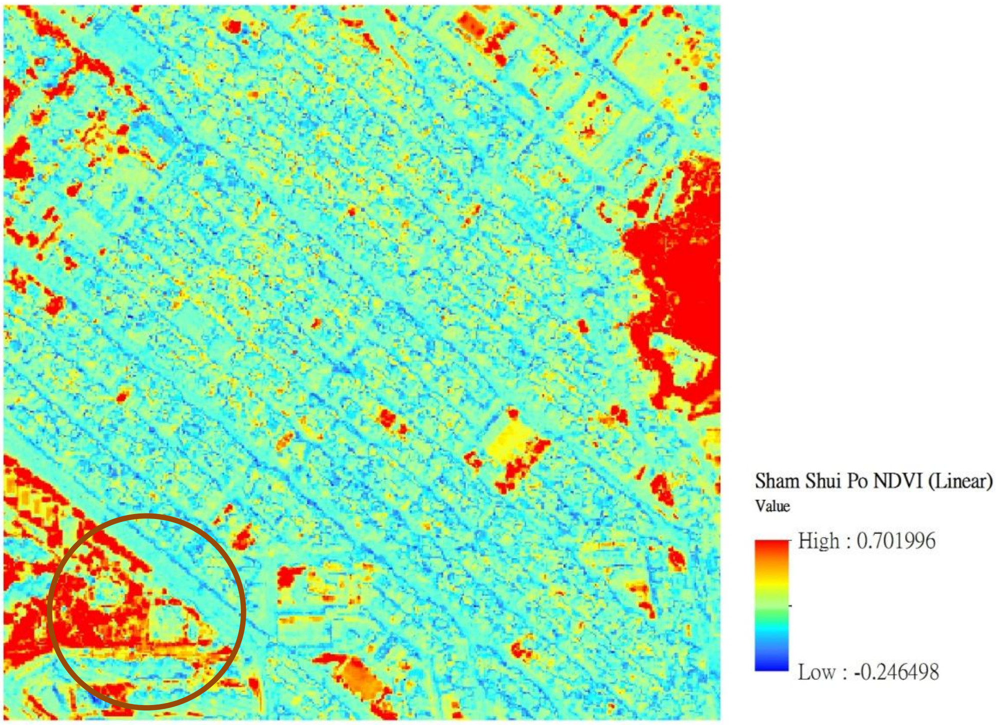

Figure 4-38 Linear enhanced NDVI of Sham Shui Po

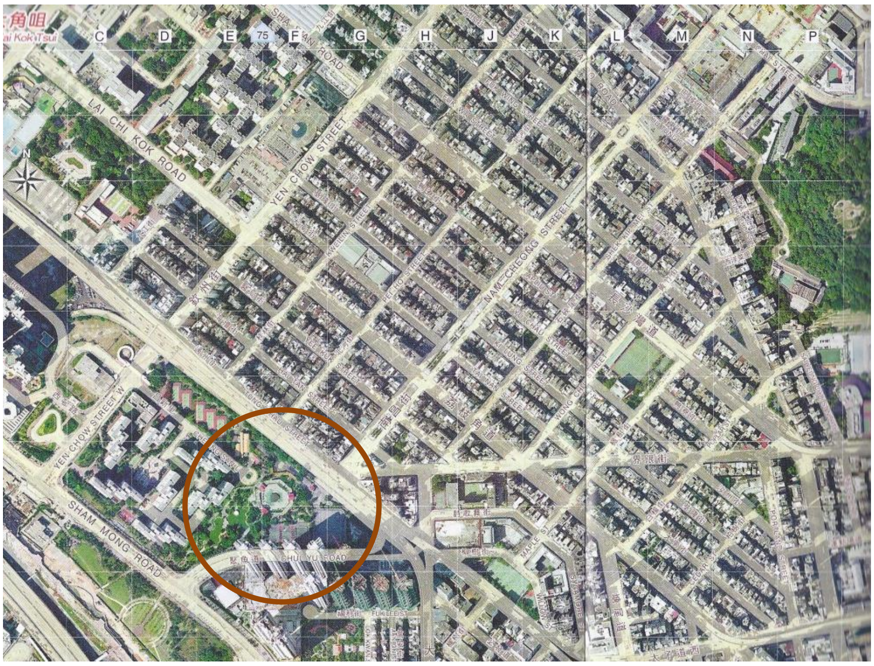

Figure 4-39 Aerial photo of Sham Shui Po

In Sham Shui Po, the result of Gamma Correction slightly improves the results of NDVI (figure 4-37). Although the NDVI range is the same as in original image, the

NDVI obtained within enhanced shadows were slightly increased. It could be seen in the circle that vegetation under shadows has a much closer values to its surrounding, but the color difference is still significant. However, when compared the results with Linear Correlation Correction (figure 4-38), the NDVI values obtained is similar to that of the surrounding. Although the enhancement result of Sham Shui Po by Linear Correlation Correction (figure 4-20) appears to be much darker for some regions, use of vegetation index is able to extract information required. Among three study areas, those vegetated areas covered by shadows were not correctly identified in their original NDVI image and was marginally improved by the Gamma Correction algorithm. However, when Linear Correlation Correction was used, the improvement in the NDVI image is significant in all study areas. The aerial photo (Figure 4-39) can be used to show that vegetation exists in the circled area.

To summarize, shadow enhancement process should not only consider the visual improvement, but also fulfill the needs for further analysis or process. Here the impact of different enhancement algorithms on vegetation index (NDVI) is demonstrated. It was found that the enhancement result produced by Linear Correlation Correction was more capable of identifying vegetated areas than that of Gamma Correction as long as out-of-range pixel values are properly managed.

Chapter 5. A second experimental test

5.1.1 <u>Shadow enhancement for the second time (Iteration)</u>

From the results shown in the previous part, the tone of shadow enhanced regions are much closer to but are still darker than those of their non-shadowed counterparts, and parts of the enhanced areas do not show much difference after the process. If shadow enhancement is considered to be an automated process in later development, then it is possible that the slightly darker regions will get closer to their non-shadowed counterparts when the process is repeated. In order to test this idea, the image of Central was selected to be enhanced again. The reason for using Central instead of the other two images is that the Central image shows different levels of enhanced results. Some regions cannot be enhanced (those in deep shadow) while some others show a good enhancing result.

Similar to the previous procedures, the shadows have to be extracted first. By using the Spectral Shape Index presented above, the Central image having undergone linear enhancement is being classified once again. The previous shadow mask is not used again because the brightness of some of the enhanced shadows is natural compared to its adjacent non-shadowed regions. If the previous shadow is used, it is possible that some of the regions are over enhanced. Figure 5-1 shows the classification results on the Spectral Shape Index of enhanced Central image.

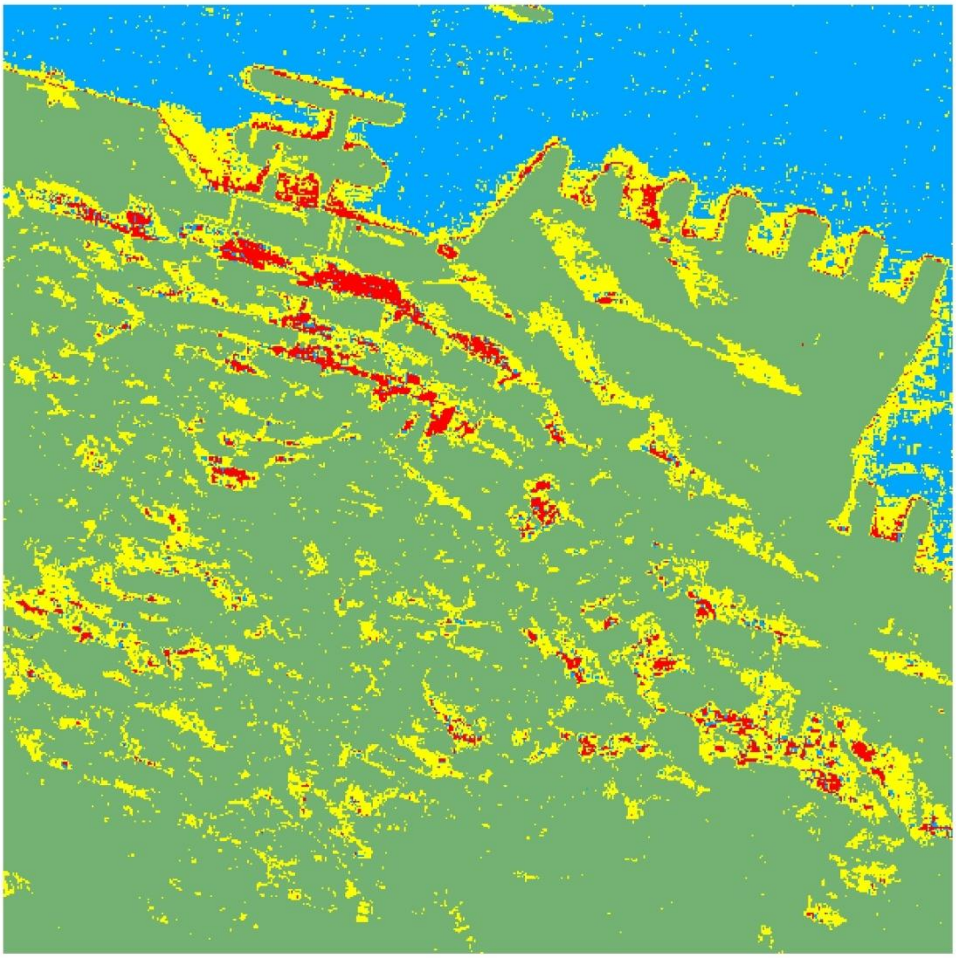

Figure 5-1 Classification results on SSI of Linear enhanced Central image

Different from the previous results which created 3 classes in total (one of them being shadows), 4 classes are produced using supervised classification due to the fact that the brightness of shadows were changed after the first enhancement. Shadows can be further classified into 2 groups based on their brightness. Inspection of the multispectral image revealed the classes representing water, dark shadow, bright shadow and non-shadow. It can be seen that part of the shadows that were enhanced the first time are no longer classified as shadows. After the shadows were extracted, the same algorithm was used to establish the linear regression models and recorded the average pixel values of shadowed and non-shadowed area pairs. Once again, the area pairs were randomly selected from the whole image and generated the regression model for each spectral band.

Table 5-1 Gamma value and Linear regression models for 2nd-iteration

	Gamma Min	Gamma Max	Linear regression model	Correlation coefficient
Blue	1.005	1.091	y = 1.213x – 23.068	0.76
Green	1.046	1.234	y = 1.104x + 38.561	0.68
Red	1.110	1.297	y = 1.284x + 38.587	0.81
NIR	1.281	1.641	y = 1.298x + 128.100	0.66

In table 5-1, the Gamma values are also presented and it can be seen that the variation among training dataset is less than the first iteration. However, it is still difficult to select one representative Gamma values for the whole images to follow. An exploratory study of applying gamma values revealed that shadows from the resulting images are of different brightness of grey. Different from the original image, the newly established regression models are not likely to make the pixel values lower after enhancement. For Red and NIR band, it is observed that both equations contain a positive constant that the resulting pixel value must be enlarged. The results are as shown below:

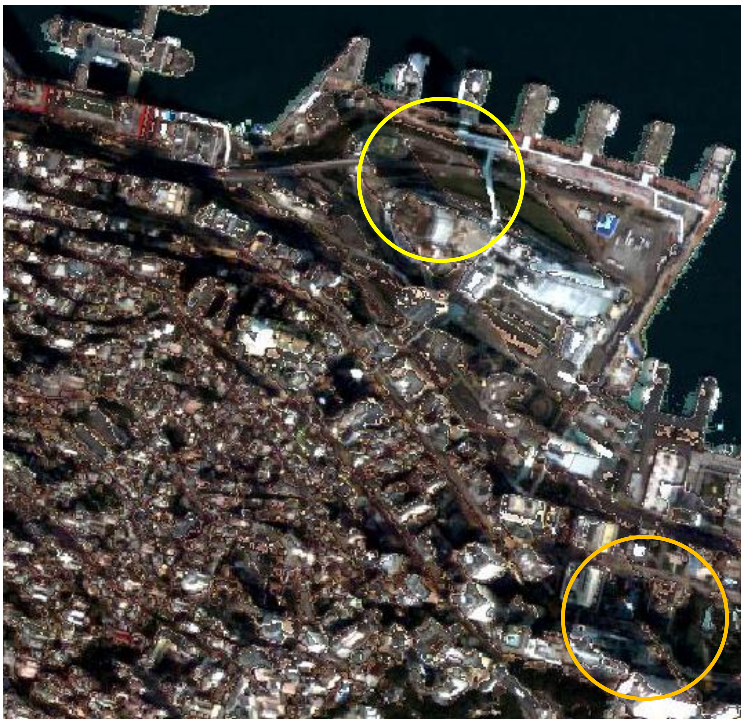

Figure 5-2 1st-iteration of Central by Linear Correlation Correction (image cropped)

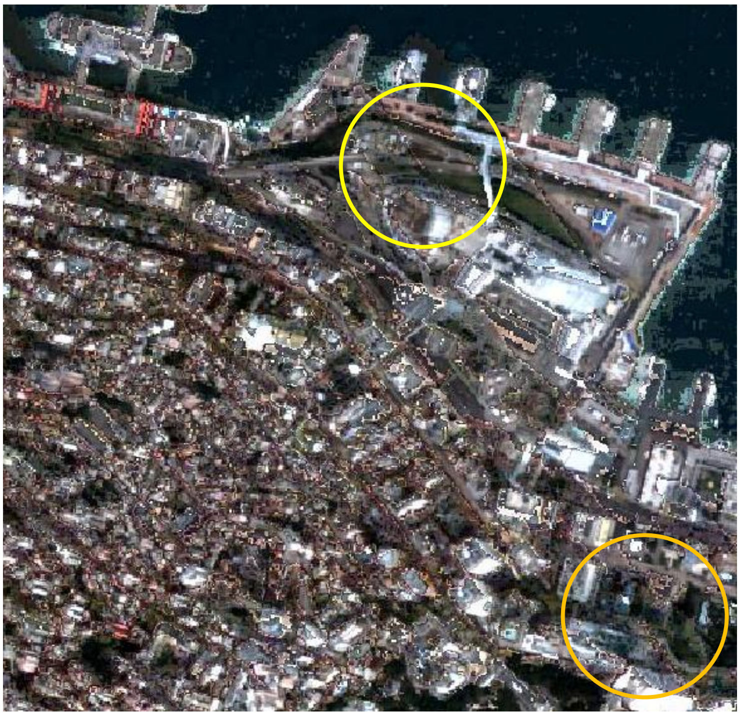

Figure 5-3 2nd-iteration of Central by Linear Correlation Correction (image cropped)

The result presented in figure 5-2 and 5-3 shows that the image quality is degraded after the second iteration was done and the water surfaces appear quite noisy. However, the areas within the two circles also show that the brightness of the shadows becomes closer to the surrounding. This indicates that shadows can be further enhanced, but the overall image quality may be lowered.

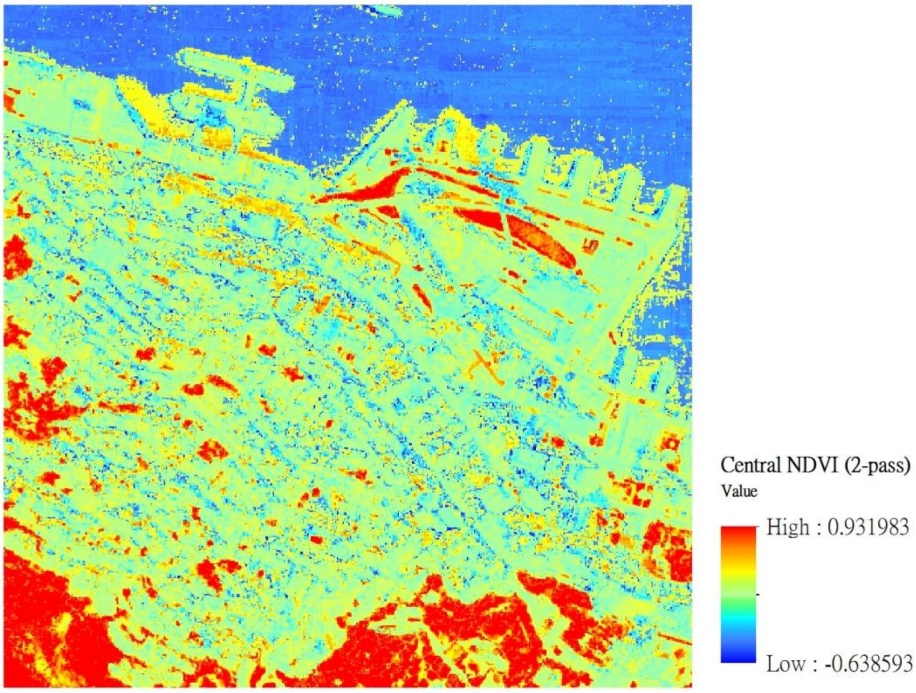

Figure 5-4 Central NDVI (2^{nd}-iteration)

The corresponding NDVI image (figure 5-4) shows similar result compared to the first iteration. It may not be easy to observe any changes in the NDVI image, therefore the difference between two NDVI images is presented (figure 5-5). It is observed that the linear regression models established here are quite different from the previous ones. The pixel values are no longer being reduced. Therefore, from figure

5-5, larger differences are found in the places where the darkest group of pixels is located.

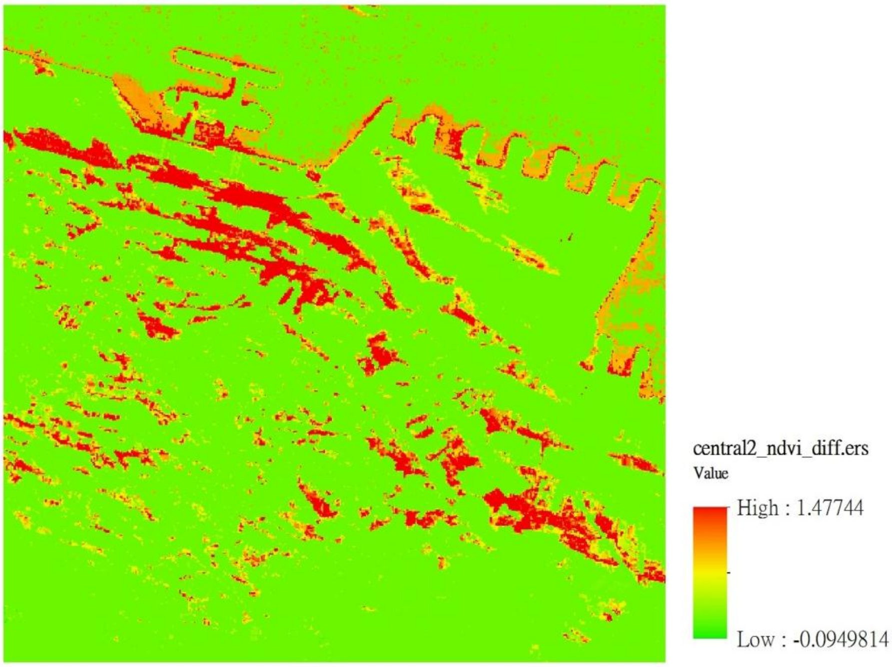

Figure 5-5 NDVI difference between two set of images - Central

5.1.2 Iteration using regression models from high contrast sampling area pairs

From the Central image having undergone first iteration of shadow enhancement, the enhanced shadows can be classified into two groups, dark shadows and bright shadows. This difference can only be observed after the first enhancement process. It is not easy to judge from the original image. In this part, the linear regression models are established based on the dark shadows and their corresponding non-shadows. The area pairs therefore have high contrast. The regression models for the randomly selected and high contrast cases and their correlation coefficients are listed in table 5-2.

Table 5-2 Regression models

Central	Regression models (random selected)	Regression models (high contrast)	Correlation coefficient
Blue	y = 1.213x – 23.068	y = 2.716x – 266.87	0.82
Green	y = 1.104x + 38.561	y = 3.511x – 394.08	0.85
Red	y = 1.284x + 38.587	y = 4.112x – 116.15	0.79
NIR	y = 1.298x + 128.1	y = 4.325x – 61.502	0.67

From the above table, it can be seen that the selection of sampling areas have a significant impact on the regression models. Using the darkest and brightest shadow pixel values in Red band as an example, pixel value 53 and 300 will behave very differently in the two regression models. Pixel value 53 and 300 will become 106.6 and 423.7 respectively when the regression model used is from random sampling areas. However, for the high contrast regression models, the results will become 101.8 and 1117.3 respectively. The resulting pixel value of the darkest group of pixels is similar, but for those brighter shadows, they will become even brighter in the produced image. The enhanced image is as shown in figure 5-6.

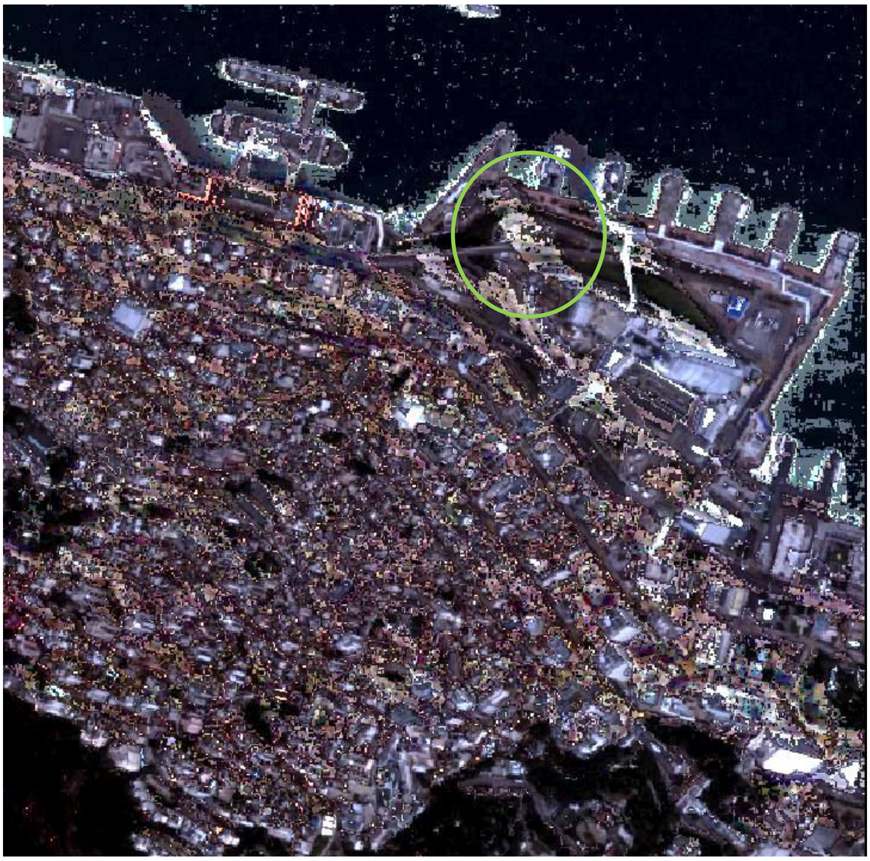

Figure 5-6 Shadow enhancement using high contrast linear regression model

The image quality is degraded when using the regression models established from high contrast sampling areas. It can be seen that some of the shadows are brighter than their adjacent non-shadowed areas (as shown in the green circle). This enhancement result shows that when shadow enhancement is an iterative process, regression models establishment should consider the brighter shadows first. For those originally darkest groups of pixels, the resulting image shows that enhancement quality is not satisfactory. This suggested that when the energy is being totally blocked and dark shadows are formed, information under these shadows is already damaged and can hardly be retrieved.

5.1.3 Shadow enhanced by non-linear functions

The problems associated with Linear Correlation Correction have been discussed previously. The darkest group of pixels is not being correctly enhanced and results in pixel values exceeding 0-2047. The problems are found to be serious mostly in the Red and NIR band, and from the distribution of the sampling data pairs. It raises the question whether a polynomial regression model is more suitable for these two bands.

Figure 5-7 and figure 5-8 presented both linear and non-linear regression models of the two spectral bands in question. From the two linear regression lines, it is clear that if the pixel values are low, the enhanced pixel values will be lowered, in some cases to less than zero. However, for the darkest pixels, polynomial (n=2) regression is closer to the reality that the pixel values are increased.

The resulting image in figure 5-9 shows that the shadow enhancement in overall visual aspect is not better than by using linear regression models (figure 5-10). However, it is observed that the dark shadows (as shown in red circle) are brighter when non-linear regression model is applied.

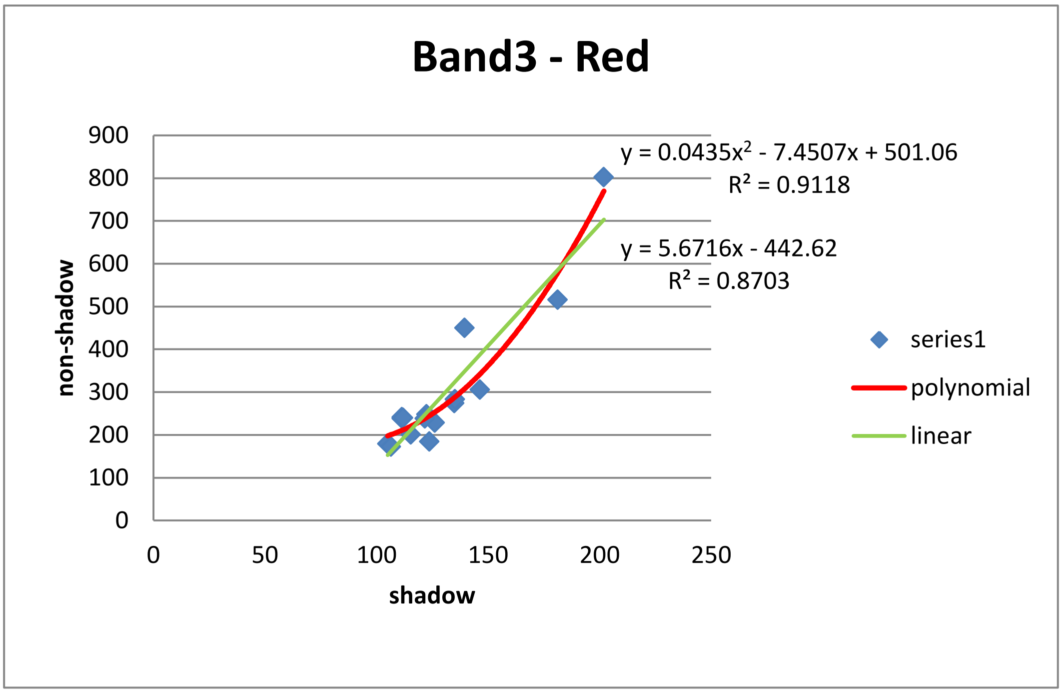

Figure 5-7 Relationship between shadow and non-shadow pairs in Central - Red

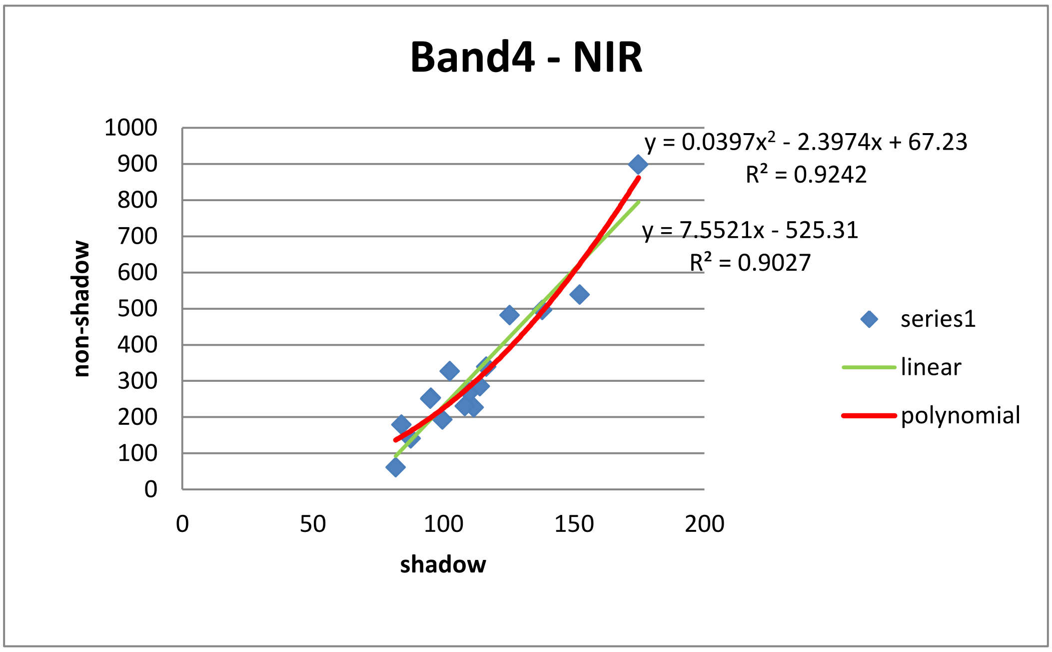

Figure 5-8 Relationship between shadow and non-shadow pairs in Central – NIR

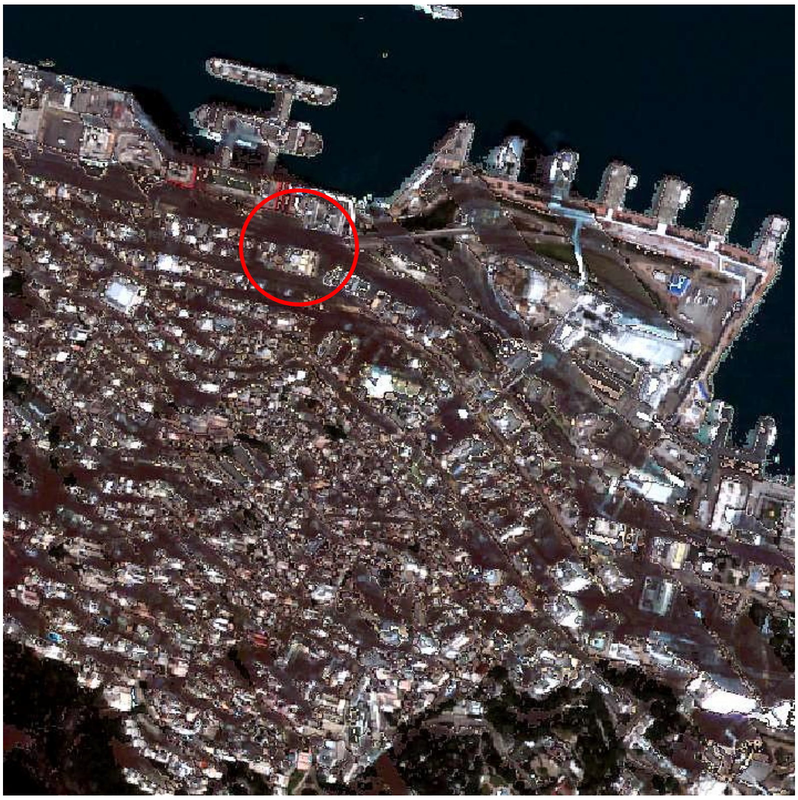

Figure 5-9 Shadow enhanced by non-linear regression model - Central

Figure 5-10 Shadow enhanced by linear regression model - Central

In order to obtain better results, it is suggested that polynomial regression is applied only on the darkest group of pixels. However, it would be another study directed at the method of separating pixel brightness into two groups and applying different regression models.

Chapter 6. Conclusions

6.1 Summary of shadow detection using Spectral Shape Index

The shadow detection algorithm applied in this study is that of the Spectral Shape Index. Under complicated environments and land covers, the detection algorithm is able to distinguish water surfaces and shadows from non-shadowed areas. However, for some surfaces that are inherently dark, they may be wrongly identified as shadows. This issue is well-known and to date has not been solved completely.

Supervised classification is selected for classifying shadows from non-shadows. However, several algorithms could be used to classify the Spectral Shape Index image. Since the study is mainly focused on the shadow enhanced image quality and improvement in identifying features under shadows, advanced classification techniques are not considered. With the use of Spectral Shape Index, most of the water features can be extracted, but it cannot accurately detect shallow water with sandy seabed. For this issue, image segmentation resulting from different color space such as HSI, HSV, $C_1C_2C_3$ and YIQ can be integrated to improve the detection accuracy. In fact, only the problem of identifying shallow water is observed and presented, but other surface types may also encounter the same problem so various testing is required on images from different locations and satellite sensors (only

Quickbird image is used in this study).

6.2 Summary of various enhancement results

Two out of three common shadow enhancement algorithms have been presented and tested. Histogram Matching was not selected due to the reported issues related to its application in complex environments. Data sampling made use of area instead of point to extract the average pixel values and to calculate Gamma parameters together with the linear regression models. Using only one pixel for establishing the regression models or estimating the Gamma values will have the chance that the selected pixel is, in fact, noise in the image. If this is the case, Gamma values estimation and linear regression models establishment will be biased. If data sampling by fixed size area, this effect should be able to be minimized.

One special concern regarding the use of area pairs is how large a sampling area can be. This will affect both Gamma estimation and the regression models. The spatial resolution of the images used is 2.44m at nadir, with 4 pixels by 4 pixels size. It is around 10m by 10m on ground. However, in places like Central, it is not easy to find shadowed and adjacent non-shadowed regions with 10m by 10m size from the satellite image. Considering the number of pixels in each sampling area and the environment limitation, 10m by 10m is almost the maximum sampling size in Hong Kong urban area. In some other cities and countries, larger sampling size can be used instead.

For the use of Gamma Correction, the shadow enhanced image is not satisfactory. The main issue is that the Gamma values estimated vary with different land covers. An ideal solution would be for each land cover to have its own set of Gamma values. When the aim of shadow enhancement is to make the classification of shadowed areas more reliable, classifying shadows before they are enhanced is a challenging task.

Generally speaking, Linear Correlation Correction is able to give better visual improvement and the image can be further used in vegetation mapping. This suggests that the Linear Correlation Correction is more capable in the enhancement of shadowed areas in satellite images that cover complicated environments. However, the results also show that choosing suitable sampling regions for regression models establishment is a critical issue. An iterative approach to the application of Linear Correlation Correction was presented. The results showed that while some enhancement was achieved, a more accurate shadow detection algorithm is required and the image quality may be degraded. If the image contains extreme dark pixels, the

Linear Correlation Correction method will not be able to enhance them and pixel values may exceed the normal range of 0-2047 (11 bit image).

In this study, the Central image has undergone Linear Correlation Correction twice and the results are presented. From the figures presented in the previous section, Linear Correlation Correction is much closer to the ideal enhancement curve while Gamma Correction is nearly parallel to the original curve. The impact of iterating the Gamma Correction was not assessed so it should be considered for further attention.

Linear Correlation Correction is not able to give good results under special cases like shadows on water surfaces. The correlation between shadows on water and non-shadow water surfaces has been investigated, and was found that the correlation coefficient is lower than 0.5 in Red, Green and Blue bands. The current result of enhancing shadows on water surface was not satisfactory and further investigation is needed on specific solution to this issue.

6.3 Summary of the assessment methods

The pixel values from a number of testing areas are used to compare the performance before and after; the vegetation index map is also used to support the findings. However, there are some other ways of measuring the information recovery quality;

for example, the concept of entropy is not discussed here for it is not easy to judge whether the information is noise or other useful details. The assessment method is limited to comparing pixel values (Bias of mean) and the probability to go one step further (NDVI performance). It may not fulfill all the expectations from different aspects.

6.4 Conclusions

In this study, three typical complex urban areas of Hong Kong demonstrating different characteristics are selected for studying shadow enhancement performance. These include high density tall buildings (more than 30 storeys), low density medium buildings (around 30 storeys or less) and high density lower buildings (mostly 8-9 storeys). The environments are complex due to the fact that shadows of a single building can fall across several types of surface (including vegetation, asphalt roads, concrete buildings, bare ground, etc.). Spectral Shape Index is used as the shadow detection method and is found that it gives acceptable classification result when both water surfaces and shadows appear in the satellite image. However, the ability of classifying shadows varies due to the differences in environments.

The performance of two existing shadow enhancement algorithms, Gamma Correction and Linear Correlation Correction are tested and compared. Results show that Linear Correlation Correction is more capable for environments having complicated land covers and gives better visual improvement. Although Linear Correlation Correction shows significant improvements in further analysis like NDVI, there are some critical issues affecting the overall quality of the enhancement. Certain solutions have been suggested, but they have their own limitations and further investigation is needed. The possibilities of iterating shadow enhancement using Linear Correlation Correction is discussed and the improvement of bright shadows is significant, but it is also a trade-off between the image quality and the recovered information. The use of non-linear regression models is tested, but the results are not satisfactory. Further investigation on combining linear and non-linear regression models could be done for better enhancing results.

To conclude, shadow enhancement could be done on urban areas having complex structure. The resulting image has its value for studying and information retrieval. When dealing with shadow enhancement in complex environments, many more issues need to be considered. The overall results show that Linear Correlation Correction is more capable in dealing with shadow enhancement in complex environments than Gamma Correction. However, the enhancement quality of dark shadows is not satisfactory and modified algorithm is tested and the result is slightly improved.

6.5 Limitations and recommendations

The use of Spectral Shape Index is demonstrated and the performance is discussed, but there are also drawbacks regarding the identification of some specific surfaces. From the Ma On Shan result, shallow water was wrongly classified as shadow. This indicates that the algorithm of Spectral Shape Index has to be revised and tested in more different environments. Only Quickbird images are used in the experiment, the performance of shadow enhancement using other satellite images should also be examined in the future.

No matter which shadow enhancement algorithm was used, the impact of penumbra (semi-shadow) could not be minimized. The penumbra size will be affected by the building's height. This is due to the fact that the distance between the object (occluder) and the surface is different. Lower buildings will have smaller penumbra size on the surface and the contrast between shadows and non-shadows is higher, while taller buildings will cast longer penumbra regions and more gradients can be observed in between. The current results leave some bright edges (being enhanced) and dark edges (not being enhanced) to some of the shadows boundaries. Therefore, further investigation is needed to examine whether applying smoothing filter or edge detection followed by specific enhancement would give better visual improvement.

From the enhancement point of view, the focus for future studies should be on how to classify the images by different illumination conditions of the scene environments. Although Linear Correlation Correction shows better visual improvement and is capable for further analysis, the pixel values in those darkest pixels cannot be correctly enhanced. If the image can be classified based on its illumination condition, two or more regression models can be established and applied separately. This will ensure that those darkest pixels are being enhanced to a certain extent. They do not remain as dark as before and are able to reduce the number of iteration required.

The problems of pixel values exceeding the normal range (dependent upon radiometric resolution) is discussed, and is mostly found in red and near-infrared bands. Some possible solutions are suggested, but they also have certain disadvantages and limitations. This is an important issue if it is intended that the enhanced image be used in further processes and be critical component for the products' quality. For this issue, it is suggested that non-linear regression models could be involved only for those darkest pixels. Linear regression model would be applied on the rest of them. Limited work has been done on testing the possibilities of combining two types of regression models for shadow enhancing.

Appendices

A. *5 sets of indices suggested for Spectral Shape Index*

Index 1:	0.5(Green+NIR) ÷ Red -1
Index 2 (used in this study):	(Green-Red) ÷ (Red+NIR)
Index 3:	(Green+NIR-2×Red) ÷ (Green+NIR+2×Red)
Index 4:	(Red+Blue) ÷ Green -2
Index 5 (suggested by Chen, et al.):	Red+Blue-2×Green

B. *Correlation between shadows and non-shadows*

Central

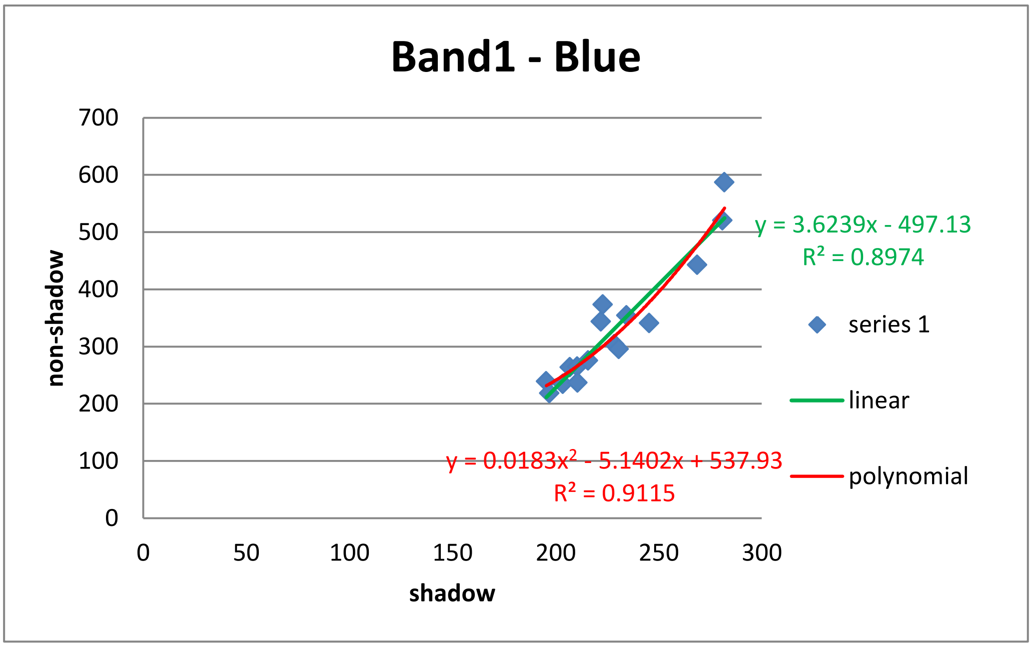

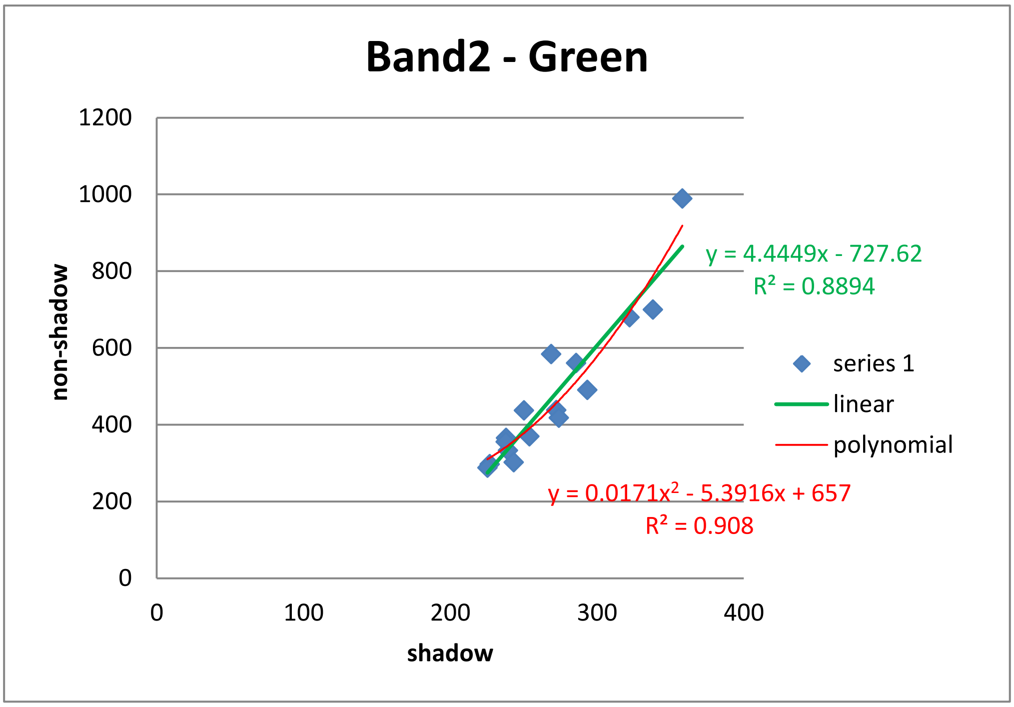
Band2 - Green
1200
1000
800
600
400
200
0
non-shadow
0
100
200
300
400
shadow
y = 4.4449x - 727.62
R² = 0.8894
series 1
linear
polynomial
y = 0.0171x² - 5.3916x + 657
R² = 0.908

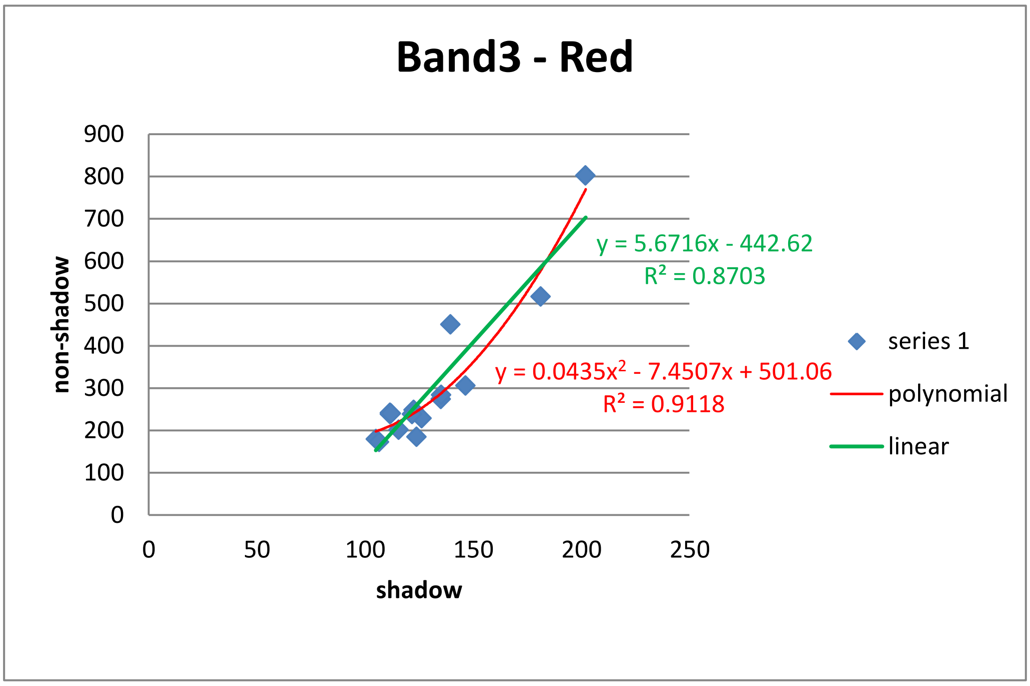
Band3 - Red
900
800
700
600
500
400
300
200
100
0
non-shadow
0
50
100
150
200
250
shadow
y = 5.6716x - 442.62
R² = 0.8703
y = 0.0435x² - 7.4507x + 501.06
R² = 0.9118
series 1
polynomial
linear

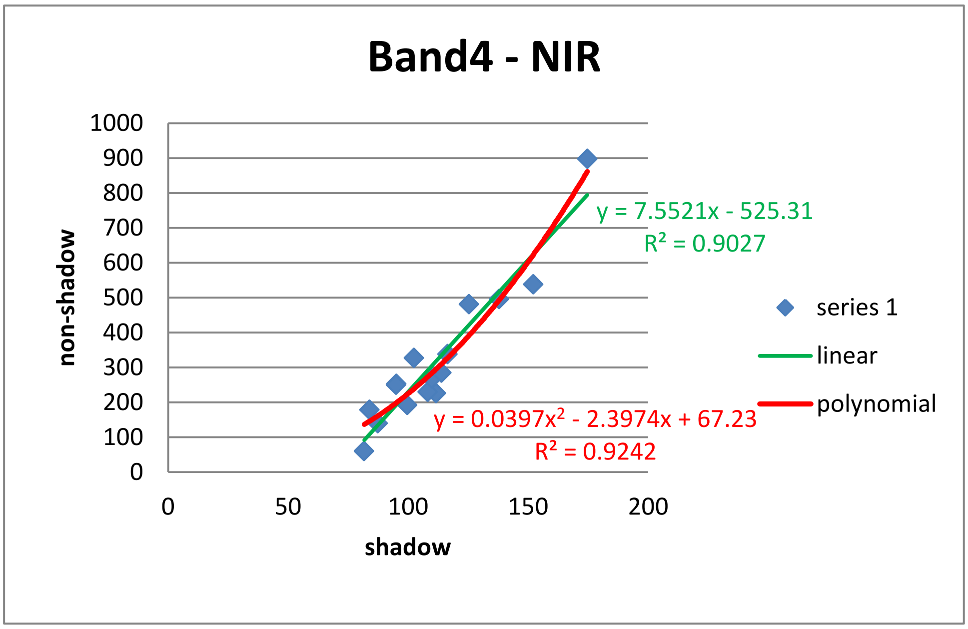

Band4 - NIR
1000
900
800
700
600
500
400
300
200
100
0
non-shadow
0
50
100
150
200
shadow
y = 7.5521x - 525.31
R² = 0.9027
y = 0.0397x² - 2.3974x + 67.23
R² = 0.9242
series 1
linear
polynomial

Ma On Shan

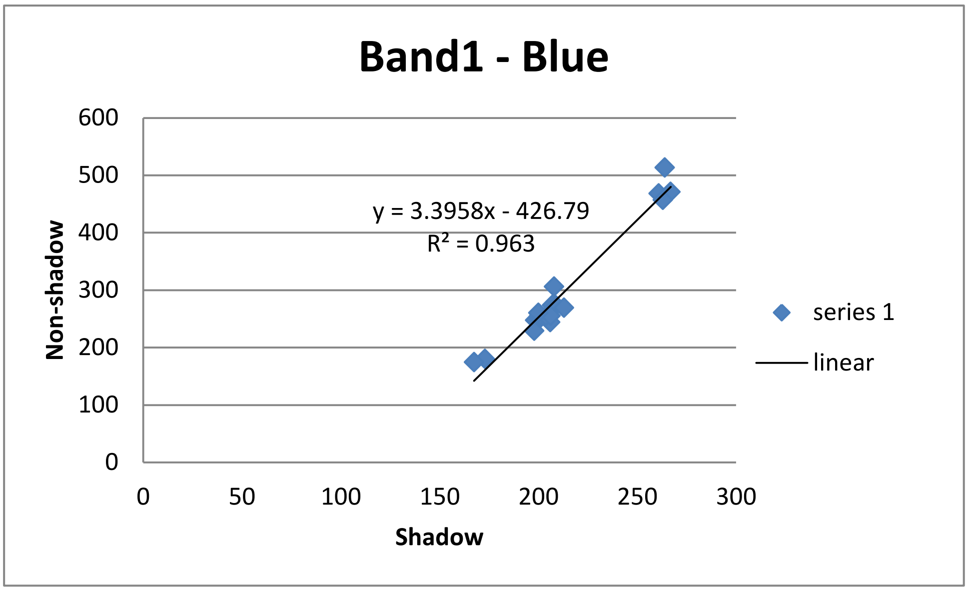
Band1 - Blue
Non-shadow
600
500
400
300
200
100
0
0
50
100
150
200
250
300
Shadow
y = 3.3958x - 426.79
R² = 0.963
series 1
linear

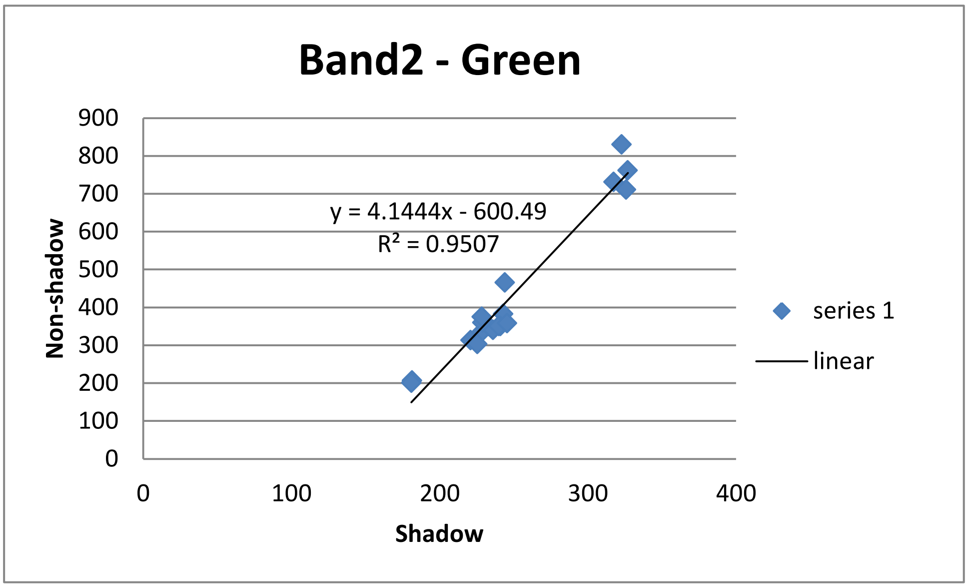
Band2 - Green
Non-shadow
900
800
700
600
500
400
300
200
100
0
0
100
200
300
400
Shadow
y = 4.1444x - 600.49
R² = 0.9507
series 1
linear

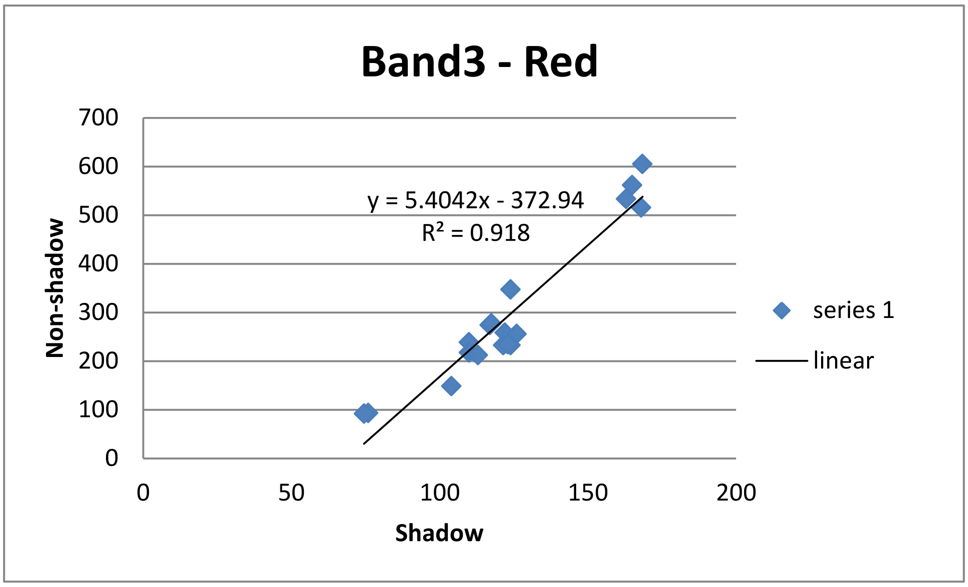
Band3 - Red
y = 5.4042x - 372.94
R² = 0.918
Non-shadow
Shadow
0
100
200
300
400
500
600
700
0
50
100
150
200
series 1
linear

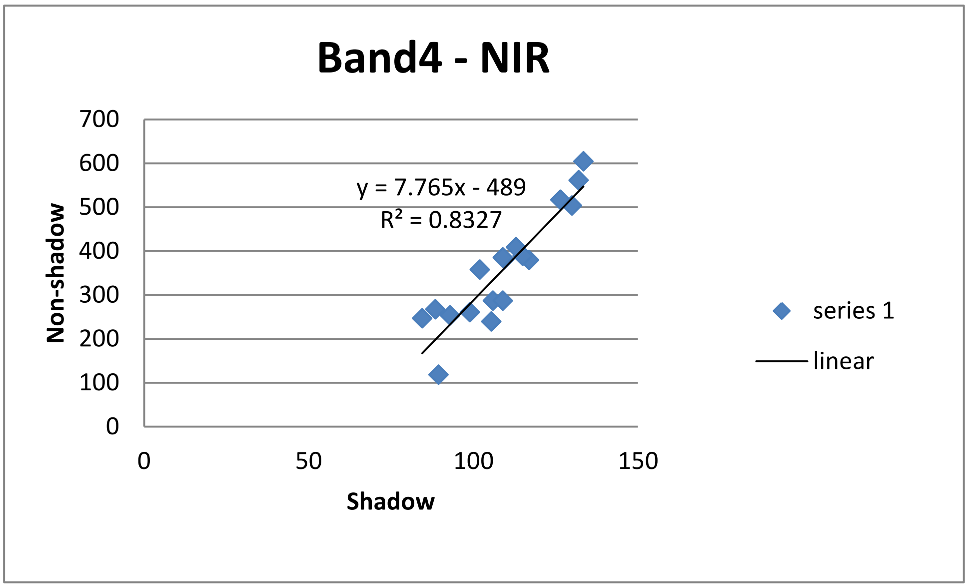
Band4 - NIR
y = 7.765x - 489
R² = 0.8327
Non-shadow
Shadow
0
100
200
300
400
500
600
700
0
50
100
150
series 1
linear

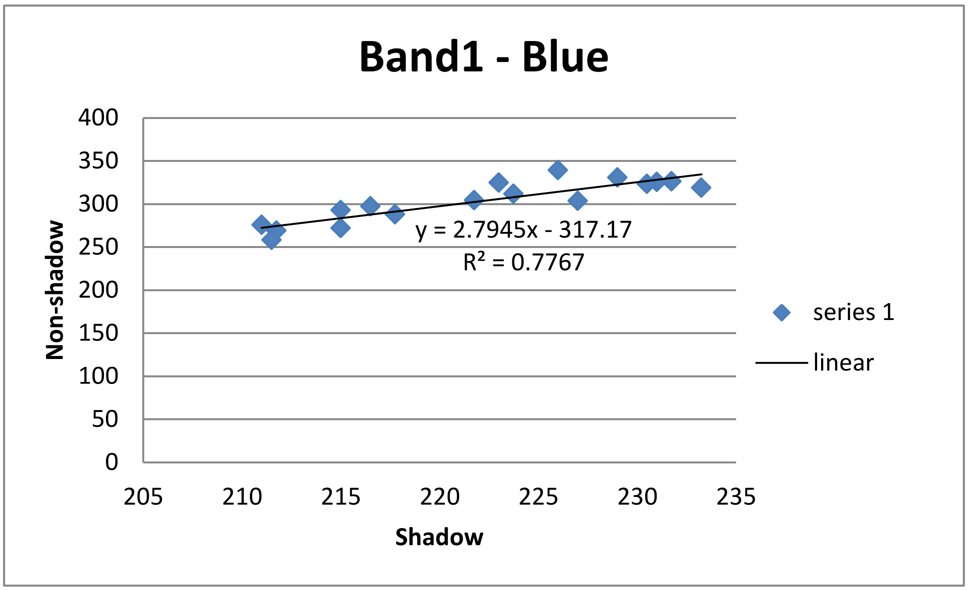
Band1 - Blue
Non-shadow
400
350
300
250
200
150
100
50
0
205
210
215
220
225
230
235
Shadow
y = 2.7945x - 317.17
R² = 0.7767
series 1
linear

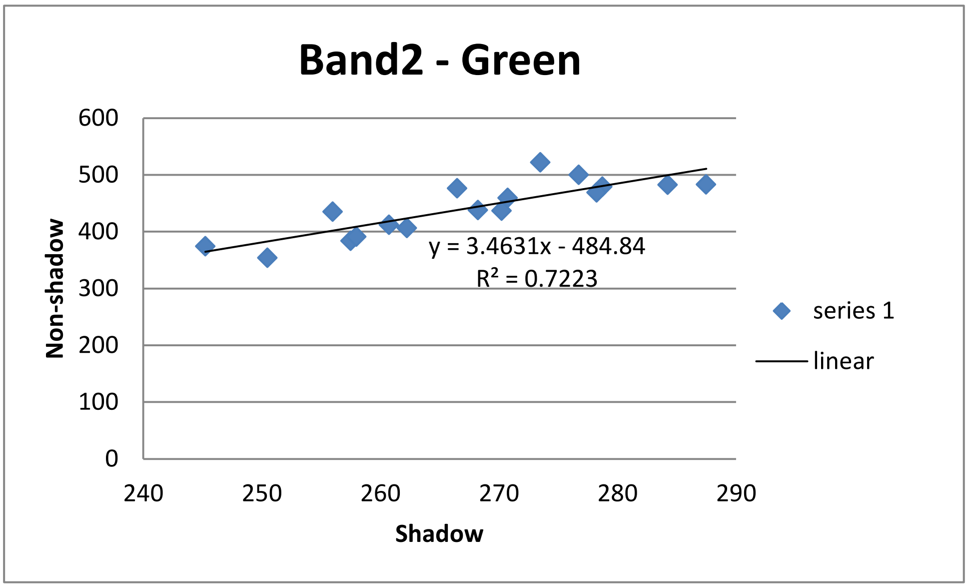
Band2 - Green
Non-shadow
600
500
400
300
200
100
0
240
250
260
270
280
290
Shadow
y = 3.4631x - 484.84
R² = 0.7223
series 1
linear

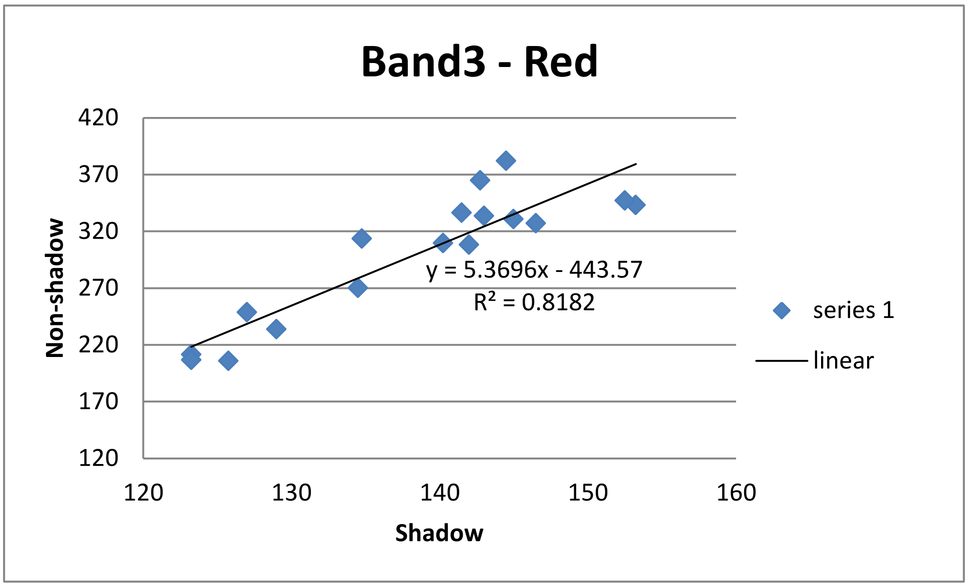
Band3 - Red
Non-shadow
420
370
320
270
220
170
120
120
130
140
150
160
Shadow
y = 5.3696x - 443.57
R² = 0.8182
series 1
linear

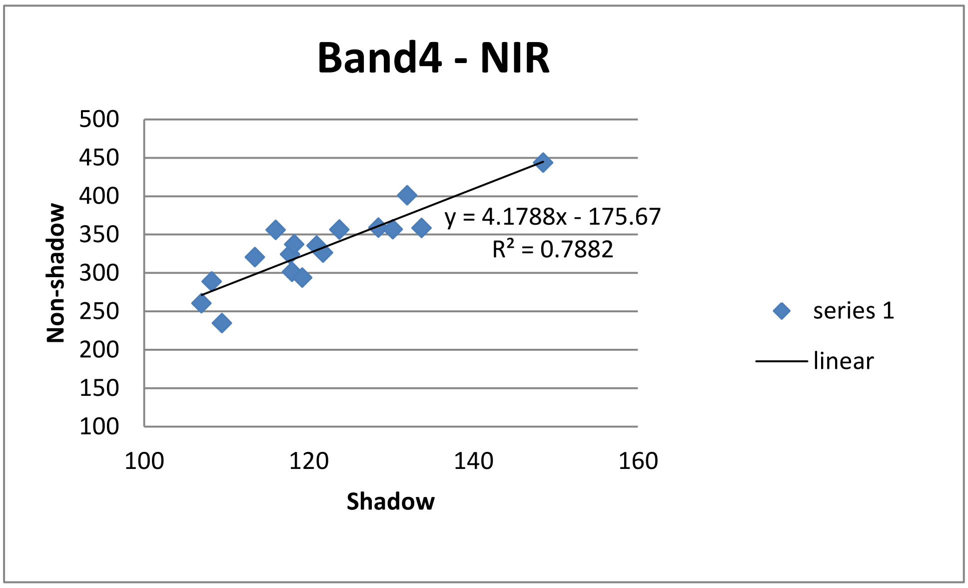
Band4 - NIR
Non-shadow
500
450
400
350
300
250
200
150
100
100
120
140
160
Shadow
y = 4.1788x - 175.67
R² = 0.7882
series 1
linear

C. Graphical representation of shadow enhancement performance

Central

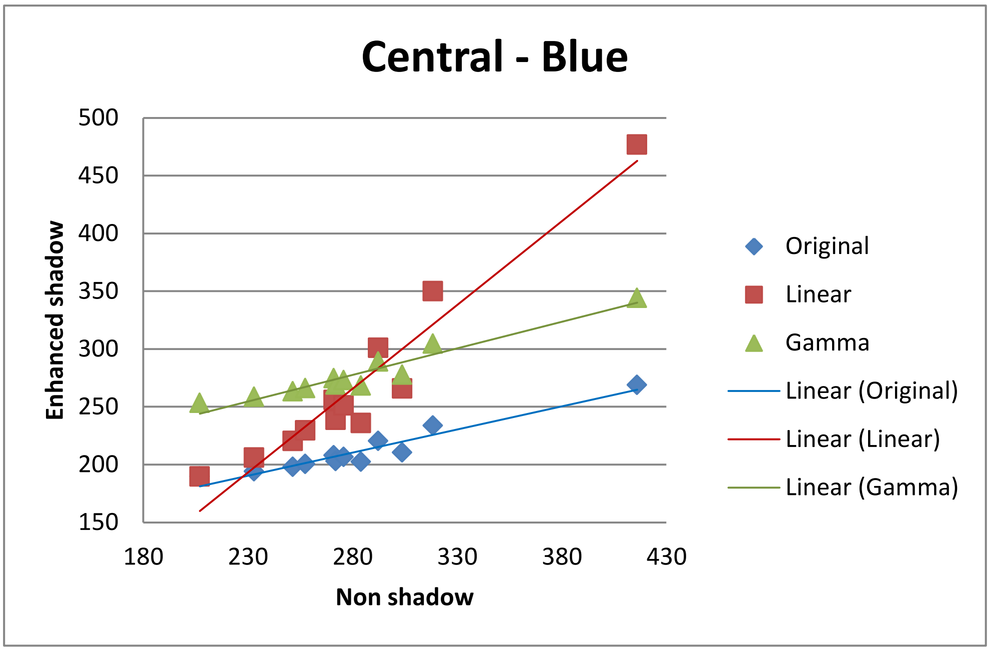

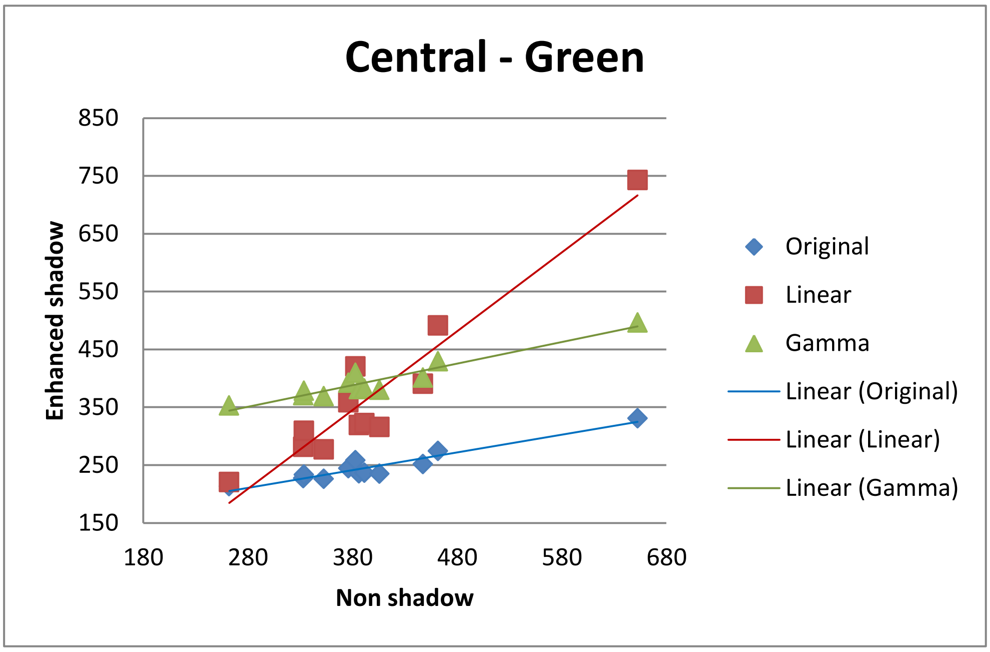

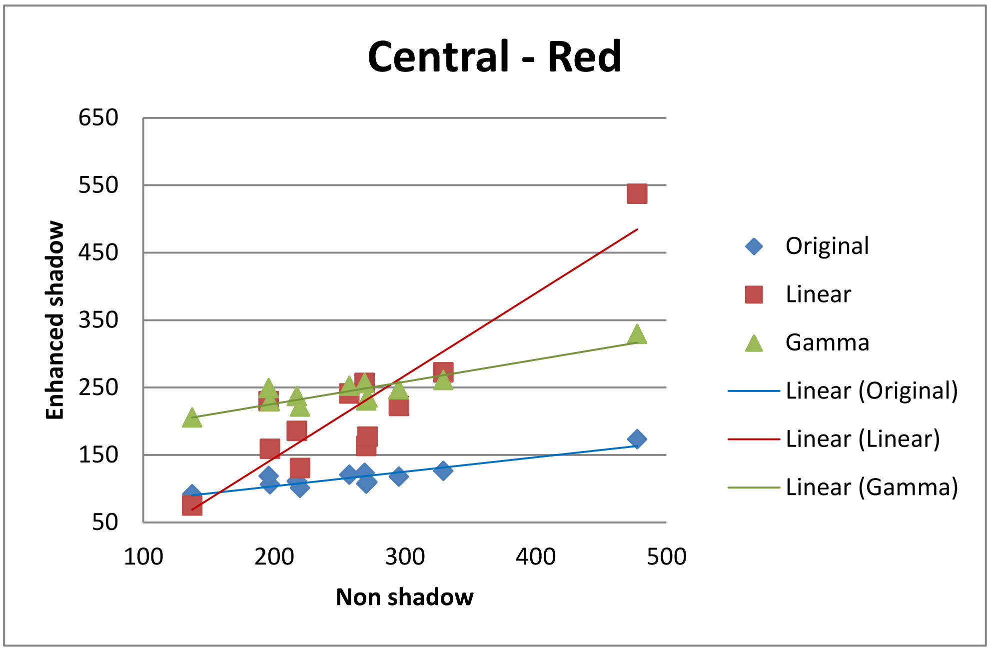

Central - Red
Enhanced shadow
650
550
450
350
250
150
50
100
200
300
400
500
Non shadow
Original
Linear
Gamma
Linear (Original)
Linear (Linear)
Linear (Gamma)

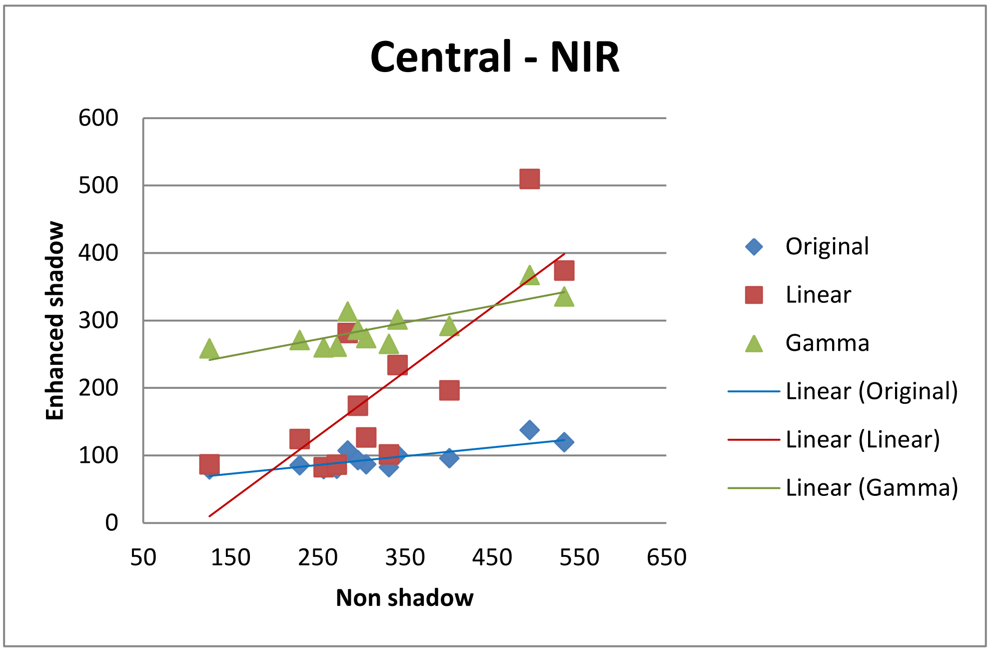

Central - NIR
Enhanced shadow
600
500
400
300
200
100
0
50
150
250
350
450
550
650
Non shadow
Original
Linear
Gamma
Linear (Original)
Linear (Linear)
Linear (Gamma)

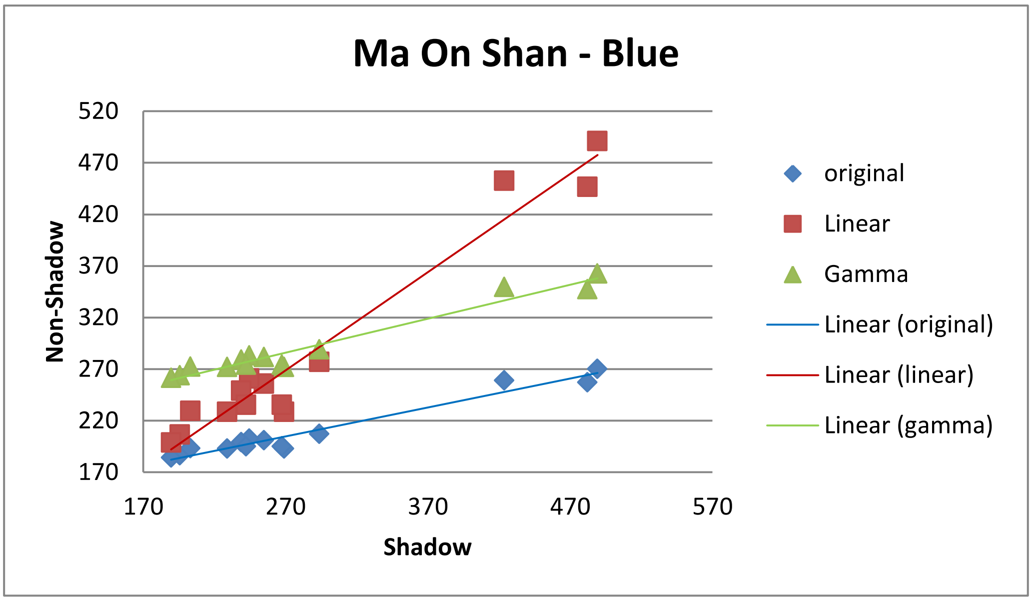
Ma On Shan - Blue
Non-Shadow
520
470
420
370
320
270
220
170
170
270
370
470
570
Shadow
original
Linear
Gamma
Linear (original)
Linear (linear)
Linear (gamma)

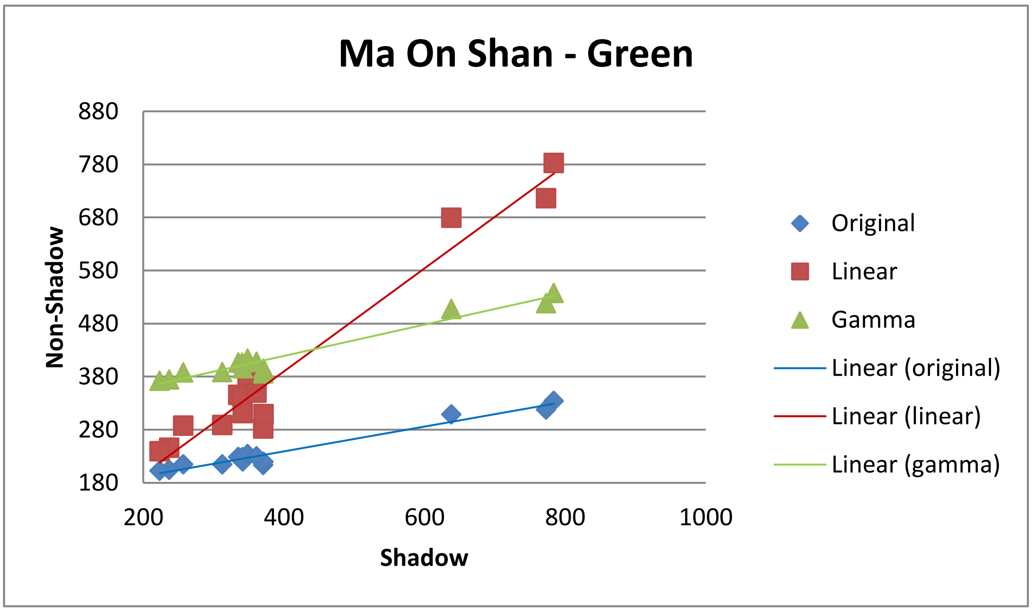
Ma On Shan - Green
Non-Shadow
880
780
680
580
480
380
280
180
200
400
600
800
1000
Shadow
Original
Linear
Gamma
Linear (original)
Linear (linear)
Linear (gamma)

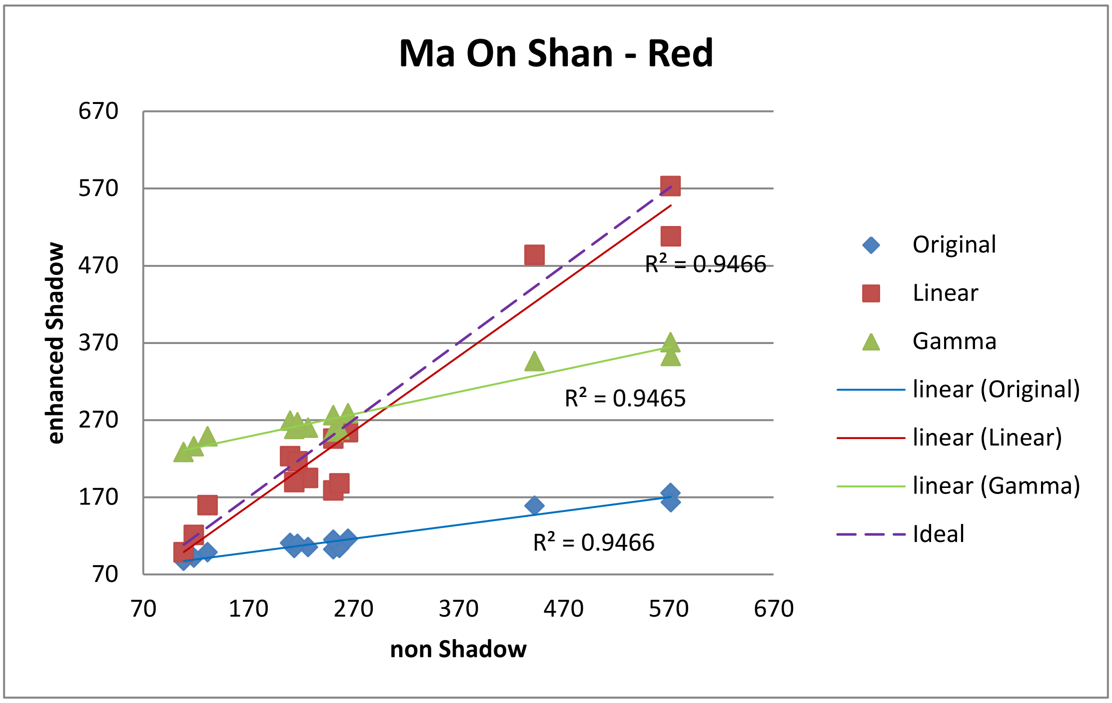

Ma On Shan - Red
670
570
470
370
270
170
70
enhanced Shadow
70
170
270
370
470
570
670
non Shadow
R² = 0.9466
R² = 0.9465
R² = 0.9466
Original
Linear
Gamma
linear (Original)
linear (Linear)
linear (Gamma)
Ideal

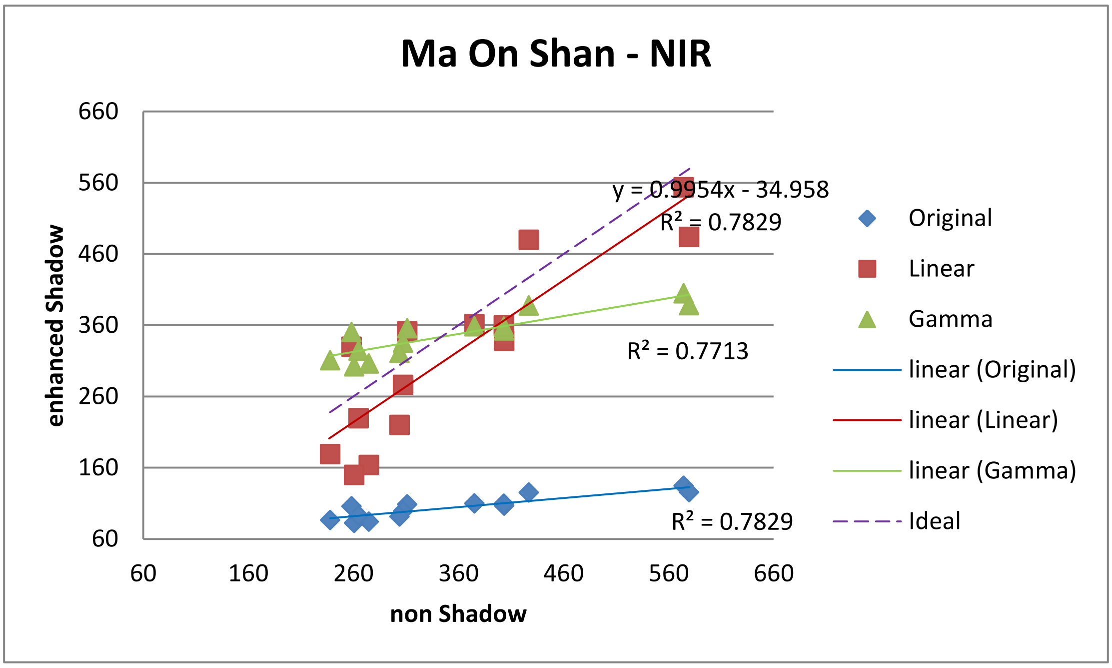

Ma On Shan - NIR
660
560
460
360
260
160
60
enhanced Shadow
60
160
260
360
460
560
660
non Shadow
y = 0.9954x - 34.958
R² = 0.7829
R² = 0.7713
R² = 0.7829
Original
Linear
Gamma
linear (Original)
linear (Linear)
linear (Gamma)
Ideal

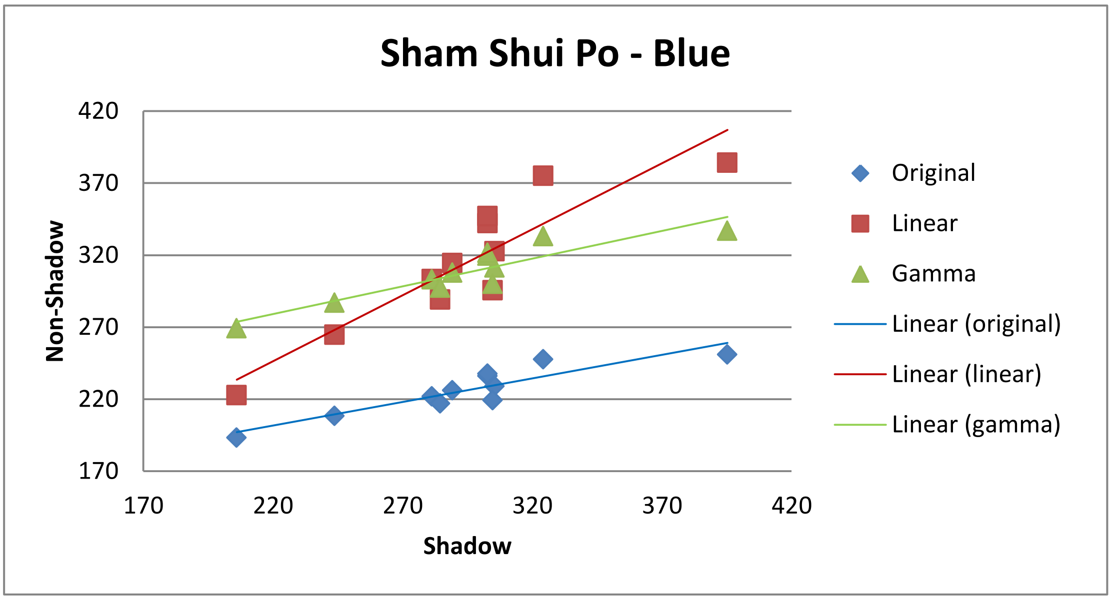
Sham Shui Po - Blue
420
370
320
270
220
170
Non-Shadow
170
220
270
320
370
420
Shadow
Original
Linear
Gamma
Linear (original)
Linear (linear)
Linear (gamma)

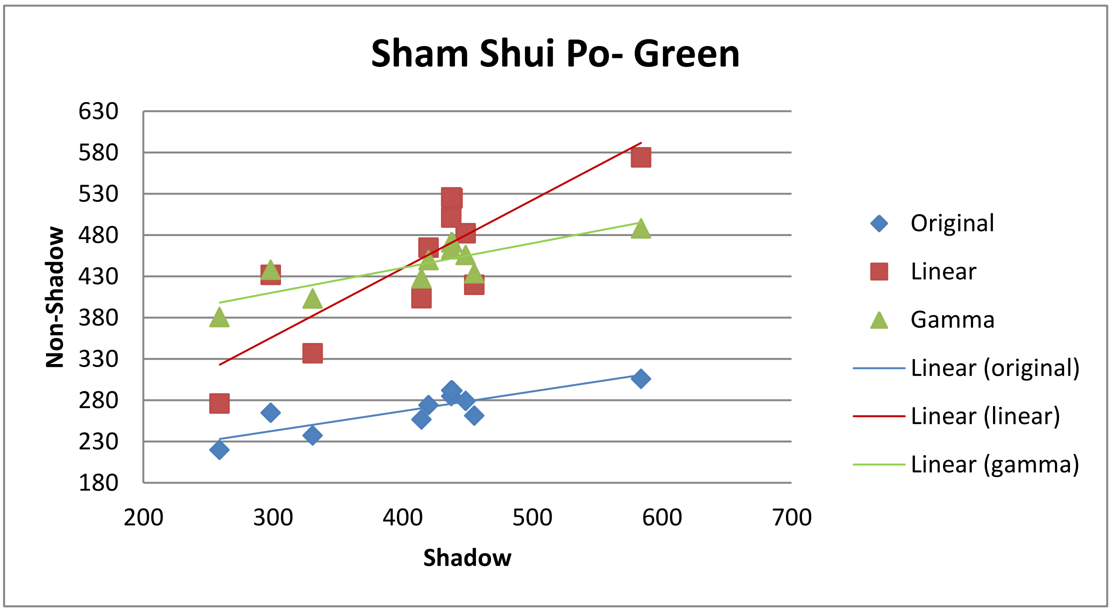
Sham Shui Po- Green
630
580
530
480
430
380
330
280
230
180
Non-Shadow
200
300
400
500
600
700
Shadow
Original
Linear
Gamma
Linear (original)
Linear (linear)
Linear (gamma)

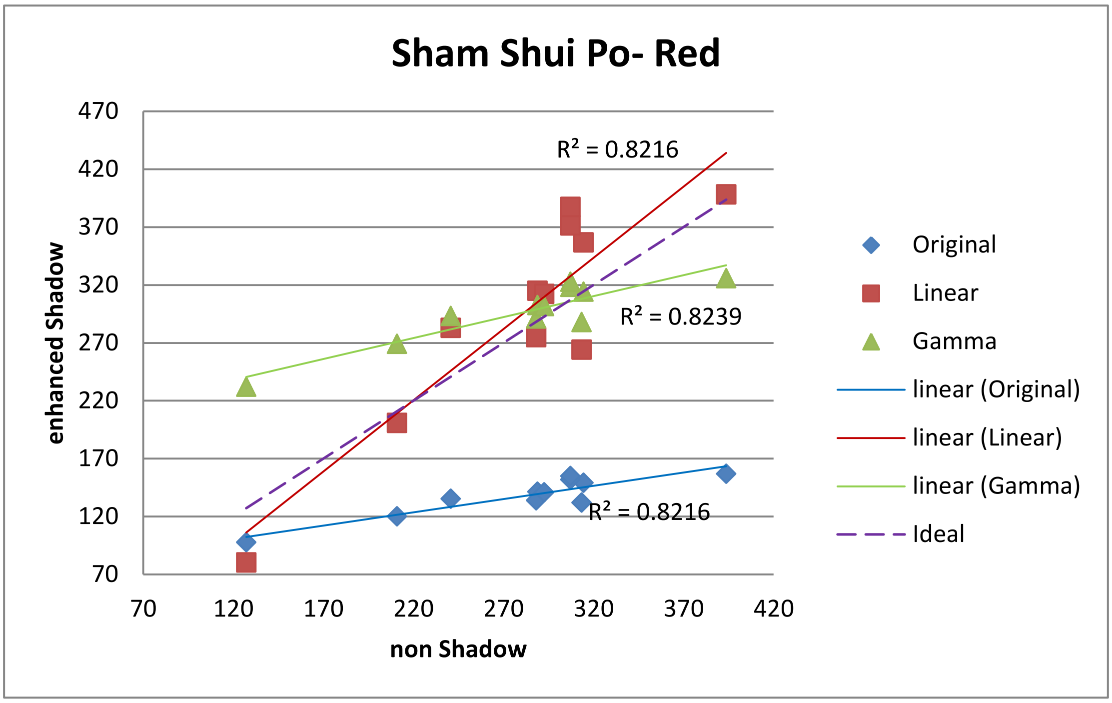
Sham Shui Po- Red
enhanced Shadow
non Shadow
470
420
370
320
270
220
170
120
70
70
120
170
220
270
320
370
420
R² = 0.8216
R² = 0.8239
R² = 0.8216
Original
Linear
Gamma
linear (Original)
linear (Linear)
linear (Gamma)
Ideal

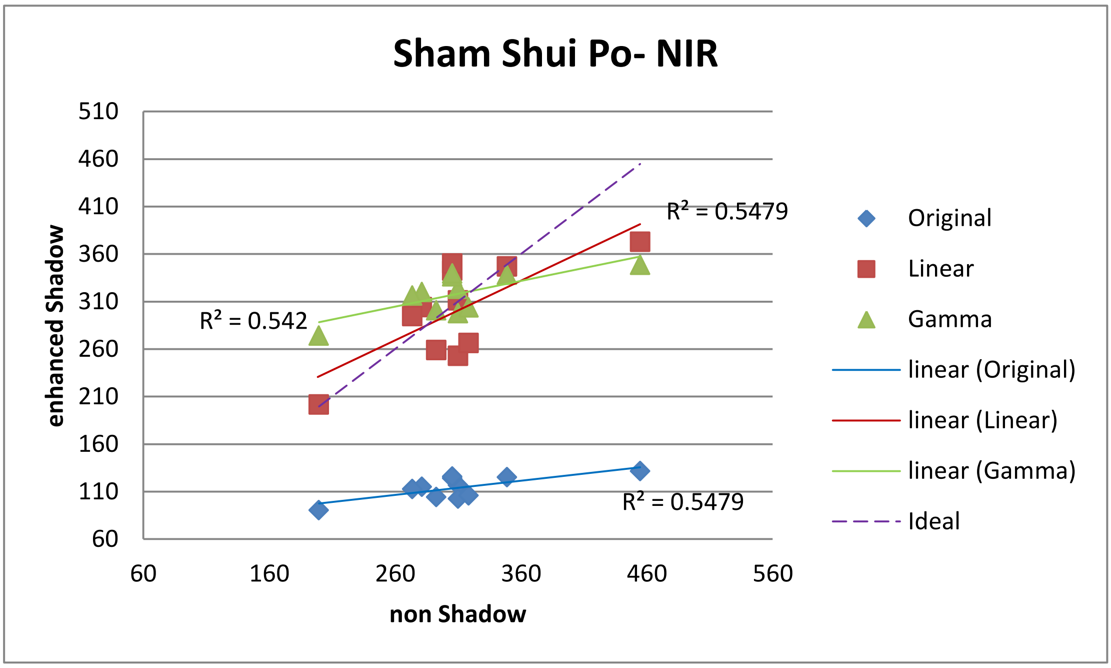
Sham Shui Po- NIR
enhanced Shadow
non Shadow
510
460
410
360
310
260
210
160
110
60
60
160
260
360
460
560
R² = 0.5479
R² = 0.542
R² = 0.5479
Original
Linear
Gamma
linear (Original)
linear (Linear)
linear (Gamma)
Ideal

References

Arevalo, V., Gonzalez, J., Valdes, J., & Ambrosio, G. (2006). Detecting Shadows in QUICKBIRD Satellite Images. *ISPRS Commission VII Mid-term Symposium "Remote Sensing: From Pixels to Processes"*, (pp. 330-335). Enschede, the Netherlands.

Cai, D., Li, M., Bao, Z., Chen, Z., Wei, W., & Zhang, H. (2010). Study on Shadow Detection Method on High Resolution Remote Sensing Image Based on HIS Space Transformation and NDVI Index. *18th International Conference on Geoinformatics, 2010* (pp. 1-4). Beijing: IEEE.

Chen, S., Su, H., Zhang, R., Tian, J., & Yang, L. (2008). The Tradeoff Analysis for Remote Sensing Image Fusion Using Expanded Spectral Angle Mapper. *Sensors*, 8, pp. 520-528.

Chen, Y., Wen, D., Jing, L., & Shi, P. (2007). Shadow information recovery in urban areas from very high resolution satellite imagery. *International Journal of Remote Sensing, 28*(15), pp. 3249-3254.

Dare, P. M. (2005). Shadow Analysis in High-Resolution Satellite Imagery of Urban Areas. *Photogrammetric Engineering & Remote Sensing, 71*(2), pp. 169-177.

Gevers, T., & Smeulders, A. W. M. (1999). Colour-based object recognition. *Pattern Recognition*, 32, pp. 453-464.

Guo, H. T., Zhang, Y., Lu, J., & Jin, G. W. (2008). Research on the building shadow extraction and elimination method. *The International Archives of the Photogrammetry, Remote Sensing and Spatial Information Sciences*, 37, (pp. 569-573). Beijing, China.

Han, S., Li, H., & Gu, H. (2008). The study on image fusion for high spatial resolution remote sensing images. *The International Archives of the Photogrammetry, Remote Sensing and Spatial Information Sciences*, 37, (pp. 1159-1164). Beijing, China.

Lau, W. L., King, B. A., & Vohora, V. K. (2001). Comparison of image data fusion techniques using entropy and INI. *Proceedings, 22nd Asian Conference on Remote Sensing, Singapore*, 1, pp. 152-157.

Massalabi, A., He, D. C., Benie, G. B., & Beaudry, E. (2004). Detecting information under and from shadow in panchromatic Ikonos images of the city of Sherbrooke. *IEEE IGARSS '04.*, pp. 2000-2003.

Massalabi, A., He, D. C., Benie, G. B., & Beaudry, E. (2004). Restitution of information under shadow in remote sensing high space resolution images: Application to IKONOS data of Sherbrooke city. *ISPRS Congress Istanbul 2004, Proceedings of Commission III.* Istanbul.

Myint, S. W., Gober, P., Brazel, A., Grossman-Clarke, S., & Weng, Q. (2011). Per-pixel vs. object-based classification of urban land cover extraction using high. *Remote Sensing of Environment*, 115, pp. 1145-1161.

Nakajima, T., Tao, G., & Yasuoka, Y. (2002). Simulated recovery of information in shadow areas on IKONS image by combing ALS data. *The 23th Asian Association of Remote Sensing (AARS) 2002.* Kathmandu, Nepal.

Nath, R., & Deb, S. (2010). Water-Body Area Extraction From High Resolution Satellite Images - An Introduction, Review and Comparison. *International Journal of Image Processing, 3*(6), pp. 353-372.

Sarabandi, P., Yamazaki, F., Matsuoka, M., & Kiremidjian, A. (2004). Shadow Detection and Radiometric Restoration in Satellite High Resolution Images. *IEEE IGARSS '04.*, 6, pp. 3744-3747.

Shu, J., & Freeman, H. (1990). Cloud shadow removal from aerial photographs. *Pattern Recognition, 23*(6), pp. 647-656.

Wang, S., & Wang, Y. (2009). Shadow Detection and Compensation in High Resolution Satellite Image Based on Retinex. *Proceedings of the Fifth International Conference on Image and Graphics (ICIG)* 2009, (pp. 209-212). Xi an, Shanxi, China.

Xia, H., Chen, X., & Guo, P. (2009). A Shadow Detection Method for Remote Sensing Images Using Affinity Propagation Algorithm. *IEEE International Conference on Systems, Man and Cybernetics (SMC) 2009,* (pp. 3116-3121). San Antonio, TX: IEEE.

Yamazaki, F., Liu, W., & Takasaki, M. (2009). Characteristic of shadow and removal of its effects for remote sensing imagery. *IEEE IGARSS '09.*, pp. 426-429.

YCEO. (2012). *CEO users guide.* Retrieved July 16, 2012, from The Yale Center for Earth Observation: http://www.yale.edu/ceo/Documentation/CEOGuide.html

Zhan, Q., Shi, W., & Xiao, Y. (2005). Quantitative analysis of shadow effects in high-resolution images of urban areas. *WG VIII/1 Joint Symposia URBAN - URS 2005.* Tempe, AZ, USA: ISPRS.

Zheng, Q., & Wang, Q. (2008). Shadow restoration method of Quickbird satellite remotely sensed imagery. *Computer Engineering and Application*, pp. 30-32.

Zhou, G. (2005). Urban Large-scale Orthoimage Standard for National Orthophoto Program. *IEEE Geoscience and Remote Sensing Symposium, 2005. IGARSS '05. Proceedings.* (pp. 1214-1217). IEEE International.